UNIVERSITY OF CALIFORNIA,
IRVINE

Macropinocytosis fuels cancer cell growth and drug resistance

DISSERTATION

submitted in partial satisfaction of the requirements
for the degree of

DOCTOR OF PHILOSOPHY

in Biological Sciences

by

Vaishali Jayashankar

Dissertation Committee:
Professor Aimee Edinger, Chair
Professor Christine Sütterlin
Professor Steve Gross
Professor Naomi Morrissette

2019

TABLE OF CONTENTS

LIST OF FIGURES

CHAPTER 3

CHAPTER 4

LIST OF TABLES

CHAPTER 4 Pg

LIST OF ABBREVIATIONS

Abbreviation	Definition
1% AA	medium containing 1% the normal amount of amino acids but standard fetal calf serum (10%)
1% AA/gluc	medium containing 1% the normal amount of amino acids and glucose but standard fetal calf serum (10%)
1% gluc	medium containing 1% the normal amount of glucose but standard fetal calf serum (10%)
22Rv1	PTEN-replete human prostate cancer cell line, not macropinocytic
4T1	mouse mammary carcinoma cell line, contextually macropinocytic
ADT	androgen deprivation therapy
ATCC	american Type Culture Collection
ATG5	autophagy related 5
BSA	bovine serum albumin
BxPC3	non-macropinocytic pancreas cancer cell line
CARS	coherent anti-Stokes Raman spectroscopy, used here to monitor lipid droplet content
CFSE	carboxyfluorescein succinimidyl ester, fluorescent protein dye
CHX	cycloheximide, protein synthesis inhibitor
CK8	cytokeratin 8, epithelial marker
CRISPR/Cas9	Clustered regularly interspaced short palindromic repeats (CRISPR)-associated protein-9 nuclease (Cas9)
CRPC	castration-resistant prostate cancer
CTLA-4	cytotoxic T-lymphocyte-associated protein 4, a protein receptor that, functioning as an immune checkpoint, downregulates immune responses; acts as an "off" switch when bound to CD80 or CD86 on the surface of antigen-presenting cells.
DAPI	4′,6-diamidino-2-phenylindole, fluorescent DNA stain excluded from live cells
DIC	Differential interference contrast

	microscopy, an optical microscopy technique used to enhance the contrast in unstained, transparent samples
DU145	macropinocytic human prostate cancer cell line, PTEN-deficient, does not express the androgen receptor
ECM	extracellular matrix
EdU	5-ethynyl-2'-deoxyuridine; an alkyne-modified thymidine analogue that is efficiently incorporated into newly synthesized DNA and fluorescently labeled through the highly-specific click (copper catalyzed azido-alkyne cycloaddition) reaction
EIPA	5-(N-Ethyl-N-isopropyl) amiloride
EOD	every other day
FL5.12	murine hematopoetic cell line dependent on IL-3; IL-3 withdrawal induces apoptosis and then cells undergo secondary necrosis; rapid doubling time (12 h) facilitates metabolic labeling
GF	Growth factor
GlcNAc	N-Acetylglucosamine, a monosaccharide used in glycosylation reactions
GlcNAlk	an alkyne-containing, clickable form of GlcNAc
HCC1569	non-macropinocytic breast cancer cell line
Hoechst	Hoeschst 33342 fluorescent DNA stain that can be used in live cells
HPG	homopropargylglycine; clickable alternative to methionine
HU	hydroxyurea, arrests DNA polymerization
IL-3	interleukin 3, required growth factor for FL5.12 cells
LC3	Microtubule-associated protein 1A/1B-light chain 3 (LC3)
LNCaP	macropinocytic, AR-positive, PTEN-deficient prostate cancer cell line; grows in fetal bovine serum without added androgen, but is androgen responsive
LTR/LysoRed/Blue	Lysotracker dyes used to stain acidic compartments
MCF7	macropinocytic breast cancer cell line

MP	macropinocytic
mPCE	mouse prostate cancer epithelial cells, derived from a tumor in a pDKO mouse
MSK-PCa1/2	macropinocytic, PTEN-deficient patient derived CRPC cells that will grow in organoid cultures and as tumors in NSG mice
Nec cells	necrotic cells
NHE	Sodium–hydrogen antiporter; blocking NHE function prevents macropinocytosis
NSCLC	non-small-cell lung carcinoma
PA-Alk	palmitic acid alkyne
PAK1	p-21 activated kinase 1
PANC1	macropinocytic pancreas cancer cell
PC3	PTEN deficient AR null human prostate cancer cell line
PDAC	pancreatic adenocarcinomas
PI3K	phosphatidylinositol 3-kinase, produces PIP_3
PIP_3	Phosphatidylinositol (3,4,5)-trisphosphate, dephosphorylated by PTEN
PDX	patient-derived xenograft; samples from patients that are transferred to mice without in vitro culture.
PTEN	Phosphatase and tensin homolog, negative regulator of the PI 3-kinase pathway
RAC1	Rho Family, Small GTP Binding *Protein*
RAS	a GTP binding oncogene
RWPE-1	PTEN-replete, non-macropinocytic, non-transformed prostate epithelial cell line
SD	standard deviation
SEM	standard error of the mean
SQ	Subcutaneous
TME	tumor microenvironment

ACKNOWLEDGMENTS

I would like to express my deepest appreciation to my committee chair, *Aimee Edinger*, whose passion for science is extremely infectious, inspiring and motivating. I was able to restart and complete my dissertation work quickly only due to Aimee's brilliant ideas, endless creativity, and her genuine investment in my success and belief in my abilities as a scientist. I'm grateful for the countless number of hours we spent discussing science and for all her honest feedback, which has helped mold me into a better scientist. Aimee is not only an exceptional and seasoned scientist, but also a great human being, whom I am proud to call a mentor and a role model. I thank her for dealing with my shenanigans.

I'm forever grateful to *Susanne Rafelski* for introducing me to the fascinating world of mitochondrial biology, which I have not stopped thinking about ever since and have committed to working on in some aspect of my scientific career.

I was extremely lucky to have committee members (*Christine Sutterlin,* *Naomi Morisseette* and *Steve Gross*) who are triple threats (great scientists, mentors and human beings). Thank you for showing genuine interest in my success and growth as a scientist.

In addition, I would like to thank *Wengi Wang* and the members of his lab, *Kavita Arora*, *David Fruman*, *Mike Mulligan* and *Justin Shaffer* as well as other faculty and staff members for sharing words of encouragement and/or providing valuable scientific feedback.

I thank *Douglas Weiser*, *Lisa Wrishnik*, *Greg Joggenward*, *Craig Vierra*, *Mitchell Singer*, *Arturo Calderon Flores* and *Madan Paidhungant* for helping me develop my love for science and teaching. I would like to thank all the talented *graduate students, postdocs, undergraduates and staff members from the Edinger and Rafelski* labs for providing valuable discussions every day and for their friendship. I thank all my classmates, roommates and lifelong friends I made throughout the years, for constant encouragement and for their patience especially the last three years.

I thank my parents *Mallika Jayashankar* and *Jayashankar Raghunathan*. Thank you for always making me see the light at the end of the tunnel and helping me keep my dreams alive and for letting me march to the beat of my own drum. I know the last three years I was absent and focused on nothing but this work but you two never made me feel guilty about it and always made sure I was OK.

Yuora Yelpaala and *April Raj-* this journey would have been much harder without the love and support from you and your families.

Financial support was provided by the through *GAANN* (P200A120207) under the supervision of *Debra Mauzy-Melitz* from 2015-2017.

CURRICULUM VITAE

Vaishali Jayashankar

3302 Natural Sciences 1, Irvine, CA 92617 | (949) 824-1035 | vjayasha@uci.edu

Education

University of California, Irvine — Ph.D., Irvine, CA [09/2012]-[06/2019]

University of the Pacific — M.S., Stockton, CA [08/2009]-[06/2012]

University of California, Davis — B.S., Davis, CA [09/2006]-[05/2008]

Research

Ph.D. candidate — University of California, Irvine [08/2016]-[06/2019]

Advisor: Dr. Aimee L. Edinger
Project title: Macropinocytosis supports cancer anabolism

- Use of molecular techniques to study novel signals that regulate macropinocytosis in cancer cells
- Identified macropinocytosis as a novel mechanism that mediates drug resistance
- Developed a click-chemistry based tool to monitor macropinocytic flux

Ph.D. candidate — University of California, Irvine [07/2013]-[08/2016]

Advisor: Dr. Susanne Rafelski
Project title: Disordered regions of tubulin maintain mitochondrial organization
Project Contributions:

- Generated yeast mutant strains to characterize signal transduction pathways that regulate mitochondrial morphology
- Analysis of synthetic lethality screens
- Identified a novel regulation between cytoskeleton elements and mitochondrial shape and function

Graduate Student Researcher — University of the Pacific [08/2009] - [06/2012]

Advisor: Dr. Douglas Weiser
Project title: Protein Phosphatase 1 β Paralogs Encode the Zebrafish Myosin Phosphatase Catalytic Subunit
Project Contributions:

- Protein phosphatase 1 β paralogs both have phosphatase

activity necessary for cell migration during gastrulation

Research Associate — Maxygen Inc [06/2008]-[05/2009]

Group: Research and Development
Goal: Support development of small molecule treatments for multiple sclerosis

Undergraduate Research Assistant — University of California, Davis [12/2006]-[05/2008]

Advisor: Dr. Mitchell Singer
Project title: Cyclic GMP promotes M. xanthus biofilm growth and fruiting body development

Publications

[Primary Papers]

1. Kubiniok, P*., McCracken, A. N*., **Jayashankar, V*,** Lorenzo, S., Vece, V., …Edinger, A. (2019). Simultaneous inhibition of nutrient and nuclear import by natural and synthetic sphingolipids. (manuscript in preparation; **equal contribution)*
2. **Jayashankar, V.,** Edinger, A.L. (2019) Macropinocytosis confers resistance to therapies targeting cancer anabolism (under review)
3. Kim, S. M., Nguyen, T. T., Ravi, A., Kubiniok, P., Finicle, B. T., **Jayashankar, V**., … Edinger, A. L. (2018). PTEN deficiency and AMPK activation promote nutrient scavenging and anabolism in prostate cancer cells. *Cancer Discovery*, **8**, 1-18
4. Carr, B. W., Basepayne, T. L., Chen, L., **Jayashankar, V.,** & Weiser, D. C. (2014). Characterization of the zebrafish homolog of zipper interacting protein kinase. *International Journal of Molecular Sciences,* **15**, 11597-11613
5. **Jayashankar, V.,** Nguyen, M. J., Carr, B. W., Zheng, D. C., Rosales, J. B., Rosales, J. B., & Weiser, D. C. (2013). Protein phosphatase 1 β paralogs encode the zebrafish myosin phosphatase catalytic subunit. *PLoS ONE,* **8**, 1-19

[Invited Reviews and Commentaries]

1. **Jayashankar, V**, Finicle, B. T., Edinger, A.L. (2018) Starving PTEN-deficient prostate cancer cells thrive under nutrient stress by scavenging corpses for their supper. *Molecular Cell Oncology*. **5**, e1472060.
2. Finicle, B, **Jayashankar, V,** Edinger, A.L. (2018) Nutrient scavenging in cancer. *Nat Rev Cancer*. **10**, 619-633.
3. **Jayashankar, V*,** Mueller, IA*, Rafelski, SM. (2015) Shaping the multi-scale architecture of mitochondria. *Equal contribution, *Current Opinions in Cell Biology*. **18**, 14-20.
4. **Jayashankar, V,** Rafelski, SM. (2014) Integrating mitochondrial organization and dynamics with cellular architecture. *Current Opinions in Cell Biology*. **26**, 34-40

Selected talks and posters

[Selected talks]

1. **2018: Developmental & Cell Departmental Retreat, Irvine, CA.** Macropinocytosis promotes survival and proliferation of nutrient deprived breast cancer cells.
2. **2018: Monthly Breast Cancer Disease Oriented Team, Stern Center for Cancer Clinical Trials and Research, Orange, CA.** Nutrient Scavenging fuels cancer cell growth.
3. **2017: Developmental & Cell Departmental Retreat, Irvine, CA.** Macropinocytosis supports breast cancer anabolism

4. **2014: ASCB meeting, Organelle Dynamics and Crosstalk in Health and Disease Section.** Novel mitochondria-microtubule crosstalk regulates mitochondrial biogenesis and morphology.
5. **2013: ASCB national conference, Intracellular Trafficking and Organelle Biogenesis.** Tubulin carboxy-terminal tails regulate mitochondrial content and morphology in budding yeast.
6. **2008: 19th Annual Undergraduate Research Conference.** Genetic Characterization of the Response Regulator orrW in Myxococcus Xanthus."

[Posters]

1. **2017: Tumor metabolism & hypoxia, Keystone Symposia.** Macropinocytosis supports survival of breast cancer cells under nutrient limiting states. **V. Jayashankar,** Aimee L. Edinger
2. **2015 Cell Biology of Yeasts meeting, Cold Spring Harbor:** Tubulin carboxy-terminal tails regulate mitochondrial structure and function. **V. Jayashankar,** Susanne M. Rafelski, Jeffrey K. Moore
3. **2015 ASCB meeting:** α-tubulin carboxy-terminal tail maintains mitochondrial structure and function in *Saccharomyces cerevisiae.* **V. Jayashankar,** Jayne Aiken, Susanne M. Rafelski, Jeffrey K. Moore
4. **2014 ASCB meeting:** Novel mitochondria-microtubule crosstalk regulates mitochondrial biogenesis and morphology. **V. Jayashankar,** Jayne Aiken, Susanne M. Rafelski, Jeffrey K. Moore
5. **2013 ASCB conference:** Tubulin carboxy-terminal tails regulate mitochondrial content and morphology in budding yeast. **V. Jayashankar**, Susanne M. Rafelski, Jeffrey K. Moore
6. **2012 ASCB conference:** Two isoforms of protein phosphatase 1 beta assemble the zebrafish myosin phosphatase. **V. Jayashankar**, D. C. Weiser; Biological Sciences, University of the Pacific, Stockton, CA
7. **2012 10th Annual National Zebrafish Genetics and Developmental Conference:** Two isoforms of protein phosphatase 1B assemble the Zebrafish Myosin Phosphatase. **V. Jayashankar**, Douglas Weiser.

Teaching and Service

[University of California, Irvine]

- **Co-Instructor** for **Bio Sci 800,** Pre-Biology STEM-UPP Course, UNEX,00361 (Summer 2015)

- **The courses that I served as a teaching assistant: BIO SCI D111** (Developmental Laboratory) Spring 2018, **BIO SCI 93H** (DNA to Organisms) Fall 2017 & Fall 2016, **BIO SCI 9B** (Biology & Chemistry of Food and Cooking) Winter 2017, **BIO SCI D135** (Diseases of the Cell) Spring 2014 & Spring 2015, **BIO SCI 93** (DNA to Organisms) Fall 2014, **BIO SCI D103** (Cell Biology) Fall 2013

- **Graduate assistance in areas of national need fellow:** As a Graduate Assistance in Areas of National Need (GAANN) fellow, I developed and facilitated multiple symposiums for undergraduate students and graduate students in the STEM field. Some of the workshops I developed included *how to become a successful undergraduate researcher, how to give a effective talk and provide feedback,* and *how to develop a teaching portfolio.*

- **Additional workshops held at teaching development conferences:**

    - **2015 RABLE , University of California, Irvine, Irvine, CA.** Bringing *Chlamydia* and conflict to the classroom: An interactive discussion activity to assess students' ability to read primary literature (Cell Biology, Instructional Methods).

    - **2014 ABLE- Oregon State University, Eugene, OR.** Assessment of the impact of *Bio Sci D140: How to Read a Science Paper* course on student attitudes towards biological research.

[University of the Pacific]

- **Lead laboratory Instructor: BIO SCI 51/61** (Principles of Biology Laboratory Course) Fall & Spring 2009-2012

[Mentorship]

- I have also mentored several undergraduate and high school research students in the **Weiser lab** (*Rojin Amiri, Jalpa Patel, Christine Hsu and Monique Iskarous*), **Rafelski lab** (*Claire Goul, Amal Yusuff and Kenji Sumikawa*), and the **Edinger lab** (*Thomas Ngo, Andrew Tang and Temoc Ramirez*)
- Judge for Intel International Science and Engineering Fair (Intel ISEF; 2015)
- Irvine Unified School District Science Fair Judge (2014)

Academic & Professional honors

- Developmental & Cell Biology Department Graduate Student Representative (2015-2016)
- ASCB Travel Award (2015)
- AGS Travel Award (2014)
- GAANN Fellowship (2014-2016)
- Cold Spring Harbor - Yeast Genetics Training Certificate of Excellence (2014)
- Hunter Nahhas Excellence Fellowship, University of the Pacific (2010)
- Scholarly research at 19th annual Undergraduate Research Conference, University of California, Davis (April 2008)
- Alpha Gamma Sigma Honor, Ohlone College, 2005-2006

Society Memberships

American Society of Cell Biology, United Mitochondrial Disease Foundation Association For Biology Laboratory Education, Association of American Colleges & Universities

References

Aimee L. Edinger, Associate Professor
Department of Developmental and Cell Biology
University of California, Irvine
(949) 824-1921
aedinger@uci.edu

Susanne M. Rafelski, Director, Assay Development
The Allen Institute for Cell Science
615 Westlake Ave N, Seattle, WA 98109
(206) 548-7000
susanner@mac.com

Douglas C. Weiser, Associate Professor
University of the Pacific
3601 Pacific Ave Stockton, CA 95211
209-946-2955
dweiser@pacific.edu

ABSTRACT OF THE DISSERTATION

Macropinocytosis fuels cancer cell growth and drug resistance

By

Vaishali Jayashankar

Doctor of Philosophy in Biological Sciences

University of California, Irvine, 2019

Professor Aimee L. Edinger, Chair

To support their accelerated non-homeostatic proliferation, cancer cells depends on access to extracellular nutrients derived from the tumor vasculature. However, dysfunctional tumor vasculature and high interstitial pressure limit tumor perfusion leaving many tumor cells nutrient-deprived. To bypass this nutrient limitation, RAS driven cancer cells recycle their own nutrients via autophagy or scavenge macromolecules from the tumor microenvironment (TME) via macropinocytosis. Oncogenic mutations in RAS promote macropinocytosis, a bulk scavenging process through which components in the TME can be non-specifically acquired. When macropinosomes fuse with lysosomes, degradative enzymes release nutrients that can support cancer cell growth and proliferation. We report macropinocytosis is not just a RAS driven phenotype but a cancer phenotype. Lipid PIP_3 generated by the PI3K pathway is necessary for closure of macropinosomes in most contexts. We identified prostate and breast cancers with hyper-activation of the PI3K pathway perform macropinocytosis in an AMPK dependent manner. AMPK mediated macropinocytosis is necessary for proliferation of PTEN-deficient cells in low nutrients but not autophagy.

Because scavenging allows cells to acquire nutrients from cell extrinsic sources, it is likely to play a greater role in promoting tumor growth than cell-autonomous autophagy, which leads to atrophy. Necrosis is observed in most solid tumors; necrotic cell debris is selectively scavenged via macropinocytosis. Nutrient-deprived macropinocytic breast cancer cells acquired not just amino acids, but also sugars, lipids, and nucleotides from necrotic cell debris (necrocytosis) suggesting macropinocytosis plays a larger role than previously appreciated in supporting cancer anabolism. In addition, necrocytosis also conferred resistance to various therapies that target de novo nucleotide synthesis, fatty acid synthesis as well standard of care genotoxic therapies resulting in the first demonstration that scavenging confers drug resistance. Together, these studies suggest that macropinocytosis inhibitors could have therapeutic value in many cancer patients, particularly in combination with conventional therapies.

CHAPTER 1

INTRODUCTION

The following introduction contains excerpts taken from our review article entitled "Nutrient Scavenging in Cancer" published in *Nature Reviews Cancer* (2018). I'm a co-author of this review. All authors contributed to substantial discussions, research and collection of references and the writing and editing of the article. B.T.F. and A.L.E. organized and planned the display figures and boxes.

I. Deregulated nutrient acquisition pathways allow tumor cells to be metabolically flexible in nutrient-deficient environments

A hallmark of cancer is uncontrolled cell growth and division mediated by gain of function mutations in oncogenes or loss of function mutations in tumor suppressors[1]. For a cell to divide, it has to be able to duplicate its biomass. The biomass of a cell for the most part, is composed of proteins, lipids and nucleotides that are synthesized from metabolic precursors[2]. Amino acids are the monomers of proteins, acetyl-CoA is a precursor of lipids, and purines and pyrimidines serve as the backbone of nucleotides. Like most rapidly proliferating cells, cancer cells require a steady supply of these building blocks to support their continuous growth. A fundamental principle of cancer development is the increased dependence and uptake of extracellular nutrients. Many oncogenic mutations increase the expression of genes encoding cell surface transporters for amino acids, glucose, monocarboxylates, fatty acids and lipoproteins. In order to get access to these nutrients, cells have to rely on the blood supply. Unlike normal tissues, blood vessels in the tumors are dilated, leaky, and torturous compromising nutrient delivery to tumor cells[3, 4]. In addition, most solid tumors have buildup of fibrotic tissue referred to as desmoplasia, which leads to high interstitial tumor pressure further compromising perfusion. How tumor cells acquire and maintain sufficient levels of nutrients under these conditions remain poorly characterized. Understanding how oncogenic mutations rewire metabolism could identify novel, effective therapeutic strategies to inhibit tumor growth by directly targeting their metabolic vulnerabilities. Targeting these vulnerabilities may be sufficient to restore sensitivity in tumors that have developed resistance to standard of care therapies, many of which target metabolism. It has been well established that

tumor cells survive in vascularly compromised environments recycling intracellular components to get access to nutrients, but recent studies have identified tumor growth also depends on the ability to scavenge nutrients directly from the tumor microenvironment (TME)[5].

A) Recycling cell-intrinsic nutrients via autophagy supports tumor cell survival.

Autophagy is a catabolic process by which cells recycle their own components after sequestering them in double-membrane-bound vesicles that are ultimately degraded upon fusion with the lysosomes and release of the digested intracellular nutrients in the cytoplasm[6]. Autophagy is necessary to maintain a balanced redox state, prevent buildup of cellular waste, maintain organelle function, and to provide access to substrates upon nutrient limitation. The role of autophagy in tumorigenesis remains highly context dependent[7]. Cumulative studies have demonstrated that autophagy contributes to tumor suppression during the early stages of tumorigenesis while promoting growth as tumors progress. Tumor suppressive roles of autophagy are attributed to its ability to reduce ROS and pro-growth inflammatory responses. Autophagy is upregulated in nutrient-deprived regions of advanced solid tumors[8, 9]. Many studies have demonstrated that autophagy allows tumor cells to survive nutrient deprivation[8, 9]. Autophagy is tightly regulated by both nutrient and energy sensing kinases, mechanistic target of rapamycin complex 1 (mTORC1) and AMP-activated protein kinase (AMPK)[5]. Under nutrient rich conditions, mTORC1 inhibits autophagosome formation by suppressing ULK1 kinase activity[10]. When the ATP: AMP ratio falls, AMPK is activated promoting autophagy by both directly activating ULK1

and indirectly by inhibiting mTORC1 through the tuberous sclerosis complex 2 (TSC2) and Raptor proteins[11].

While blocking autophagy often reduces both tumor volume and the number of viable, proliferating cells, it is impossible for autophagy to fuel cell-autonomous growth. When a cell reallocates its own resources through recycling, there is no opportunity for growth; autophagic cells eventually face atrophy (Fig. 1). It is conceivable autophagy is necessary for maximal growth of the macroscopic tumor because it promotes cell survival; these viable cells can proliferate only if they are able to acquire extrinsic nutrients or macromolecules from the TME. It is important to keep in mind that nutrients generated by non-cell autonomous autophagy thus performed by supporting cells in the TME or cells in normal tissues may support tumor cell growth and proliferation because the tumor cells are receiving cell-extrinsic nutrients[12-14].

B) Acquiring cell-extrinsic nutrients via scavenging supports tumor cell growth

By definition, scavengers search for and collect items that can be re-purposed into useful material. In the context of tumor metabolism, we define scavenging as removing macromolecules synthesized by other cells from the TME and breaking them down into components that can be used for ATP production and/or anabolism. All scavenging mechanisms rely on successful completion of four distinct steps: uptake, trafficking to the lysosome, lysosomal proteolysis, and export of the monomeric amino acids to the cytosol (Fig. 2). The building blocks that make up these scavenged

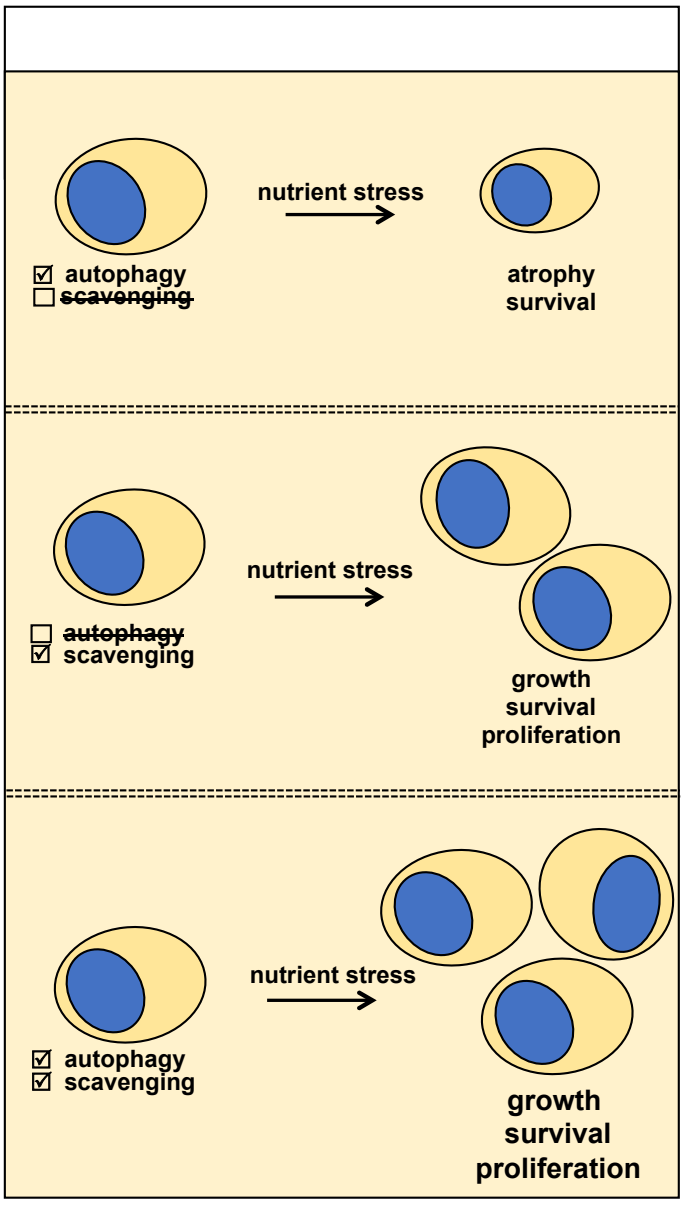

Fig. 1: Contributions of cell autonomous autophagy vs. scavenging to tumor survival and proliferation. In nutrient-limiting conditions, recycling intracellular components via cell autonomous autophagy fuels survival, but cannot support growth, as intracellular recycling leads to atrophy. Because scavenging provides access to extracellular macromolecules, it can support both survival and proliferation. Tumor cells that acquire nutrients via both strategies may exhibit the greatest proliferative advantage. *This model is experimentally validated in Chapter 1.*

molecules that are released after lysosomal degradation can be used for biosynthesis or ATP generation. Several scavenging pathways have been identified to support cancer cell proliferation in low-nutrient environments include: scavenging of extracellular matrix proteins via integrins, receptor-mediated albumin uptake and catabolism, the engulfment and degradation of entire live cells via entosis and macropinocytic consumption of multiple components of the tumor microenvironment (Fig. 2) and are reviewed in depth in[5] but briefly summarized below.

Selective scavenging- receptor mediated endocytosis of proteins

The TME contains variety of extracellular matrix (ECM) proteins including collagen, laminin and fibronectin produced by supporting fibroblasts[5]. Integrins, heterodimeric cell surface receptors link ECM components to the cytoskeleton[15]. Recent reports suggest a novel, pro-growth role for integrins: fueling anabolism by mediating ECM scavenging in both nutrient deprived normal and transformed cells. α5β1 integrin-bound fibronectin is endocytosed and degraded in the lysosome of ovarian cancer cells likely supplying amino acids[16]. Given that ECM proteins are heavily glycosylated, sugars may also be liberated by ECM scavenging[17]. Many other integrin scavenged ECM proteins are degraded in the lysosomes suggesting additional opportunities for retrieving amino acids and sugars[18, 19]. AMPK activation increases integrin-mediated ECM scavenging and promotes lysosomal degradation of ligand-bound integrin coupling scavenging to energy deprivation[16, 20-22]. Importantly, integrin receptors are over-expressed in many cancer classes and correlate with poor prognosis[23, 24]. Whether ECM scavenging

supports anabolism in these cancer classes remain to be identified. Albumin, produced primarily by the liver, is the most abundant plasma protein[25]. Consistent with the idea that the main function of albumin is as a carrier molecule and not a fuel source, albumin is generally recycled after its receptor-mediated endocytosis[26]. The intracellular neonatal Fc receptor (FcRn) inhibits lysosomal degradation of albumin by binding with high affinity to albumin in acidic endosomes and promoting its recycling back to the extracellular space[27]. Many cancer cells have reduced FcRn expression, a state that is favorable for receptor-mediated albumin scavenging. Forced over-expression of FcRn in prostate cancer cells is sufficient to prevent albumin scavenging, reduce intracellular glutamate levels and slow xenograft growth[28]. Conversely, knockdown of endogenous FcRn in breast cancer cells increases intracellular glutamate levels and dramatically accelerates tumor growth[28]. Importantly, albumin has up to seven fatty acid-binding sites and thus may provide cancer cells with fatty acids as well as amino acids when digested[29]. In summary, these selective protein scavenging strategies are likely employed by various cancer classes to support biosynthesis and growth.

Selective scavenging in bulk- Cannibalism and murder via entosis

Cancer cells engulf and digest their living neighbors within large endolysosomes through a process termed entosis[5]. Therefore, entosis requires both autophagy proteins like microtubule-associated protein 1A/1B-light chain 3 (LC3) and lysosome-mediated cell digestion[30]. During entosis, RHOA and RHO-associated protein kinase (ROCK) activation in the “loser cell” that is encapsulated, promotes myosin-dependent invasion

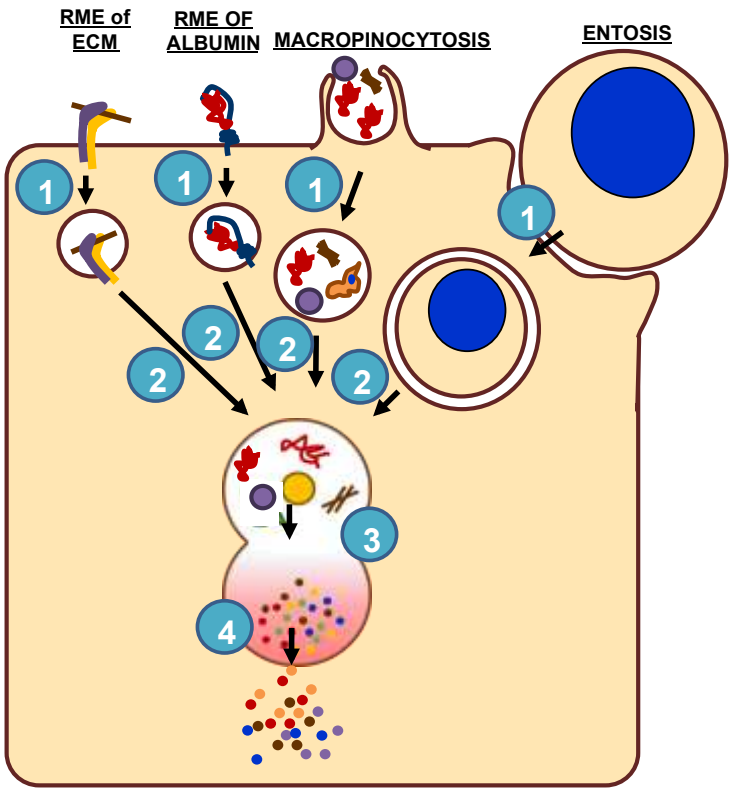

Fig. 2: Cancer cells successfully utilize multiple, parallel scavenging strategies. Receptor mediated scavenging of albumin and extracellular proteins, live cell cannibalism by entosis and protein scavenging by macropinocytosis are strategies employed by cancers to overcome nutrient limitation. Successful scavenging requires four distinct steps: (1) uptake of macromolecules, (2) trafficking and fusion of endocytic intermediates with lysosomes, (3) catabolism of macromolecules in lysosomes and (4) release of the liberated nutrients into the cytosol. Each of these steps is regulated by multiple signaling inputs. ECM, extracellular matrix; RME, receptor-mediated endocytosis.

into the winner cell. Therefore, entosis relies on biophysical forces produced by the invading cell rather than relying on signals from the host cell. The most energetically compromised cells in the population may be marked as loser cells since within a population of starved cells, AMPK activity is greatest within loser cells and is required for their uptake into winner cells[31]. This process may have arisen as a cell suicide pathway; 'loser' cells are likely the most energetically compromised and sacrifice themselves by serving as the fuel source necessary to support the growth and proliferation of winner cells that are not as seriously compromised. Though entosis supports proliferation of winner cells *in vitro*, determining the extent to which entosis contributes to cancer cell anabolism and tumor heterogeneity in vivo will require the identification of proteins that selectively control this process, rendering the complete molecular dissection of this process a high priority in the field.

Power of non-selective bulk scavenging- cancer's big bite via macropinocytosis

Macropinocytosis is a non-selective form of endocytosis through which cells assimilate both extracellular fluid and macromolecules by generating large, uncoated endocytic vesicles (macropinosomes) that range in diameter from 0.2 to 5.0 μm (FIG. 3)[32]. Macropinocytosis has been extensively studied in *Dictyostelium discoideum* and in mammalian cells including macrophages, dendritic cells, growth factor-stimulated fibroblasts and A-431 carcinoma cells in a variety of different contexts, including viral entry, antigen processing, and metabolism. Unlike other forms of endocytosis, macropinocytosis is not dependent on the recruitment of specific receptors, cargos or

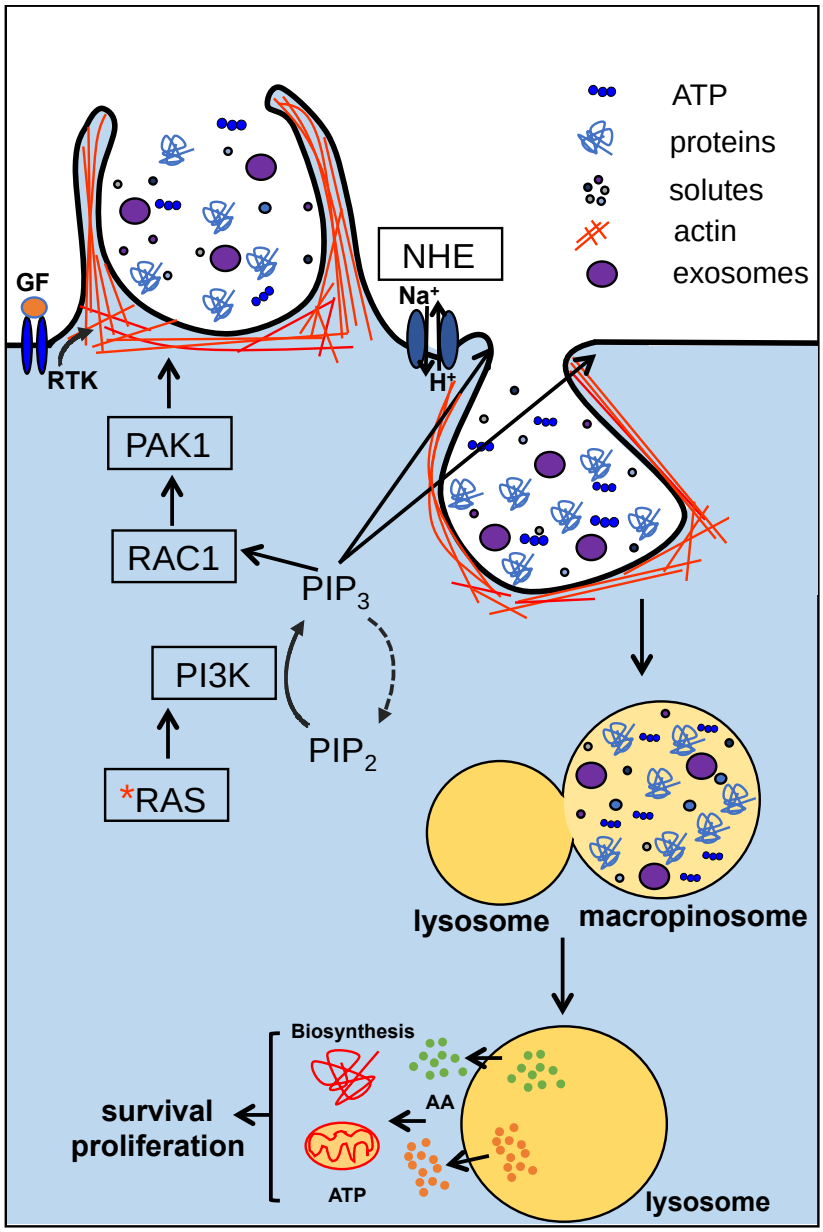

Fig. 3: Macropinocytosis allows cancer cells to proliferate in nutrient-limiting conditions. RAS and PI3K orchestrate actin-driven membrane ruffling and macropinosome formation. Growth factor signals or oncogenic mutations that constitutively activate the Ras signaling pathways trigger constitutive macropinocytosis. Macropinocytosis allows non-selective uptake of, proteins, solutes, exosomes and extracellular fluid. Lysosomal catabolism of the macromolecules present in macropinosomes provides anabolic substrates. Amino acid depletion leads to the inactivation of mTORC1, which enhances lysosomal catabolism of macropinocytosed proteins. *Findings from this dissertation work have led to advances in this model; these advances are depicted in the discussion section as Fig. 1.*

adaptor proteins[32, 33]. The functional relevance of macropinocytosis during tumor progression has only recently been identified. Consistent with macropinocytosis being non-selective, it can provide tumor cells with access to a plethora of fuel present in the TME including, but not limited to albumin, ECM proteins, and exosomes[5]. The anabolic value of macropinocytosis for cells in poorly perfused tumors is likely high, making it vital to understand the oncogenic signals that regulate macropinocytosis, and the pervasiveness as well as the true contributions of macropinocytosis to cancer anabolism will be reviewed in more depth below and will be the focus of this dissertation work.

II. Oncogene driven macropinocytosis supports cancer cell anabolism

Multiple oncogenic signals trigger macropinocytosis

RAS, a GTP binding protein transduces signals from the cell surface mediated by growth factors and G-proteins to promote cell growth, differentiation, migration, cytoskeletal rearrangements as well as many other cellular processes[34]. The three human RAS genes inclduing Kirsten rat sarcoma viral oncogene homolog (*KRAS*), neuroblastoma RAS viral (v-ras) oncogene homolog (*NRAS*) and Harvey rat sarcoma viral oncogene homolog (*HRAS*)] encode RAS proteins[35]. Activating mutations in these genes lock RAS in an constitutively active state. These mutations in K-RAS, N-RAS and H-RAS genes in total occur approximately in 30% of all human cancers[36]. RAS activation is sufficient to induce macropinosome formation because it activates the small GTPases RAC1, and CDC42, which stimulate membrane ruffles by promoting actin polymerization and the class 1 PI3K which generates a signature lipid PIP_3 necessary

for macropinosome closure (FIG. 3)[32, 37, 38]. How RAC1 and CDC42 are recruited to specific sites to induce macropinosome formation remain unclear. Agents that disrupt actin polymerization downstream from RAC activation block macropinosome formation[5]. Amiloride is a compound best known for its ability to inhibit channels formed by the Epithelial Sodium Channel (ENaC)/Degenerin (Deg) family of proteins as well as sodium hydrogen ion exchangers (NHE)[39]. RAC inactivation is also the mechanism by which the amiloride blocks macropinocytosis[40]. By decreasing acidification at the plasma membrane, amiloride blocks the plasma membrane recruitment and activation of Rac1 and Cdc42 GTPases preventing macropinosome formation without affecting the fate of other endocytic compartments[41]. RAC1 and Cdc42 recruitment to the plasma membrane is necessary for their interaction with their effector proteins required for promoting actin remodeling. Though amiloride has been used as a NHE inhibitor, NHE is not its primary target. Therefore, more specific NHE inhibitors were derived including 5-(*N*-ethyl-*N*-isopropyl) amiloride (EIPA) which inhibits multiple isoforms of NHE and cariporide a NHE1 specific inhibitor[5, 32]. Which NHE isoforms are necessary for macropinocytosis remain to be identified. In fact, sensitivity to amilioride class of compounds is a defining feature of macropinocytosis.

Phosphoinositides are produced by the phosphorylation of phospholipid phosphatidylinositol (PI) on the 3, 4, and 5 positions of its inositol ring[42]. Spatiotemporal generation of various phosphoinositides is regulated by the heterodimeric PI3K family of lipid kinases that are necessary for macropinosome formation[43]. Class I PI3 kinases phosphorylate $PI(4,5)P_2$ converting it to $PI(3,4,5)P_3$ (PIP_3). Both plasma membrane

remodeling and macropinosome closure require PIP_3 in most cell types reported[43]. Whether activating mutations in the PI3 kinase pathway are sufficient to induce macropinocytosis in tumor cells was, at the time my thesis was initiated, unknown. Importantly, hyperactivation of the PI3K pathway is one of the most commonly occurring events in human cancers making it crucial to identify if these cancer classes perform macropinocytosis[44].

Contributions of RAS driven macropinocytosis to tumor anabolism and growth

A) Macropinocytosis supports protein scavenging in RAS driven cancers

Initially demonstrated in oncogenic KRAS-driven models of pancreatic cancer, macropinocytosis has also been documented in urinary bladder, colon and lung cancer cells with activating mutations in *HRAS*, *NRAS* or *KRAS*[45-49]. The functional significance of macropinocytosis in tumor anabolism has been best characterized in pancreatic ductal adenocarcinomas (PDAC), a lethal form of cancer characterized by hyperactivated KRAS signaling, profound desmoplasia, poor perfusion and increased hypoxia[45, 47, 50, 51]. Macropinocytosis is observed in human PDAC patient tumor cells as well as murine PDAC xenograft and autochthonous tumor models[45-47]. Metabolic analysis from human PDAC tumor samples suggests PDAC cells are deprived of both glutamine and glucose despite their ability to sustain rapid cell growth[47]. Glutamine-addicted, *KRAS*-transformed PDAC cells continue to proliferate despite glutamine, leucine or essential amino acids deprivation by catabolizing macropinocytosed albumin into amino acids, pyruvate, lactate and tricarboxylic acid (TCA) cycle intermediates[45-47]. Recent studies have also shown scavenged exogenous proteins

contribute to the amino pools of PDAC tumors *in vivo*[46]. These cumulative findings have identified a pivotal role for macropinocytosis in contributing to cancer cell biomass and growth.

B) Macropinocytosis supports PDAC tumor growth

Macropinocytosis inhibition with EIPA slowed the growth of macropinocytic, *KRAS*^{G12D} harboring tumor xenograft but not non-macropinocytic, *KRAS*-wild-type pancreatic tumor xenografts, suggesting that macropinocytosis promotes tumor growth in vivo[45]. However, EIPA was delivered for only 1 week and the KRAS-negative xenografts are slow-growing and thus that EIPA is selectively toxic to macropinocytic cells remains in doubt given that altering pH will have broad effects on tumor biology and growth. Further research is required to assess whether macropinocytosis inhibitors could benefit human patients harboring RAS mutant tumors. Use of genetically engineered mouse models with deletions in essential autophagy genes has helped identify pivotal role autophagy plays in cancer progression, initiation and drug resistance[7]. Tools to selectively inhibit macropinocytosis and identification of signals that regulate macropinocytosis are necessary for understanding the role macropinocytosis plays in tumorigenesis.

C) Tumor microenvironment determines functional implications of macropinocytosis

The extent to which macropinocytosis can drive tumor growth depends on the quantity and quality of the material that can be scavenged. Leaky tumor vasculature and suboptimal lymphatic drainage leads to high albumin levels in the tumor interstitium

providing a potential source of amino acids for macropinocytic tumor cells[52]. Because it is physiologically relevant, albumin is the cargo that has been provided in virtually all in vitro studies evaluating the contribution of macropinocytosis to tumor anabolism. However, as macropinocytosis is a non-selective uptake route, many components of the TME are likely to be engulfed in macropinosomes. ECM proteins can also be scavenged via macropinocytosis[46, 53]. Scavenging multiple different proteins would afford a more balanced ratio of amino acids than solely consuming albumin. Exosomes, approximately 100 nm vesicles released into the TME by both normal and transformed cells, are also consumed via both macropinocytosis dependent and independent pathways[54-57]. Exosomes contain RNA, proteins, and metabolic intermediates and could supply multiple biosynthetic pathways. Extracellular ATP levels can also be much higher in tumors than in normal tissues. In a non-small-cell lung carcinoma (NSCLC) xenograft tumor model, with the use of a non-hydrolyzable fluorescent form of ATP it was identified that ATP is internalized by macropinocytosis[58]. Uptake of extracellular ATP is known to induce resistance to various chemotherapeutic drugs in cancer cells and may promote survival of hypoxic or glucose deprived tumor cells. However, all TME components identified thus far can be taken up by both macropinocytic independent and dependent mechanisms. Therefore, identification of fuel sources that are abundant in the TME of many different tumor classes and are selectively taken up via macropinocytosis is necessary to determine the extent to which macropinocytosis supports anabolism.

III. Significance and organization of chapters

As summarized above macropinocytosis, an evolutionarily conserved feeding mechanism can also fuel starving cancer cells. Oncogene driven macropinocytosis has received attention in the recent years in RAS driven cancers. This dissertation addresses many open questions that remain in the macropinocytosis and tumor metabolism field summarized in the box below.

Chapter 2 and 3: Is macropinocytosis a RAS associated phenotype?
Hypothesis: Macropinosome formation will be supported in cancers with elevated levels of the lipid $PIP_{3.}$

Chapter 2 and 3: Can stress signals coordinate macropinosome formation?
Hypothesis: Nutrient stress promotes macropinocytosis via AMPK activation.

Chapter 2: Are there physiologic components in the tumor microenvironment that can be selectively scavenged via macropinocytosis?
Hypothesis: Necrotic cells prevalent in most nutrient deprived solid tumors can be scavenged via macropinocytosis.

Chapter 3: Can macropinocytosis confer therapeutic resistance?
Hypothesis: Acquiring cell extrinsic nutrients can allow cells to bypass anabolic therapies that target biosynthesis and nutrient import.

Box 1: Open questions in the macropinocytosis and tumor metabolism field addressed in this dissertation work.

In **Chapter 2**, we identify that *macropinocytosis is not just a KRAS-driven phenotype.* Prostate tumors, which frequently contain mutations in PTEN, a PI3K antagonist were demonstrated to be macropinocytic in vitro and in vivo and *blocking macropinocytosis limits prostate tumor growth*, even causing some regressions. In addition, we identified AMPK activity as a general requirement for macropinosome formation suggesting that nutrient stress promotes not just autophagy but also macropinocytosis. However,

macropinocytosis but not autophagy is necessary for AMPK driven proliferation under nutrient stress. Albumin, the primary anabolic cargo used to study macropinocytosis is taken up independently of macropinocytosis in prostate cancer cells. We coined the term *"necrocytosis"* to describe the selective uptake of necrotic cell debris via macropinocytosis. *Necrocytosis supports protein synthesis* in both nutrient replete and limited states as well as helps *starved prostate cancer cells maintain lipid droplets*.

In **Chapter 3**, we demonstrate that breast cancers with mutations in KRAS or the PI3K pathway can also use necrocytosis to fuel growth when nutrients are limiting unlike albumin. Necrocytosis *provides not just amino acids but also sugars, lipids and nucleotides* thus supporting multiple biosynthetic pathways*.* Consistent with the idea scavenging can override a block in biosynthesis; we provide the first demonstration that *macropinocytosis confers resistance to various therapies targeting metabolism*. Thus, therapeutic value of standard of care therapies in lethal and difficult to treat, macropinocytic cancer classes such as pancreas, prostate, and TNBC are likely to *benefit from macropinocytosis inhibitors, particularly when used in combination with cytotoxic and metabolic therapies.*

The **conclusion in chapter 4** will summarize the most impactful findings from this dissertation work, discuss the strategies to successfully target scavenging, and outline future directions and remaining knowledge gaps in the tumor macropinocytosis field.

References

1. Selwan, E.M., Finicle, B.T., Kim, S.M. & Edinger, A.L. Attacking the supply wagons to starve cancer cells to death. *FEBS Lett* **590**, 885-907 (2016).
2. Vazquez, A. *et al.* Cancer metabolism at a glance. *J Cell Sci* **129**, 3367-3373 (2016).
3. Forster, J.C., Harriss-Phillips, W.M., Douglass, M.J. & Bezak, E. A review of the development of tumor vasculature and its effects on the tumor microenvironment. *Hypoxia (Auckl)* **5**, 21-32 (2017).
4. Pandol, S., Edderkaoui, M., Gukovsky, I., Lugea, A. & Gukovskaya, A. Desmoplasia of pancreatic ductal adenocarcinoma. *Clin Gastroenterol Hepatol* **7**, S44-47 (2009).
5. Finicle, B.T., Jayashankar, V. & Edinger, A.L. Nutrient scavenging in cancer. *Nat Rev Cancer* **18**, 619-633 (2018).
6. Xie, Z., Klinosky D.J. Autophagosome formation: core machineray and adpatations. *Nature Cell Biology* **9,** 1102-1109 (2007).
7. White, E. The role for autophagy in cancer. *J Clin Invest* **125**, 42-46 (2015).
8. Degenhardt, K. *et al.* Autophagy promotes tumor cell survival and restricts necrosis, inflammation, and tumorigenesis. *Cancer Cell* **10**, 51-64 (2006).
9. Amaravadi, R., Kimmelman A.C., White, E. Recent insights into autophagy in cancer. *GENES & DEVELOPMENT* **30,** 1913-1930 (2016).
10. Jung, C.H., Ro, S.H., Cao, J., Otto, N.M. & Kim, D.H. mTOR regulation of autophagy. *FEBS Lett* **584**, 1287-1295 (2010).
11. Kim, J., Kundu, M., Viollet, B. & Guan, K.L. AMPK and mTOR regulate autophagy through direct phosphorylation of Ulk1. *Nat Cell Biol* **13**, 132-141 (2011).
12. Sousa, C.M. *et al.* Pancreatic stellate cells support tumour metabolism through autophagic alanine secretion. *Nature* **536**, 479-483 (2016).
13. Katheder, N.S. *et al.* Microenvironmental autophagy promotes tumour growth. *Nature* **541**, 417-420 (2017).
14. Yang, A. *et al.* Autophagy Sustains Pancreatic Cancer Growth through Both Cell-Autonomous and Nonautonomous Mechanisms. *Cancer Discov* **8**, 276-287 (2018).
15. Seguin, L., Desgrosellier, J.S., Weis, S.M. & Cheresh, D.A. Integrins and cancer: regulators of cancer stemness, metastasis, and drug resistance. *Trends Cell Biol* **25**, 234-240 (2015).
16. Rainero, E. *et al.* Ligand-Occupied Integrin Internalization Links Nutrient Signaling to Invasive Migration. *Cell Rep* **10**, 398-413 (2015).
17. Roth, Z., Yehezkel, G. & Khalaila, I. Identification and Quantification of Protein Glycosylation. *International Journal of Carbohydrate Chemistry* **2012**, 1-10 (2012).
18. Memmo, LM., McKeown-Longo, P. The αvβ5 integrin functions as an endocytic receptor for vitronectin. *Journal of cell science* **111**, 425-433 (1998).
19. Wienke, D., MacFadyen, J.R. & Isacke, C.M. Identification and characterization of the endocytic transmembrane glycoprotein Endo180 as a novel collagen receptor. *Mol Biol Cell* **14**, 3592-3604 (2003).

20. Muranen, T. *et al.* Starved epithelial cells uptake extracellular matrix for survival. *Nat Commun* **8**, 13989 (2017).
21. Ross, E. *et al.* AMP-Activated Protein Kinase Regulates the Cell Surface Proteome and Integrin Membrane Traffic. *PLoS One* **10**, e0128013 (2015).
22. Steinberg, F., Heesom, K.J., Bass, M.D. & Cullen, P.J. SNX17 protects integrins from degradation by sorting between lysosomal and recycling pathways. *J Cell Biol* **197**, 219-230 (2012).
23. Bianconi, D., Unseld, M. & Prager, G.W. Integrins in the Spotlight of Cancer. *Int J Mol Sci* **17** (2016).
24. Desgrosellier, J.S. & Cheresh, D.A. Integrins in cancer: biological implications and therapeutic opportunities. *Nat Rev Cancer* **10**, 9-22 (2010).
25. Merlot, A.M., Kalinowski, D.S. & Richardson, D.R. Unraveling the mysteries of serum albumin-more than just a serum protein. *Front Physiol* **5**, 299 (2014).
26. Roopenian, D.C. & Akilesh, S. FcRn: the neonatal Fc receptor comes of age. *Nat Rev Immunol* **7**, 715-725 (2007).
27. Sand, K.M. *et al.* Unraveling the Interaction between FcRn and Albumin: Opportunities for Design of Albumin-Based Therapeutics. *Front Immunol* **5**, 682 (2014).
28. Dalloneau E, Baroukh N, Mavridis K, Maillet A, Gueugnon F, Courty Y, Petit A, Kryza T, M Del Rio, Guyetant S, Castaneda DC, Dhommee C, Arnoult C. Downregulation of the neonatal Fc receptor expression in non-small cell lung cancer tissue is associated with a poor prognosis. *Oncotarget* **7**, 54415–54429 (2016).
29. Bern, M., Sand, K.M., Nilsen, J., Sandlie, I. & Andersen, J.T. The role of albumin receptors in regulation of albumin homeostasis: Implications for drug delivery. *J Control Release* **211**, 144-162 (2015).
30. Florey, O. & Overholtzer, M. Macropinocytosis and autophagy crosstalk in nutrient scavenging. *Philos Trans R Soc Lond B Biol Sci* **374**, 20180154 (2019).
31. Hamann, J.C. *et al.* Entosis Is Induced by Glucose Starvation. *Cell Rep* **20**, 201-210 (2017).
32. Kerr, M.C. & Teasdale, R.D. Defining macropinocytosis. *Traffic* **10**, 364-371 (2009).
33. Watts, C. & Swanson, J.A. Macropinocytosis. *Trends in cell biology* **5**,424-428 (1995).
34. Fernandez-Medarde, A. & Santos, E. Ras in cancer and developmental diseases. *Genes Cancer* **2**, 344-358 (2011).
35. Hobbs, G.A., Der, C.J. & Rossman, K.L. RAS isoforms and mutations in cancer at a glance. *J Cell Sci* **129**, 1287-1292 (2016).
36. Kodaz H, Eskisehir Hastanesi A, Onkoloji Klinigi T. Frequency of RAS Mutations (KRAS, NRAS, HRAS) in Human Solid Cancer. *Eur J Med Oncol* **1**, 1–7 (2000).
37. D. Bar-Sagi, J.R. Feramisco Induction of membrane ruffling and fluid-phase pinocytosis in quiescent fibroblasts by ras proteins Science **233**, 1061-1068 (1986).
38. Buckley, C.M. & King, J.S. Drinking problems: mechanisms of macropinosome formation and maturation. *FEBS J* **284**, 3778-3790 (2017).

39. Qadri, Y.J., Song, Y., Fuller, C.M. & Benos, D.J. Amiloride docking to acid-sensing ion channel-1. *J Biol Chem* **285**, 9627-9635 (2010).
40. Koivusalo, M. *et al.* Amiloride inhibits macropinocytosis by lowering submembranous pH and preventing Rac1 and Cdc42 signaling. *J Cell Biol* **188**, 547-563 (2010).
41. West, M.A. Distinct endocytotic pathways in epidermal growth factor-stimulated human carcinoma A431 cells [published erratum appears in J Cell Biol 1990 Mar;110(3):859]. *The Journal of Cell Biology* **109**, 2731-2739 (1989).
42. Falkenburger, B.H., Jensen, J.B., Dickson, E.J., Suh, B.C. & Hille, B. Phosphoinositides: lipid regulators of membrane proteins. *J Physiol* **588**, 3179-3185 (2010).
43. Egami, Y., Taguchi, T., Maekawa, M., Arai, H. & Araki, N. Small GTPases and phosphoinositides in the regulatory mechanisms of macropinosome formation and maturation. *Front Physiol* **5**, 374 (2014).
44. Yuan, T.L. & Cantley, L.C. PI3K pathway alterations in cancer: variations on a theme. *Oncogene* **27**, 5497-5510 (2008).
45. Commisso, C. *et al.* Macropinocytosis of protein is an amino acid supply route in Ras-transformed cells. *Nature* **497**, 633-637 (2013).
46. Davidson, S.M. *et al.* Direct evidence for cancer-cell-autonomous extracellular protein catabolism in pancreatic tumors. *Nat Med* **23**, 235-241 (2017).
47. Kamphorst, J.J. *et al.* Human pancreatic cancer tumors are nutrient poor and tumor cells actively scavenge extracellular protein. *Cancer Res* **75**, 544-553 (2015).
48. Redelman-Sidi, G. *et al.* The Canonical Wnt Pathway Drives Macropinocytosis in Cancer. *Cancer Res* **78**, 4658-4670 (2018).
49. Tajiri, H. *et al.* Targeting Ras-Driven Cancer Cell Survival and Invasion through Selective Inhibition of DOCK1. *Cell Rep* **19**, 969-980 (2017).
50. Cannon A, Thompson C, Hall BR, Jain M, Kumar S, Batra SK. Desmoplasia in pancreatic ductal adenocarcinoma: insight into pathological function and therapeutic potential. *Genes Cancer* **9**, 78–86 (2018).
51. Koong, A. C. et al. Pancreatic tumors show high levels of hypoxia. Int. J. Radiat. *Oncol. Biol. Phys* **48**, 919–922 (2000).
52. G. Stehle, H. Sinn, A. Wunder, H.H. Schrenk, J.C. Stewart, G. Hartung, W. Maier-Borst, D.L. Heene Plasma protein (albumin) catabolism by the tumor itself—implications for tumor metabolism and the genesis of cachexia. *Crit. Rev. Oncol* **26**, 77-100 (1997).
53. Olivares, O. *et al.* Collagen-derived proline promotes pancreatic ductal adenocarcinoma cell survival under nutrient limited conditions. *Nat Commun* **8**, 16031 (2017).
54. Thery, C., Zitvogel, L. & Amigorena, S. Exosomes: composition, biogenesis and function. *Nat Rev Immunol* **2**, 569-579 (2002).
55. Zhao, H. *et al.* Tumor microenvironment derived exosomes pleiotropically modulate cancer cell metabolism. *Elife* **5**, e10250 (2016).
56. Nakase, I., Kobayashi, N.B., Takatani-Nakase, T. & Yoshida, T. Active macropinocytosis induction by stimulation of epidermal growth factor receptor

and oncogenic Ras expression potentiates cellular uptake efficacy of exosomes. *Sci Rep* **5**, 10300 (2015).
57. Kamerkar, S. *et al.* Exosomes facilitate therapeutic targeting of oncogenic KRAS in pancreatic cancer. *Nature* **546**, 498-503 (2017).
58. Qian, Y., Wang, X., Li, Y., Cao, Y. & Chen, X. Extracellular ATP a New Player in Cancer Metabolism: NSCLC Cells Internalize ATP In Vitro and In Vivo Using Multiple Endocytic Mechanisms. *Mol Cancer Res* **14**, 1087-1096 (2016).

CHAPTER 2

PTEN deficiency and AMPK activation promote nutrient scavenging and anabolism in prostate cancer cells

Contributions:

This chapter is derived from our manuscript that is published *Cancer Discovery.* This work was a result of a close collaboration between many authors with Seong Kim, Tricia Nguyen and Archna Ravi as the leading contributors. I conducted majority of the experiments that were necessary during the peer review process. Main figures: Fig. 2C-H; Fig 3. A-B; Fig 4D. . All statistical analysis. Supplemental Figures: Fig. 2B and 2D-F; Fig. 3B and 3D-E; Fig. 4A-D and 4F-G; Fig. 8A-B . All statistical analysis.

Detailed declaration of contributions:

Figure 2 and related supplementary Figures:

I was able to demonstrate that AMPK is necessary for proliferation of macropinocytic PTEN deficient MEFs which provides an example of pro-tumorgenic role for AMPK rather than it's perception as a tumor suppressor. Importantly, AMPK driven macropinocytosis but not autophagy was necessary for PTEN deficient MEFs to proliferate in low nutrients suggesting scavenging nutrients via macropinocytosis provides a greater anabolic contribution than recycling nutrients via autophagy. In addition, inhibiting macropinocytosis did not upregulate autophagy or vice-versa.

Figure 3 and related supplementary Figures:

RAS is a potent driver of macropinocytosis. I was able to identify AMPK is necessary for RAS driven macropinocytosis not just PI3K pathway driven macropinocytosis. Therefore, targeting AMPK may be a beneficial strategy for cancers driven by the PI3K pathway or RAS.

Figure 4 and related supplementary Figures:

PTEN-deficient prostate cancers performed robust macropinocytosis. By using genetic tools, I was able to demonstrate both PTEN loss, AMPK activity as well as RAC1 activity was necessary for macropinocytosis.

Figure 5 and related supplementary Figures:

Necrotic cells are selectively taken by through macropinocytosis. I was able to identify that necrotic cells are localized in the same compartments as a well-established marker for macropinosomes suggesting necrotic cell debris is taken up by macropinosomes.

I also conducted all the statistical analysis.

PTEN deficiency and AMPK activation promote nutrient scavenging and anabolism in prostate cancer cells

Seong M. Kim[1,*], Tricia T. Nguyen[1,*], Archna Ravi[1,*], Peter Kubiniok[2], Brendan T. Finicle[1], Vaishali Jayashankar[1], Leonel Malacrida[3,4], Jue Hou[5], Jane Robertson[1], Dong Gao[6], Jonathan Chernoff[7], Michelle A. Digman[3], Eric O. Potma[5], Bruce J. Tromberg[5], Pierre Thibault[2], and Aimee L. Edinger[1,#]

[1]Department of Developmental and Cell Biology, University of California Irvine, Irvine CA 92697
[2]Department of Chemistry, Université de Montréal, Quebec, Canada H3C 3J7
[3]Laboratory for Fluorescence Dynamics, University of California Irvine, Irvine CA 92697
[4]Departamento de Fisiopatología, Hospital del Clínicas, Facultad de Medicia, Universidad de la República, Montevideo-Uruguay 11600
[5]Laser Microbeam and Medical Program, Beckman Laser Institute and Medical Clinic, University of California, Irvine CA 92697
[6]Key Laboratory of Systems Biology, Institute of Biochemistry and Cell Biology, Shanghai Institutes for Biological Sciences, Chinese Academy of Sciences, Shanghai, 200031, China
[7]Cancer Biology Program, Fox Chase Cancer Center, Philadelphia, PA, 19111

*These authors contributed equally to this work.

Running title: PTEN loss and AMPK promote nutrient scavenging

Keywords: macropinocytosis; prostate cancer; scavenging; AMPK; PTEN; cancer metabolism, necrosis

ABSTRACT

We report that PTEN-deficient prostate cancer cells use macropinocytosis to survive and proliferate under nutrient stress. PTEN loss increased macropinocytosis only in the context of AMPK activation revealing a general requirement for AMPK in macropinocytosis and a novel mechanism by which AMPK promotes survival under stress. In prostate cancer cells, albumin uptake did not require macropinocytosis, but necrotic cell debris proved a specific macropinocytic cargo. Isotopic labeling confirmed that macropinocytosed necrotic cell proteins fueled new protein synthesis in prostate cancer cells. Supplementation with necrotic debris, but not albumin, also maintained lipid stores suggesting that macropinocytosis can supply nutrients other than amino acids. Non-transformed prostatic epithelial cells were not macropinocytic, but patient-derived prostate cancer organoids and xenografts and autochthonous prostate tumors all exhibited constitutive macropinocytosis, and blocking macropinocytosis limited prostate tumor growth. Macropinocytosis of extracellular material by prostate cancer cells is a previously unappreciated tumor-microenvironment interaction that could be targeted therapeutically.

STATEMENT OF SIGNIFICANCE: As PTEN-deficient prostate cancer cells proliferate in low nutrient environments by scavenging necrotic debris and extracellular protein via macropinocytosis, blocking macropinocytosis by inhibiting AMPK, RAC1, or PI3 kinase may have therapeutic value, particularly in necrotic tumors and in combination with therapies that cause nutrient stress.

INTRODUCTION

Cancer cells up-regulate nutrient acquisition pathways to fuel oncogene-driven anabolism and proliferation (1). However, as tumors grow, their abnormal vasculature leads to the development of areas of extracellular nutrient limitation. Nutrient import pathways become substrate-limited and fail to meet nutrient demand, leading to tumor necrosis (2). Macropinocytosis, a process by which cells non-selectively engulf extracellular material via plasma membrane ruffling (3-5), allows cancer cells with activating mutations in RAS to use extracellular proteins such as albumin as fuel when amino acids are limiting (6-9). Downstream of RAS, $PI(3,4,5)P_3$ (PIP_3) and RAC1-GTP are both necessary for macropinosome formation. RAC1 activation induces the actin remodeling and membrane ruffling necessary to form macropinosomes by activating PAK kinases (10, 11). PIP_3 produced by type I PI3Ks is required for macropinosome closure; in some cell types, PIP_3 is also required for membrane ruffling (12, 13). The lipid phosphatase PTEN opposes PI3K pathway signaling by converting PIP_3 to $PI(4,5)P_2$ (14). PTEN is the most frequently deleted tumor suppressor gene in prostate cancer (15, 16); monoallelic PTEN deletion occurs in up to 60% of localized prostate cancers and complete loss of PTEN is commonly associated with increased risk of metastasis and the development of lethal, castration-resistant disease (16, 17). Consistent with the central role of PIP_3 in macropinocytosis, we report that PTEN-deficient prostate cancer cells use macropinocytosis to support anabolism and survival in nutrient-limiting environments. Interestingly, PTEN loss was not sufficient to trigger macropinocytosis in all contexts, revealing a previously unappreciated requirement for AMPK activation to support RAC1 activation and macropinosome formation. Robust

macropinocytosis-independent albumin uptake in prostate cancer cells also led to the discovery that necrotic cell debris is a specific macropinocytic cargo suggesting that macropinocytosis can supply many nutrients, not just amino acids. Taken together, these studies provide critical insights into how nutrient-responsive signaling pathways coordinate the adaptive response to nutrient limitation and suggest a novel mechanism by which the microenvironment impacts prostate tumor growth.

RESULTS

PTEN loss promotes macropinocytosis in fibroblasts under nutrient-limiting conditions. Oncogenic mutations constitutively drive anabolism and limit adaptive metabolic changes under nutrient stress (18). Nevertheless, tumor cells with activating mutations in RAS are paradoxically resistant to amino acid deprivation because they can degrade macropinocytosed proteins in the lysosome to produce amino acids (6-8). PI3K pathway activation is essential for macropinocytosis downstream of RAS (4, 5, 19). To assess whether activating the PI3K pathway would be sufficient to drive macropinocytosis and confer resistance to nutrient stress, uptake of the macropinocytic cargos 70 kD dextran and bovine serum albumin (BSA) was measured in PTEN null and wild type murine embryonic fibroblasts (PTEN KO and WT MEFs, respectively) in the presence or absence of the NHE inhibitor 5-(N-ethyl-N-isopropyl) amiloride (EIPA). The dextran or BSA index (percent of cell area that contains dextran or BSA) was calculated using Image J and established protocols (Supplemental Methods and Supplementary Fig. S2.1A) (20). EIPA inhibits RAC1 activation indirectly by reducing the submembranous pH (21). While EIPA has pleiotropic effects on cells (22), it is

selective for macropinocytosis among endocytic pathways and does not inhibit the clathrin-mediated endocytosis of the EGFR or the transferrin receptor (23, 24). Neither PTEN WT nor PTEN KO MEFs took up dextran or BSA in complete medium (Fig. 2.1A-C). However, incubation in medium containing only 1% the amount of glucose and amino acids present in standard DMEM (1% AA/gluc) dramatically enhanced both dextran and BSA uptake selectively in PTEN KO MEFs. This increased uptake was sensitive to EIPA, the RAC inhibitor EHT1864, the PAK inhibitor FRAX597, and to dominant-negative RAC1 T17N expression (Fig. 2.1A,C,D and Supplementary Fig. S2.1B) consistent with internalization via macropinocytosis. Chemical inhibitors of PI3K and PTEN confirmed that PTEN's catalytic activity suppresses macropinocytosis. Inhibiting PTEN with bpV(pic) was sufficient to stimulate macropinocytosis in PTEN WT MEFs in low-nutrient medium (Fig. 2.1E) but not complete medium (not shown). Conversely, inhibiting Class I PI3K with a combination of the α or β isoform-selective inhibitors BYL719 and AZD8186 prevented macropinocytosis in PTEN KO MEFs in 1% AA/gluc (Fig. 2.1F). Together, these results suggest that PI3K pathway activation by PTEN loss is sufficient to promote macropinosome formation selectively under nutrient-limiting conditions.

When macropinocytic cells are subjected to amino acid limitation, albumin supplementation (2-5%) stimulates proliferation (6-8). A caveat to this approach is that albumin also enters cells through receptor-mediated endocytosis (RME), and supplementation with BSA promotes survival and proliferation even in non-macropinocytic cells, albeit to a lesser degree (7). Similar to published data from

control LSL and KRAS G12D MEFs (7), supplementation with 2% BSA increased proliferation of both PTEN WT and KO MEFs in 1% AA/gluc medium, although macropinocytic PTEN KO MEFs proliferated more (Fig. 2.1G). The value of macropinocytosis was much more apparent in unsupplemented 1% AA/gluc medium as macropinocytic PTEN KO MEFs were able to proliferate while non-macropinocytic PTEN WT MEFs died. Albumin is the principal protein in fetal calf serum (Supplementary Fig. S2.2A). Because BSA uptake by macropinocytosis was much more efficient than uptake by RME (Fig. 2.1A,C), the 0.3% albumin contributed by the serum in the 1% AA/gluc medium was likely sufficient to support survival only in macropinocytic PTEN KO MEFs. Macropinocytic KRAS G12D-expressing MEFs, but not matched non-macropinocytic LSL MEFs, also survived in unsupplemented 1% AA/gluc medium (Supplementary Fig. S2.2B). In both KRAS G12D MEFs and PTEN KO MEFs, this survival advantage was fully reversed by EIPA (Fig. 2.1H and Supplementary Fig. S2.2B,C). Importantly, EIPA was minimally and equally toxic to macropinocytic and non-macropinocytic MEFs in complete medium (Fig. 2.1H and Supplementary Fig. S2.2B). Similar to EIPA, EHT1864 (allosteric RAC inhibitor) and FRAX597 (PAK inhibitor) were selectively toxic to PTEN KO MEFs relying on macropinocytosis for nutrients (Supplementary Fig. S2.2D,E). Furthermore, reconstitution with PTEN blocked macropinocytosis and eliminated the survival advantage of PTEN KO MEFs in low nutrient medium (Fig. 2.1I and Supplementary Fig. S2.2F). Taken together, these results demonstrate that macropinocytosis confers a survival and proliferative advantage on PTEN KO MEFs in low-nutrient medium.

AMPK activation is necessary for macropinocytosis. Unexpectedly, PTEN KO MEFs that proliferated in 1% AA/gluc medium (Fig. 2.1G and 2.2A) died when deprived of only amino acids (Fig. 2.2A and Supplementary Fig. S2.3A). This result suggested that glucose withdrawal stimulated growth. Cells sense and respond to glucose depletion by activating AMPK (25). Strikingly, the allosteric AMPK activator A769662 stimulated robust proliferation in 1% AA medium in PTEN KO MEFs but not in PTEN WT MEFs (Fig. 2.2A). AMPK promotes the macropinocytosis-dependent entry of Ebola and vaccinia viruses (26, 27). Either glucose depletion or A769662 was sufficient to stimulate dextran uptake in PTEN KO but not WT MEFs (Fig. 2.2B and Supplementary Fig. S2.3B). In contrast, amino acid depletion failed to trigger macropinocytosis in PTEN KO MEFs (Fig. 2.2B). These results suggest that PTEN loss is not sufficient to drive macropinocytosis; AMPK activation is also necessary. Consistent with this model, PTEN deletion from MEFs lacking both AMPK catalytic subunit isoforms (28) failed to trigger macropinocytosis in 1% AA/gluc medium (Fig. 2.2C and Supplementary Fig. S2.3C,D). The expression of a dominant-negative AMPK mutant or treatment with the AMPK inhibitor Compound C also blocked macropinocytosis in PTEN KO MEFs in 1% AA/gluc (Supplementary Fig. S2.3E,F). Although glucose deprivation or A769662 was sufficient to stimulate dextran uptake in PTEN KO MEFs in the presence of normal amino acid levels, co-localization of dextran and Lysotracker Red was reduced relative to 1% AA/gluc (Fig. 2.2B). This result is consistent with previous reports that mTORC1 inactivation is necessary for efficient macropinosome-lysosome fusion in MEFs (7, 29). In keeping with its role in macropinocytosis, AMPK was necessary for PTEN null cells to proliferate in 1% AA/gluc medium (Fig. 2.2D). Taken together, these results

demonstrate that AMPK activation is necessary for PTEN-deficient MEFs to form macropinosomes and proliferate under nutrient-limiting conditions.

AMPK activation drives autophagy by activating ULK1 and inactivating mTORC1 (30-32). Autophagy is often necessary for maximal tumor growth (33). To dissect the relative contribution of autophagy and macropinocytosis to AMPK-driven cell proliferation in low nutrients (Fig. 2.2A), dominant-negative PTEN C124S was introduced into MEFs that were either capable of autophagy but deficient in macropinocytosis due to PAK1 deletion or capable of macropinocytosis but deficient in autophagy due to ATG5 deletion. PTEN C124S expression in either PAK1 WT or ATG5 WT MEFs led to macropinocytosis upon AMPK activation with A769662 similar to results in PTEN null MEFs (Fig. 2.2E,F and Supplementary Fig. S2.4A-D). Deletion of PAK1, but not ATG5, eliminated macropinocytosis. Conversely, deletion of ATG5, but not PAK1, blocked autophagy (Supplementary Fig. S2.4E-G). Consistent with their effect on macropinocytosis (Fig. 2.2E), PTEN C124S expression combined with A769662 drove proliferation in PAK1 WT, but not PAK1 KO, MEFs in amino acid deficient medium (Fig. 2.2G). Compensatory up-regulation of autophagy was not observed when macropinocytosis was blocked by PAK1 deletion, however, autophagy was slightly elevated basally in PAK1 KO MEFs relative to PAK1 WT controls (Supplementary Fig. S2.4E and not shown). Intriguingly, A769662 stimulated proliferation in both ATG5 WT and KO MEFs expressing PTEN C124S in low amino acids (Fig. 2.2H). Autophagy-deficient PTEN C124S ATG5 KO MEFs may have proliferated less than autophagy-competent PTEN C124S ATG5 WT MEFs, but

autophagy was not necessary for proliferation in amino acid deficient medium. Taken together, these studies demonstrate that AMPK drives proliferation in nutrient-stressed cells by inducing macropinocytosis. While autophagy may promote proliferation by sparing macropinocytosis-derived nutrients for anabolic processes, cell-autonomous autophagy is not sufficient to support cell division.

How AMPK stimulates macropinosome formation was next investigated. AMPK activates RAC1 in certain contexts (34), and RAC1 activation is required for membrane ruffling during macropinocytosis (4, 5, 19). We measured RAC1-GTP levels and localization using a dual-chain RAC1 Förster resonance energy transfer (FRET) biosensor and fluorescence lifetime imaging microscopy (FLIM) (35). When the biosensor (PAK1 effector domain-YPET fusion) binds CyPet-RAC1-GTP, the resulting FRET quenches the fluorescence lifetime of the donor (CyPET). Detecting FRET by monitoring donor lifetime rather than following the ratio of acceptor:donor fluorescence intensity has the key advantage that measurements are independent of protein concentration, while the phasor approach to fluorescence lifetime data analysis can provide a global view of the RAC1 activation state in an image by transforming the histogram of time delays in each pixel into a phasor (Supplementary Fig. S2.5A). When the AMPK activator A769662 was added to PTEN KO MEFs in complete medium, RAC1-GTP levels increased, particularly in the cell periphery (Fig. 2.2I and Supplementary Fig. S2.5B,C). A769662 also stimulated robust AMPK and RAC1 activation and membrane ruffling in PTEN WT MEFs indicating that PTEN deficiency was not required for RAC1 activation. Macropinosome closure leads to RAC1

inactivation (36). Thus, productive macropinosome formation in PTEN KO MEFs (Fig. 2.1A) may lead to reduced total RAC1-GTP levels relative to PTEN WT MEFs. Confirming the specificity of the assay, RAC1-GTP levels did not increase in the absence of A769662, and adding the RAC inhibitor EHT1864 60 min after A769662 restored donor lifetime to basal levels (Supplementary Fig. S2.5D,E). Using standard ratiometric techniques to monitor the localization and dynamics of RAC1 activation in real time, dynamic waves of RAC1-GTP were seen in the periphery of A769662-stimulated PTEN WT and KO cells; consistent with dextran uptake results, circular macropinosome-like structures bounded by activated RAC1 were observed only in PTEN KO MEFs (Fig. 2.2J and Supplementary Video S2.1-2). Thus, AMPK activation promotes macropinocytosis by increasing RAC1 activation (Fig. 2.2I), but RAC1 activation is not sufficient to trigger macropinosome formation in the presence of PTEN (Fig. 2.2I,K and Supplementary Fig. S2.3B).

Whether AMPK activation was a general requirement for macropinocytosis or selectively required in PTEN-deficient cells was not clear. The LKB1 tumor suppressor is mutated in up to 30% of NSCLC, including tumor cells with activating mutations in KRAS (37). LKB1 is reported to be the major AMPK-activating kinase under metabolic stress (38). It was therefore of interest to determine whether LKB1 and AMPK are required for RAS-driven macropinocytosis. Introduction of KRAS G12D drove macropinocytosis in AMPK WT but not AMPK DKO MEFs (Fig. 2.3A). Consistent with these results, DN-AMPK expression or Compound C blocked dextran uptake in KRAS G12D MEFs (Fig. 2.3B,C). Thus, AMPK activity is also necessary for KRAS-driven

macropinocytosis. In contrast, KRAS G12D expression stimulated equally robust macropinocytosis in LKB1 WT and KO MEFs (Fig. 2.3D) consistent with studies showing that LKB1 loss reduces but does not eliminate AMPK activity. Moreover, the LKB1-deficient, KRAS G12S-expressing NSCLC cell line A549 exhibited a high macropinocytic index that was dramatically reduced by Compound C or DN-AMPK expression (Fig. 2.3E,F). These results suggest that AMPK activation is a general requirement for macropinosome formation.

PTEN-deficient prostate cancer cells exhibit constitutive macropinocytosis. At diagnosis, the majority of prostate tumors exhibit PTEN deficiency or mutation and complete loss of PTEN is closely linked to the castration resistance and metastasis that render prostate cancer a lethal disease (16). Our results in MEFs suggest that macropinocytosis may supply PTEN-deficient prostate cancers with fuel for biosynthesis and growth. For initial *in vitro* studies, human prostate cancer cells with PTEN deletion (PC3, LNCaP) or deficiency (DU145) and mouse prostate cancer epithelial (mPCE) cells derived from a tumor in a *Pten*$^{flox/flox}$*;tp53*$^{flox/flox}$*;PB-Cre4* mouse, an established model for castration-resistant prostate cancer (CRPC), were utilized (18, 39). All of these PTEN-deficient prostate cancer cell lines exhibited robust, EIPA-sensitive dextran uptake in 1% AA/gluc medium (Fig. 2.4A). In contrast, the immortalized but non-transformed PTEN-replete prostate epithelial cell line RWPE-1 did not exhibit macropinocytosis under nutrient deprivation or in the presence of A769662 (Fig. 2.4B). These results suggests that prostatic epithelial cells are not normally macropinocytic and that macropinocytosis is a cancer-associated phenotype that stems from the loss of

PTEN function. In keeping with this model, PTEN reconstitution or the pan-PI3K inhibitor ZSTK474 blocked dextran uptake in prostate cancer cells (Fig. 2.4C,D). As observed in MEFs (Fig. 2.2C, 2.3A-C, and Supplementary Fig. S2.3E-F), AMPK activation was also necessary for macropinocytosis in prostate cancer cells, as Compound C or expression of DN-AMPK blocked macropinocytosis to a similar extent as RAC inhibition (Fig. 2.4C,D and Supplementary Figure S2.6A). Given this requirement for AMPK activation, it was somewhat surprising that prostate cancer cells exhibited equally robust dextran uptake in complete and nutrient-deficient media (Fig. 2.4E,F). Neither nutrient deprivation nor A769662 increased the amount of dextran taken up by prostate cancer cells over 30 min, a time point when steady state was reached (Fig. 2.4F and Supplementary Fig. S2.6B,C). However, when the dextran pulse was shortened to 5 min, A769662 increased uptake in both PC3 and LNCaP prostate cancer cells (Fig. 2.4G and Supplementary Fig. S2.6D). These results are consistent with studies demonstrating that AMPK activity is basally elevated in prostate tumors relative to normal tissue (40). AMPK also stimulates autophagy, and blocking macropinocytosis in prostate cancer cells did not further increase autophagic flux (Supplementary Fig. S2.6E). Together, these results confirm that PTEN loss and AMPK activation promote macropinosome formation in prostate cancer cells even in complete medium.

Albumin uptake is independent of macropinocytosis in prostate cancer cells. Having established that PTEN-deficient prostate cancer cells exhibit robust macropinocytosis (Fig. 2.4), whether prostate cancer cells could use macropinocytosis

to support growth and survival in low nutrients was evaluated. BSA is routinely used as a fuel in assays designed to measure whether macropinocytosis supports proliferation and survival in low nutrients (6-8). However, BSA is taken up by multiple mechanisms (41). Efficient BSA uptake in MEFs required macropinocytosis (Fig. 2.1A,C), and thus this cargo could be used to dissect the role of macropinocytosis in resistance to nutrient stress in MEFs (Figs. 2.1G-I and 2.2A,D,G,H). In contrast, prostate cancer cells took up similar amounts of BSA in the presence or absence of macropinocytosis (Supplementary Fig. S2.7A-C). As expected, LDL and transferrin, two classic RME cargos, were taken up with equal efficiency in the presence or absence of EIPA suggesting that BSA entry via RME would also be EIPA-resistant (Supplementary Fig. S2.7D,E). Consistent with this model, dominant-negative dynamin1 K44A expression inhibited uptake of transferrin and BSA, but not dextran (Supplementary Fig. S2.7F); RME but not macropinocytosis is dynamin-dependent (5). Because these experiments indicated that albumin efficiently enters prostate cancer cells through macropinocytosis-independent pathways, an alternative, physiologically relevant and purely macropinocytic cargo was sought to determine whether macropinocytosis can support prostate cancer anabolism.

Necrotic cell debris is taken up by prostate cancer cells solely by macropinocytosis. As tumors grow, tortuous and poorly formed vasculature leads to necrosis in regions where oxygen and nutrient delivery are inadequate to meet tumor cell demand (2). Necrosis is present in many aggressive, high-grade tumors, including prostate cancers and RAS-driven tumors, and correlates with negative patient outcomes

and resistance to radiation and chemotherapy (42-48). Macropinosomes are large structures, ranging from 0.2 to 5 μM in diameter. Necrotic cell debris could be small enough to be engulfed via macropinocytosis, while live or apoptotic cells should be too large to enter via this mechanism. To test this idea, murine hematopoietic FL5.12 cells were fluorescently labeled with carboxyfluorescein diacetate succinimidyl ester (CFSE) and then killed using different protocols. FL5.12 cells were ideal for these studies because apoptotic death upon withdrawal of the cytokine IL-3 avoids the need to remove a cytotoxic drug before supplying the corpses as fuel for prostate cancer cells. A necrotic FL5.12 cell preparation was prepared by allowing sufficient time after IL-3 withdrawal for secondary necrosis to occur (48-72 h). As shown in Fig. 5A and B, freshly killed apoptotic FL5.12 cells are intact, Annexin V- and CFSE-positive, and label with the fluorescent vital dye DAPI. In contrast, necrotic FL5.12 cell preparations contain only cell fragments that retain CFSE- and Annexin V-positivity. As expected, live FL5.12 cells are CFSE-positive but do not stain with DAPI or Annexin V. Consistent with their relative sizes, CFSE-labeled necrotic debris but not apoptotic or live FL5.12 cells were engulfed by macropinocytic mPCE and DU145 cells (Fig. 2.5C). Importantly, uptake of necrotic debris was was fully EIPA-sensitive, only observed in macropinocytic cells, and green necrotic debris fully co-localized with red dextran in macropinosomes (Fig. 2.5C and Supplementary Fig. S2.8A,B). The selective uptake of necrotic debris but not intact cell corpses or live cells clearly differentiates this process from efferocytosis (phagocytosis of apoptotic cells) (49) or entosis (engulfment of viable cells by cancer cells)(50). To confirm that necrotic debris could be accommodated within macropinosomes, co-labeling studies were performed. When prostate cancer cells

were fed both red and green dextrans, macropinosomes were uniformly yellow in the merged image as expected (Supplementary Fig. S2.8C,D). In contrast, when red and green necrotic debris were added simultaneously, macropinosomes were either red or green demonstrating that large cell fragments in the necrotic cell preparation were taken up via macropinocytosis (Supplementary Fig. S2.8D,E). Taken together, these experiments demonstrate that necrotic debris enters cells solely via macropinocytosis.

Whether macropinocytosis could drive prostate cancer cell proliferation in low-nutrient medium was measured using necrotic debris as fuel. Because macropinocytosis in prostate cancer cells did not depend on glucose depletion (Fig. 2.4E,F), only amino acids were limited to allow maximal macropinocytosis-driven proliferation. The addition of necrotic cell debris significantly stimulated the proliferation of mPCE, PC3, and DU145 cells in amino acid-deficient medium (Fig. 2.5D). Macropinocytosis was required to derive a benefit from necrotic debris as PTEN reconstitution eliminated both macropinocytosis (Fig. 2.4C) and the enhanced prostate cancer cell proliferation (Fig. 2.5E). Necrotic debris also supported the proliferation of nutrient-deprived macropinocytic KRAS G12D MEFs and PANC-1 pancreatic cancer cells but not non-macropinocytic LSL MEFs or BxPC3 pancreatic cancer cells (Supplementary Fig. S2.8F,G). In fact, adding necrotic debris increased death in nutrient-deprived non-macropinocytic LSL MEFs or BxPC3 cells confirming that the necrotic cell preparation did not contain sufficient soluble amino acids to support growth. In summary, macropinocytic cells can use necrotic cell debris to support anabolism under nutrient stress.

To confirm that macropinocytosed material fueled prostate cancer anabolism, we assessed amino acid-sensitive mTORC1 signaling. Amino acids produced by the degradation of macropinosomes can re-activate mTORC1 (7). As expected, shifting prostate cancer cells to amino acid-deficient medium reduced mTORC1-dependent phosphorylation of p70S6 kinase at Thr389 (Fig. 2.5F). Supplementation with necrotic debris at a concentration of 0.05% protein restored mTORC1 signaling in an EIPA-sensitive manner. BSA supplementation (2%) also restored Thr389 phosphorylation, but this effect was incompletely reversed by EIPA as expected given that BSA uptake is macropinocytosis-independent in prostate cancer cells (Fig. 2.5F and Supplementary Fig. S2.7A,B). Interestingly, necrotic debris increased mTORC1 signaling in an EIPA-sensitive manner even in complete medium suggesting that macropinocytosis also fuels prostate cancer growth in nutrient-replete conditions (Fig. 2.5F). Importantly, necrotic cell debris did not itself contribute to the pThr389 p70S6K signal. These results suggest that necrotic debris supplies amino acids to nutrient-deprived macropinocytic prostate cancer cells.

To directly test whether proteins scavenged via macropinocytosis are broken down into amino acids to build biomass, we developed a novel isotopic labeling strategy (Fig. 2.6A). To label the macropinocytic cargo, FL5.12 cells were grown in stable isotope labeling with amino acids in cell culture (SILAC) medium containing $^{13}C_3$,$^{15}N_1$ lysine (K4) and $^{13}C_6$,$^{15}N_4$ arginine (R10) for more than 10 generations. Complete labeling of the FL5.12 proteome was confirmed by LC-MS/MS. Necrotic debris containing only fully-

labeled (K4R10, heavy, 14 Da mass shift) peptides, depicted in green in Fig. 2.6A-C, was produced from these FL5.12 cells and fed to macropinocytic prostate cancer cells whose proteins contained only unlabeled amino acids (K0R0, light, depicted in blue). Proliferation assays were conducted in medium containing only unlabeled amino acids, and thus the only source of isotopically labeled amino acids was the proteins in the necrotic debris. When prostate cancer cells fed necrotic debris are harvested and their proteins digested with LysC, peptides that contain both lysine and arginine can be present in four different isotopic forms (Fig. 2.6A-C). Peptides produced independently of macropinocytosis will be unlabeled (K0R0, light, blue). Peptides that contain one unlabeled and one labeled amino acid (K4R0 producing a 4 Da shift or K0R10 producing a 10 Da shift, mixed peaks, red) must have been synthesized in prostate cancer cells using both a labeled amino acid obtained via macropinocytosis and an unlabeled amino acid obtained from the medium. Fully isotopically labeled peptides (K4R10 producing a 14 Da shift, heavy, green) could come from either undigested, heavy-labeled FL5.12 proteins or represent proteins synthesized in prostate cancer cells using both heavy-labeled arginine and lysine obtained via macropinocytosis. An example isotopic profile for the LysC peptide ^{219}FDRGYISPYFINTSK^{233} from the mitochondrial heat shock protein HSPD1 exhibits these four classes of peptides (Fig. 2.6C). To summarize, peptides that are K0R0 were generated independent of macropinocytosis, K4R0 and K0R10 peptides can only be generated if macropinocytosis supplies amino acids, and peptides that are K4R10 are either from engulfed but undigested FL5.12 proteins or proteins synthesized in prostate cancer cells using two labeled amino acids derived from macropinocytosis.

To calculate the maximum biomass derived from macropinocytosis, we assumed that all K4R10 peptides (heavy, green) were synthesized in prostate cancer cells using lysine and arginine derived from macropinocytosis (see Supplementary Methods for details). The minimum amount of protein biomass derived from macropinocytosis was calculated by assuming all of these K4R10 peptides were derived from engulfed but undigested FL5.12 proteins. Using this approach, we found that in amino acid-deficient medium, at least 35-37% of proteins and as much as 60-71% of prostate cancer cell protein biomass was derived from macropinocytosed protein (Fig. 2.6D,E and Supplementary Fig. S2.9A). Moreover, even in complete medium where free, unlabeled amino acids were abundant, between 14% and 25% of the prostate cancer cell protein biomass was derived from macropinocytosed protein. To complement the LysC approach, we performed tryptic digests of proteins isolated from human DU145 prostate cancer cells fed heavy-labeled necrotic debris generated from murine FL5.12 cells. In this scenario, uniquely human peptides that contain an isotopically-labeled amino acid (K4 or R10) must have been synthesized using amino acids acquired via macropinocytosis. This approach produced similar estimates of the contribution of macropinocytosis to the amino acid pool for protein synthesis (Supplementary Fig. S2.9B). In summary, isotopic labeling conclusively demonstrates that macropinocytosed protein contributes to prostate cancer biomass even in nutrient-replete conditions.

Cellular corpses are rich sources of other building blocks besides amino acids. Lipids and cholesterol in particular are key drivers of prostate cancer growth (51, 52). Fatty

acids and cholesterol are stored in lipid droplets, and depleting these lipid pools suppresses prostate cancer proliferation (51-53). Lysosomal degradation of lipid droplets increases in response to amino acid or glucose depletion as triglycerides in these droplets are utilized to fuel mitochondrial metabolism (53, 54). Using label-free Coherent Anti-stokes Raman Spectroscopy (CARS) to detect C-H stretching vibration signals from lipids (52), lipid droplet content declined significantly in glucose- and amino acid-restricted prostate cancer cells as expected (Fig. 2.6F and Supplementary Fig. S2.9C). Supplying necrotic cell debris completely restored lipid droplet content in an EIPA-sensitive manner. As noted earlier (Supplementary Fig. S2.7D), EIPA did not interfere with LDL uptake and it did not decrease lipid droplet content when added in complete medium (Supplementary Fig. S2.9D). Interestingly, supplementation with 2% BSA did not restore lipid droplet content in nutrient-deprived prostate cancer cells (Fig. 2.6F). This suggests that the membranes and lipids present in necrotic debris rather than proteins are responsible for maintaining lipid stores and that prostate cancer cells can scavenge multiple nutrients from cell corpses.

Prostate cancer cells exhibit macropinocytosis under physiologic conditions. To assess whether normal and transformed prostate epithelial cells perform macropinocytosis under more physiologic conditions, we evaluated dextran uptake in prostate organoids derived from C57BL/6 mice and from *Pten*$^{flox/flox}$*;tp53*$^{flox/flox}$*;PB-Cre4* mice that develop autochthonous prostate tumors. PTEN-deficient prostate cancer spheroids but not PTEN-replete normal prostate epithelial organoids exhibited EIPA-sensitive macropinocytosis in nutrient-replete standard 3D culture medium (Fig. 2.7A)

(55). Macropinocytosis in prostate cancer organoids was sensitive to Compound C suggesting that AMPK activation was also required in this context (Supplementary Fig. 2.10A). Primary, metastatic tumor cells from CRPC patients can also be propagated in 3D culture where they form tumor organoids that exhibit histological features that mimic the original patient tumor (56). A patient sample deficient in both PTEN and p53, MSK-PCa1, also exhibited constitutive macropinocytosis in 3D culture (Fig. 2.7B). Patient-derived xenografts (PDX) were also evaluated *in situ*. Subcutaneous PTEN- and p53-deficient PDX prostate tumors (Jackson Laboratory PDX model TM00298) also exhibited EIPA-sensitive dextran uptake *in vivo* following intra-tumoral injection of dextran (Fig. 2.7C). Similarly, autochthonous tumors in *Pten*$^{flox/flox}$*;tp53*$^{flox/flox}$*;PB-Cre4* mice exhibited robust macropinocytosis of intravenously delivered 70 kD FITC-Ficoll; uptake was again sensitive to systemic EIPA administration (Fig. 2.7D). Macropinocytosis was not observed in the prostates of normal mice given 70 kD FITC-Ficoll intravenously (Fig. 2.7E). Importantly, in all cases where macropinocytic uptake was not detected (e.g. in EIPA-treated and wild-type animals), Evan's Blue dye that was co-injected with the dextran or Ficoll was present in the tumor or tissue confirming successful delivery of dextran or Ficoll and EIPA. These results demonstrate that PTEN-deficient prostate cancer cells, but not normal prostate epithelial cells, exhibit robust macropinocytosis in 3D culture and *in vivo*.

To evaluate whether prostate tumors rely on macropinocytosis for growth, C57BL/6 mice bearing subcutaneous prostate cancer isografts were treated with EIPA. Consistent with a role for macropinocytosis in driving prostate tumor growth *in vivo*,

alternate day subcutaneous injections of EIPA inhibited both 70 kD FITC-Ficoll uptake and prostate tumor growth, even producing some regressions, without affecting body weight (Fig. 2.7F-H and Supplementary Fig. S2.10B-E). Again, Evan's Blue dye co-injected with Ficoll robustly labeled tumors that failed to take up FITC-Ficoll in the presence of EIPA confirming successful IV injection and that EIPA delivered with this dosing protocol inhibits macropinocytosis (Supplementary Fig. S2.10E). While all prostate tumor cells we evaluated exhibited macropinocytosis, xenograft growth of a non-macropinocytic pancreatic cancer cell line is not affected by EIPA (6). Taken together, these results in cell lines, organoid cultures, and mouse models support the conclusion that prostate cancers use macropinocytosis to acquire extracellular nutrients to fuel growth and proliferation both *in vitro* and *in vivo*.

DISCUSSION

This study defines macropinocytosis as a previously unrecognized fuel source in prostate cancer, a tumor class known for its enigmatic nutrient dependencies. This discovery could lead to new therapeutic approaches to this lethal disease. Despite the introduction of second-generation androgen inhibitors such as enzalutamide and abiraterone acetate, CRPC patients still develop resistance to all available targeted drugs; chemotherapy with docetaxel affords limited clinical benefit and produces significant toxicity (57, 58). Our finding that prostate cancer cells use macropinocytosis to support anabolism suggests that inhibiting this pathway could provide a novel, safe, and effective strategy to target metabolism in late-stage prostate cancer. Macropinocytosis inhibition could synergize with inhibitors of androgen signaling.

Androgen deprivation therapy triggers tumor cell death, but castration-resistant disease eventually emerges. The growth of PTEN-deficient tumor cells that survive androgen deprivation therapy may be fueled in part by the macropinocytic catabolism of the corpses of their deceased, androgen-dependent brethren. Similarly, cell death resulting from chemotherapy or radiation therapy may paradoxically increase the nutrient pool available to the surviving PTEN-deficient tumor cells. Inhibitors of lysosomal function such as chloroquine that are often used as autophagy inhibitors may limit prostate cancer cell growth in part by blocking macropinosome degradation. The synthetic sphingolipid SH-BC-893 works upstream from chloroquine, preventing macropinosome-lysosome fusion; SH-BC-893's anti-neoplastic activity in prostate cancer models may stem in part from its ability to block macropinocytosis (18). While EIPA is generally considered to have poor pharmacological properties, it inhibited both macropinocytosis and tumor growth in mice following systemic administration without obvious toxicity (Fig. 7F-H, and Supplementary Fig. S10B-E). It will be important to evaluate the sensitivity of autochthonous and metastatic prostate tumors to macropinocytosis inhibitors alone and in combination with standard of care therapies in future studies to provide a more complete picture of their potential clinical value.

The discovery that AMPK activation is a general requirement for macropinosome formation in cancer cells dramatically extends our understanding of the regulation of this process. By increasing RAC1-GTP levels, AMPK activation stimulates macropinosome formation (Fig. 2.2I-K and Supplementary Fig. S2.5). The relatively slow kinetics of RAC1 activation by A769662 (Fig. 2.2I), while somewhat unexpected, are consistent

with prior work (59). Our finding that A769662 activates RAC1-GTP even more efficiently in PTEN WT MEFs than in PTEN KO cells (Fig. 2.2I) without stimulating dextran uptake (Supplementary Fig. S2.3B) seems at first contradictory. However, macropinosome maturation leads to RAC1 inactivation (36), and RAC1 may be trapped in the GTP-bound state in PTEN WT MEFs. Closure of macropinosomes in the presence of elevated PIP_3 may prevent the accumulation of RAC1-GTP in PTEN KO MEFs. Intriguingly, the RAC GEFs ARHGEF6 and ARHGEF7 may be substrates for AMPK (60). Additional studies will be required for a full mechanistic understanding of how macropinocytosis is regulated by signal transduction cascades.

While previous studies evaluating the role of macropinocytosis in cancer deprived cells of individual or classes of amino acids (6-8), we utilized media that was either deficient in all amino acids or in both amino acids and glucose. It is difficult to accurately model the nutrient stress that tumors will experience in their normal microenvironment, but inadequate perfusion is likely to restrict access to multiple nutrients simultaneously. The 1% nutrient condition was selected because nutrient titration experiments indicated that this was the least severe reduction in nutrients that killed the majority of wild type MEFs within 48 h. The specific nutrient conditions employed can influence conclusions regarding the importance of macropinocytosis. When PTEN KO MEFs are deprived of only amino acids, they do not exhibit macropinocytosis (Fig. 2.2B). Amino acid limitation would only be relieved by autophagy, a catabolic process that cannot by itself drive cell-autonomous growth (Fig. 2.2F). In contrast, combined glucose and amino acid stress (1% AA/gluc) activates AMPK and stimulates macropinocytosis (Fig. 2.2B) thereby

providing amino acids from the degradation of albumin in the medium. That AMPK-driven macropinocytosis is responsible for the growth-stimulatory effects of glucose deprivation is supported by the observations that: 1) A769662 enhances proliferation in macropinocytosis-competent amino acid-deprived PTEN KO MEFs but not non-macropinocytic PTEN WT MEFs (Fig. 2.2A), 2) PAK1 is necessary for A769662 to drive macropinocytosis and proliferation in PTEN-deficient MEFs in low nutrients (Fig. 2.2F), and 3) A769662 can drive proliferation in PTEN-deficient MEFs in low nutrients even in the absence of autophagy (Fig. 2.2H). Thus, it is not glucose limitation per say but rather AMPK-induced macropinocytosis that stimulates proliferation in Fig. 2.2A. Indeed, direct AMPK activation in full glucose (1% AA medium + A769662) permits almost twice as much proliferation as AMPK activation by glucose limitation (1% AA/gluc). It is worth noting that, while autophagy is not sufficient to fuel proliferation in low nutrient medium, autophagy is necessary for maximal macropinocytosis-driven proliferation (Fig. 2.2H), most likely because it spares amino acids derived from macropinocytosis for anabolism. In conclusion, the seemingly paradoxical effect of glucose deprivation on the proliferation of amino acid-deprived MEFs is readily explained by the stimulation of macropinocytosis.

An intriguing implication of this study is that AMPK inhibitors could be deployed against cancer cells as macropinocytosis inhibitors. AMPK is a negative regulator of macromolecular synthesis and often classified as a tumor suppressor based on its ability to limit anabolism and stimulate catabolic processes (25). On the other hand, multiple studies suggest that AMPK plays a supportive role in established tumors similar

to the reciprocal role of autophagy as a suppressor of tumor initiation and a driver of tumor progression (38, 61-64). Indeed, many studies indicate that AMPK promotes prostate cancer progression (40). AMPK stimulates autophagy, and autophagy inhibitors have been incorporated into combination therapies based on the premise that blocking the stress response will sensitize tumor cells to other drugs. Like autophagy, macropinocytosis may provide a bypass system that could rescue tumor cells from metabolic stress induced by other agents. Our finding that AMPK promotes not just autophagy but also macropinocytosis suggests that AMPK inhibitors could be effective against macropinocytic tumors alone or as a part of drug combinations.

Histologic evidence of tumor necrosis is a negative prognostic indicator that is correlated with recurrence and aggressive, metastatic disease in multiple solid tumors, including prostate cancer and RAS-driven malignancies (42-46). Our observations that necrotic cell corpses are a rich source of proteins and lipids capable of driving both PTEN-deficient prostate cancer cell and KRAS-driven pancreatic cancer cell growth (Fig. 2.5D,E and Supplementary Figs. S2.8F,G) may partially explain this correlation. Necrosis may enhance tumor growth by triggering inflammation (65) while at the same time providing a fuel source for the cytokine-driven growth of macropinocytic tumor cells. The correlation between inflammatory markers and necrosis is imperfect (47), and in some tumors necrosis may promote cancer cell anabolism primarily by providing metabolic substrates rather than by stimulating a pro-tumorigenic immune response. It is important to recognize that any extracellular material small enough to fit in a macropinosome could be consumed and catabolized through this pathway; cargo that

are taken up by selective pathways, for example albumin, would still be taken up non-selectively by macropinocytosis. It is also significant that necrotic cell debris was supplied here at only 0.05 – 0.1% protein, a 20-40 fold lower concentration than BSA, suggesting that relatively small amounts of necrosis could have a significant impact on tumor growth. Rather than attempting to define the relative anabolic value of different macropinocytic cargos *in vivo*, the most critical next step is to uncover more specific ways to disrupt macropinocytosis than the chemical tools currently available in order to better define the importance of this nutrient scavenging pathway for tumor initiation and progression. Therapeutically, any inhibitor of macropinocytosis would simultaneously block the uptake of BSA, necrotic debris, and any other extracellular cargos. While the contribution that dead cell catabolism makes to tumor cell growth is difficult to quantify, the uptake of necrotic debris through macropinocytosis (necrocytosis) defines a new way the microenvironment likely supports tumor cell anabolism.

These studies also highlight that caution is required when using BSA as a tool to evaluate the contribution of macropinocytosis to anabolism and growth as there are significant, cell line-specific differences in the relative amount of BSA that is taken up through macropinocytosis and dynamin-dependent processes like RME (Fig. 2.1A,B and Supplementary Fig. S2.7A,B,F). In cell lines that take up BSA efficiently in the absence of macropinocytosis (Supplementary Fig. S2.7A,B), necrotic cell debris provides an alternative, physiologically-relevant substrate that is taken up solely by macropinocytosis (Fig. 2.5C). Moreover, necrotic cells are likely a more complete diet than extracellular protein. The observation that necrotic debris, but not extracellular

protein, can maintain lipid droplets in nutrient-restricted cells (Fig. 2.6F) is strong evidence that the membrane component of dead cells can be efficiently recycled via macropinocytosis. From a technical perspective, using necrotic cell debris as macropinocytic cargo has the advantage of facile fluorescent (Fig. 2.5A-C and Supplementary Fig. S2.8A-E) or isotopic (Fig. 2.6A-E) labeling, permitting both tracing of the engulfed material and analysis of its ultimate fate. Importantly, the novel SILAC labeling approach we developed to show that macropinocytosed proteins contribute amino acids to protein synthesis in nutrient-replete as well as -limited media is readily adoptable by other research groups. We anticipate that the use of necrotic cells as cargo will facilitate future studies defining the role of macropinocytosis in tumor cell growth.

In conclusion, while the anabolic value of macropinocytosis in tumor cells is now well accepted, there remains an unmet need for specific agents that block only macropinosome formation or degradation to better define the importance of this process in tumor growth and progression, particularly *in vivo*. While their pleiotropic actions somewhat complicate the dissection of the role of macropinocytosis in cancer, NHE inhibitors, AMPK inhibitors, and SH-BC-893 may actually prove to be superior therapeutic agents for the very reason that they possess multifaceted and complementary anti-neoplastic effects (18).

METHODS

Cell culture. DMEM or RPMI containing 1% of the normal amount of amino acids and/or glucose was generated by preparing DMEM or RPMI lacking amino acids and/or glucose from chemical components and mixing it 99:1 with complete medium. In all experiments, the medium was supplemented with 10% standard fetal calf serum which supplies amino acids, glucose, and albumin. LNCaP (2016), PC3 (2011), DU145 (2011), A549 (2013), PANC-1 (2013), BxPC3 (2017), and RWPE-1 (2012) were obtained from the ATCC in indicated years. mPCE cells and PTEN WT/KO MEFs were generated in the Edinger lab (2015); other MEF lines were obtained from collaborating labs in 2003 (LSL/KRAS G12D), 2007 (AMPK WT/DKO and ATG5 WT/KO), or 2017 (PAK1 WT/KO). Cell lines were cultured for ≤ 3 wk at which point a frozen low passage (≤ 4 wk after receipt) stock was thawed. Cell lines were authenticated by evaluating the expression patterns of androgen receptor (PC3, DU145, LNCaP, mPCE) and gene deletions (MEFs, LNCaP, PC3, mPCE) at least every 6 months. Cells were tested for *Mycoplasma* at least every 4 months (VENOR GeM PCR kit, Sigma). Before they were used in experiments, PAK1 WT and KO MEFs were cured of *Mycoplasma* by culture in ciprofloxacin for 2 months (PCR confirmed); all other cell lines tested negative. Additional details in Supplementary Methods.

Light Microscopy. Unless otherwise indicated, fluorescent dextran (1 mg/mL), Alexa 488 BSA (0.5 mg/ml), or Alexa 488 transferrin (0.5 mg/ml) were added in combination with Lysotracker Red (1:10,000 dilution) and Hoechst 33342 for 30 min, cells were washed three times with PBS, and live cells evaluated on a spinning disc confocal

microscope. Dextran index was calculated using ImageJ software as detailed in (20) and Supplementary Fig. S1A. When nutrient-deficient medium was used, 70 kD dextran or BSA uptake was measured after a 16 h incubation; cells were pre-incubated with 50 μM A769662 for 2 h. EIPA was used at 50-75 μM and added 1 h prior to dextran addition. In Dil-LDL uptake assays, cells were incubated in media with 10% charcoal-stripped serum for 24 h then 20 μg/ml Dil-LDL was added ± EIPA for 2 h.

SILAC labeling. FL5.12 cells were incubated in SILAC media containing "heavy" ^{13}C- or ^{15}N-labeled arginine (R10) and lysine (K4) for >10 divisions. FL5.12 cells were then killed by IL-3 withdrawal; cells were maintained at high density and 72 h allowed for secondary necrosis to produce necrotic debris. Supernatant was fully aspirated from necrotic cell pellets which were used directly or stored at -80°C. In isotopic labeling experiments, prostate cancer cells were washed with PBS after 72 h, lysed, and proteins digested with trypsin or Lys-C and analyzed by mass spectrometry as described in the Supplementary Methods.

RAC1 activity assays. MEFs were transfected with biosensors generously provided by the Hahn Laboratory (University of North Carolina): (1) RAC1 FLARE dual-chain biosensor (CyPet-RAC1 and YPet-PBD); (2) RAC1 constitutively-active dual-chain biosensor (CyPet-RAC1-Q61L and YPet-PBD); or (3) CyPet-RAC1 donor alone. Cells were imaged 24 h after transfection and stimulated with 50 μM A769662 where indicated. FLIM-FRET measurements of the RAC1 FLARE biosensors were acquired

and processed using the SimFCS software package developed at the Laboratory for Fluorescence Dynamics (www.lfd.uci.edu) as described in the Supplementary Methods.

Lipid droplet content measurement by CARS. The CARS imaging system is described in detail in (66). Cells were fixed with 4% formaldehyde and imaged with a 60X water objective. The laser power on the sample was at 10 mW with 10 ms pixel dwell time. The lipid droplet area was estimated from CARS images using a customized Matlab program. Four components Otsu thresholding method was used to separate the lipid droplets, cell cytoplasm, cell nucleus and the background. The lipid droplet area was defined as the number of pixels covered by lipid droplets over the number of pixels covered by cytoplasm.

***In vivo* experiments.** Experiments conducted in mice were performed in accordance with the Institutional Animal Care and Use Committee of University of California, Irvine. Prostate isografts were produced by injecting 5 million mPCE cells subcutaneously in the flank of 5 wk old C57BL/6 mice. Once tumors reached 100 mm^3, animals were randomly assigned to either the vehicle (1% DMSO in PBS) or EIPA (7.5 mg/kg subcutaneously every other day) group (n=10-11). Tumor volume was calculated using the formula volume (mm^3) = length [mm] x (width [mm])^2 x 0.52. For *in vivo* dextran uptake analysis, JAX PDX TM00298 tumors were intratumorally injected with 2 mg Oregon Green dextran dissolved in 1% Evan's Blue Dye 1 h after intraperitoneal (i.p.) injection with vehicle or 10 mg/kg EIPA. Ten wk old male C57BL/6, *Pten*$^{flox/flox}$;*p53*$^{flox/flox}$;*PB-Cre4*,or C57BL/6 mice with or without mPCE isografts were

intravenously injected with 250 mg/kg FITC-Ficoll dissolved in 1% Evan's Blue Dye 1 h after i.p. injection of vehicle or 10 mg/kg EIPA or 1.5 h after subcutaneous injection of 7.5 mg/kg EIPA as indicated.

Statistical methods and data analysis. Significance was determined using two-tailed t-tests. *, $P < 0.05$; **, $P < 0.01$; ***, $P < 0.001$; n.s., not significant ($P > 0.05$). Tukey's method was used to correct for multiple comparisons.

AUTHOR CONTRIBUTIONS: Conceptualization, SMK, AR, TTN, BTF, VJ, and ALE; Methodology, SMK, AR, TTN, PK, BTF, LM, JH, MAD, EOP, BJT, PT, and ALE; Investigation, SMK, AR, TTN, PK, BTF, LM, JH, VJ, and JR; Resources, DG and JC; Writing - original draft, SMK, AR, TTN, PK, LM, MAD, PT, ALE; Writing – review and editing, all authors; Visualization, SMK, AR, TTN, PK, BTF, LM, JH, and ALE; Supervision, MAD, EOP, BJT, PT, and ALE; Funding Acquisition, MAD, EOP, BJT, PT, and ALE**.**

ACKNOWLEDGEMENTS: The authors thank Yu Chen (MSKCC) for generously providing MSK-PCa1 and David Fruman (UC Irvine) for comments on the manuscript. This work was supported by grants to ALE from the NIH (R01 GM089919), CDMRP (W81XWH-11-1-0535), the American Cancer Society (RSG-11-111-01-CDD), and UCI Applied Innovation. BJT, EOP, JH were supported by NIH/NIBIB Biomedical Technology Research Center LAMMP: P41EB015890 (Laser Microbeam and Medical Program, LAMMP). SMK was supported by GAANN P200A120207. LM and MAD were supported in part by Grants NIH-P41-RR03155 and NIH-P50-GM076516. Core facilities at UCI were supported by Cancer Center Support grant P30 CA62203. Proteomics work was supported by Canada Research Chairs in Proteomics and Bioanalytical Mass Spectrometry (PT), the Genome Canada Genomics Innovation Network (PT), and the National Science and Engineering Research Council (311598, PT). PK is supported by a Vanier scholarship.

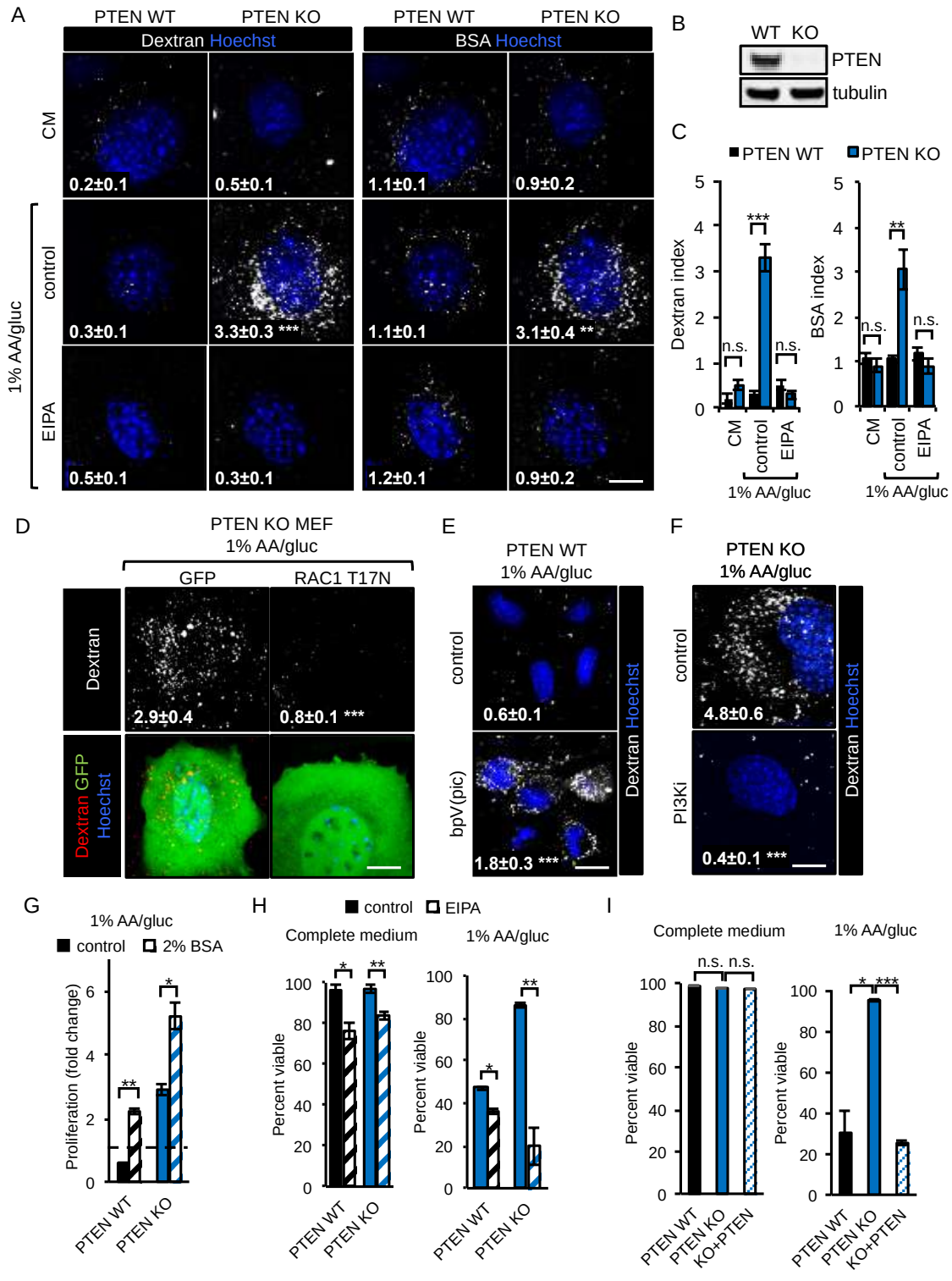
A
PTEN WT
PTEN KO
PTEN WT
PTEN KO
Dextran Hoechst
BSA Hoechst
CM
1% AA/gluc
control
EIPA
0.2±0.1
0.5±0.1
1.1±0.1
0.9±0.2
0.3±0.1
3.3±0.3 ***
1.1±0.1
3.1±0.4 **
0.5±0.1
0.3±0.1
1.2±0.1
0.9±0.2
B
WT KO
PTEN
tubulin
C
PTEN WT
PTEN KO
Dextran index
BSA index
n.s.
***
**
CM
control
EIPA
1% AA/gluc
D
PTEN KO MEF
1% AA/gluc
GFP
RAC1 T17N
Dextran
Dextran GFP Hoechst
2.9±0.4
0.8±0.1 ***
E
PTEN WT
1% AA/gluc
control
bpV(pic)
Dextran Hoechst
0.6±0.1
1.8±0.3 ***
F
PTEN KO
1% AA/gluc
control
PI3Ki
Dextran Hoechst
4.8±0.6
0.4±0.1 ***
G
1% AA/gluc
control
2% BSA
Proliferation (fold change)
PTEN WT
PTEN KO
H
control
EIPA
Complete medium
1% AA/gluc
Percent viable
PTEN WT
PTEN KO
I
Complete medium
1% AA/gluc
n.s.
Percent viable
PTEN WT
PTEN KO
KO+PTEN

Figure 2.1. PTEN loss promotes growth and survival in nutrient-limiting conditions by promoting macropinocytosis. A) 70 kD Dextran or BSA uptake in complete medium (CM) or 1% AA/gluc ± EIPA (50 μM). **B**) Western blot demonstrating loss of PTEN in PTEN KO MEFs. **C**) Quantification of dextran uptake (dextran index) and BSA uptake (BSA index) from panel (A). **D**) Dextran uptake was quantified in GFP-positive PTEN KO MEFs in 1% AA/gluc 24 h after transfection with plasmids encoding GFP or GFP and dominant-negative RAC1 T17N. **E)** Dextran uptake in PTEN WT MEFs in 1% AA/gluc ± 1 h pretreatment with the PTEN inhibitor bpV(pic) (10 μM). **F)** Dextran uptake in PTEN KO MEFs in 1% AA/gluc ± 1 h pretreatment with the PI3K inhibitors (PI3Ki) BYL719 (2.5 μM) and AZD8186 (250 nM). **G)** Proliferation of PTEN WT or KO MEFs after 72 h in 1% AA/gluc ± 2% BSA. **H)** Viability of PTEN WT and KO MEFs in CM or 1% AA/gluc ± EIPA. **H)** Viability of PTEN WT, PTEN KO, or PTEN KO MEFs reconstituted with PTEN in CM or 1% AA/gluc after 48 hr. In all panels, means ± SEM shown, n ≥ 3. Using a paired, two-tailed t test, *, $P \leq 0.05$; **, $P \leq 0.01$; ***, $P \leq 0.001$, n.s. not significant. Uptake index (dextran or BSA) is indicated in images in white; ≥ 25 cells were examined. Scale bar, 20 μm. See also Supplementary Figures S1 and S2.

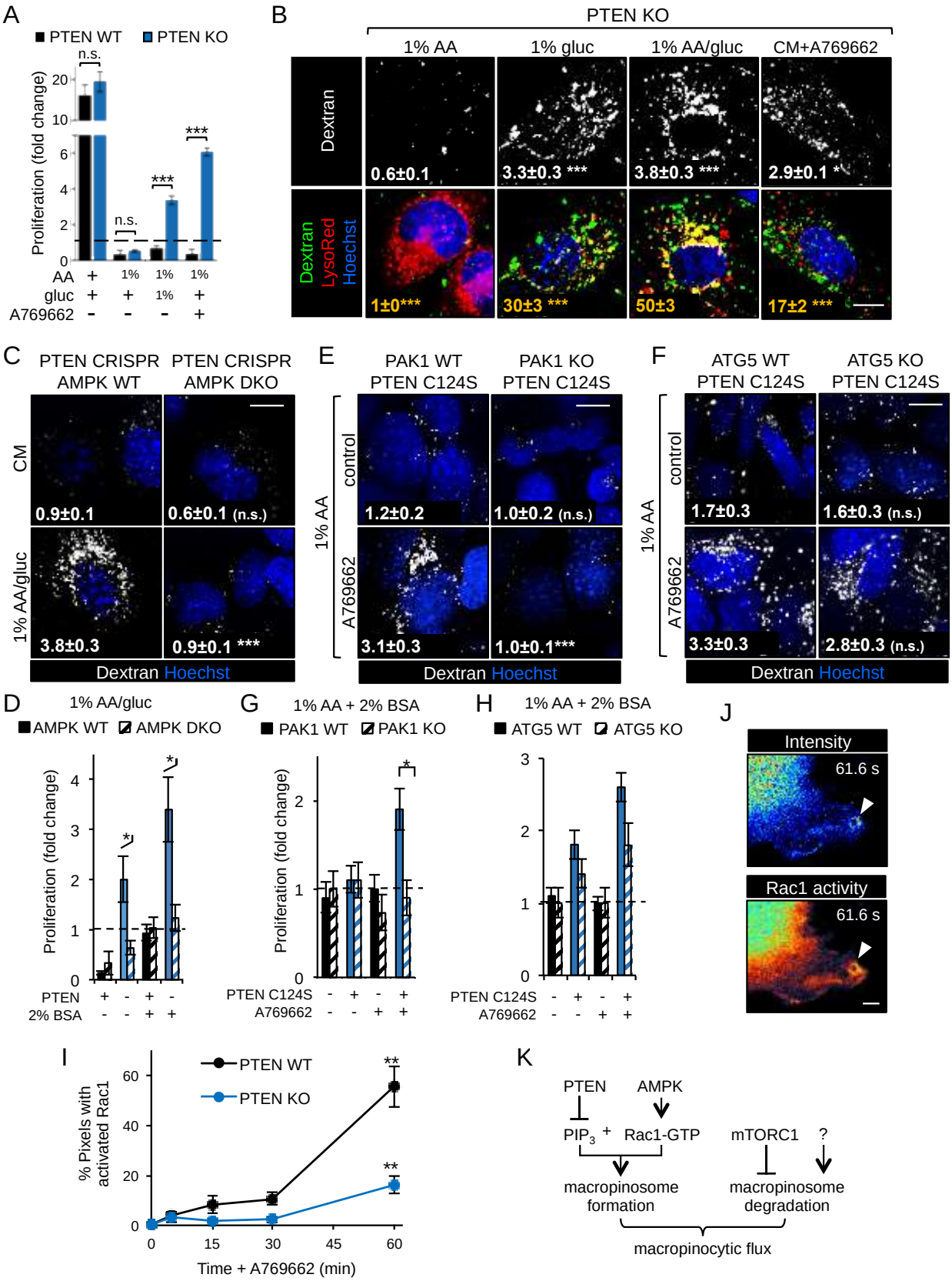
A
PTEN WT
PTEN KO
n.s.
Proliferation (fold change)
20
10
6
4
2
0
***
***
n.s.
AA + 1% 1% 1%
gluc + + 1% +
A769662 - - - +
B
PTEN KO
1% AA
1% gluc
1% AA/gluc
CM+A769662
Dextran
0.6±0.1
3.3±0.3 ***
3.8±0.3 ***
2.9±0.1 *
Dextran LysoRed Hoechst
1±0***
30±3 ***
50±3
17±2 ***
C
PTEN CRISPR AMPK WT
PTEN CRISPR AMPK DKO
CM
1% AA/gluc
0.9±0.1
0.6±0.1 (n.s.)
3.8±0.3
0.9±0.1 ***
Dextran Hoechst
E
PAK1 WT PTEN C124S
PAK1 KO PTEN C124S
1% AA
control
A769662
1.2±0.2
1.0±0.2 (n.s.)
3.1±0.3
1.0±0.1***
Dextran Hoechst
F
ATG5 WT PTEN C124S
ATG5 KO PTEN C124S
1% AA
control
A769662
1.7±0.3
1.6±0.3 (n.s.)
3.3±0.3
2.8±0.3 (n.s.)
Dextran Hoechst
D
1% AA/gluc
AMPK WT AMPK DKO
Proliferation (fold change)
4
3
2
1
0
*
*
PTEN + - + -
2% BSA - - + +
G
1% AA + 2% BSA
PAK1 WT PAK1 KO
Proliferation (fold change)
2
1
0
*
PTEN C124S - + - +
A769662 - - + +
H
1% AA + 2% BSA
ATG5 WT ATG5 KO
3
2
1
0
PTEN C124S - + - +
A769662 - - + +
J
Intensity
61.6 s
Rac1 activity
61.6 s
I
PTEN WT
PTEN KO
% Pixels with activated Rac1
60
40
20
0
**
**
0
15
30
45
60
Time + A769662 (min)
K
PTEN
AMPK
PIP3
+
Rac1-GTP
mTORC1
?
macropinosome formation
macropinosome degradation
macropinocytic flux

Figure 2.2. AMPK activation is necessary for macropinocytosis in PTEN-deficient cells. **A**) Proliferation of PTEN WT or KO MEFs after 72 h in complete or nutrient-deficient medium ± A769662 (10 μM). Where indicated, amino acids and/or glucose were reduced to 1% the level in complete medium. **B**) Dextran uptake (white, statistics relative to CM control) or dextran-lysosome co-localization (yellow, statistics relative to 1%AA/gluc) in PTEN KO MEFs in the indicated media ± A769662 (50 μM). **C**) Dextran uptake in AMPK WT or DKO MEFs ± CRISPR/Cas9-mediated PTEN deletion in CM or 1% AA/gluc; statistics relative to AMPK replete cells. **D**) Proliferation of MEFs null for AMPK and/or PTEN as indicated after 96 h in 1% AA/gluc medium ± 2% BSA. **E,F**) Dextran uptake in PAK1 WT or KO (E) or ATG5 WT or KO (F) MEFs expressing dominant-negative PTEN C124S in 1% AA ± A769662; statistics relative to PAK1 (E) or ATG5 (F) replete cells. **G,H**) Proliferation of PAK1 WT or KO MEFs (G) or ATG5 WT or KO MEFs (H) ± PTEN C124S after 72 h in 1% AA medium supplemented with 2% BSA ± A769662 (10 μM). **I**) FLIM-FRET-phasor analysis of RAC1 activation in PTEN WT or KO MEFs in CM ± A769662 (50 μM); statistics relative to T=0. **J**) Single frames from Supplementary Videos 1 and 2 showing ratiometric GP-FRET (RAC1 activity) and RAC1-CyPet intensity in the periphery of a PTEN KO MEF stimulated with A769662 for 2 h. Arrowheads indicate macropinosomes. Scale bar, 5 μm. **K**) Summary of signaling pathways regulating macropinocytic flux. Means ± SEM shown, n ≥ 3 in all panels. In panels D, G, and H, a two-way ANOVA was performed with Tukey's correction for multiple comparisons. In all other panels, a paired two-tailed t test was employed. *, $P \leq 0.05$; **, $P \leq 0.01$; ***, $P \leq 0.001$; n.s., not significant. Scale bar, 20 μm except in (J). For imaging, ≥ 25 cells were examined. See also Supplementary Figures S3-5 and Supplementary Videos S1-2.

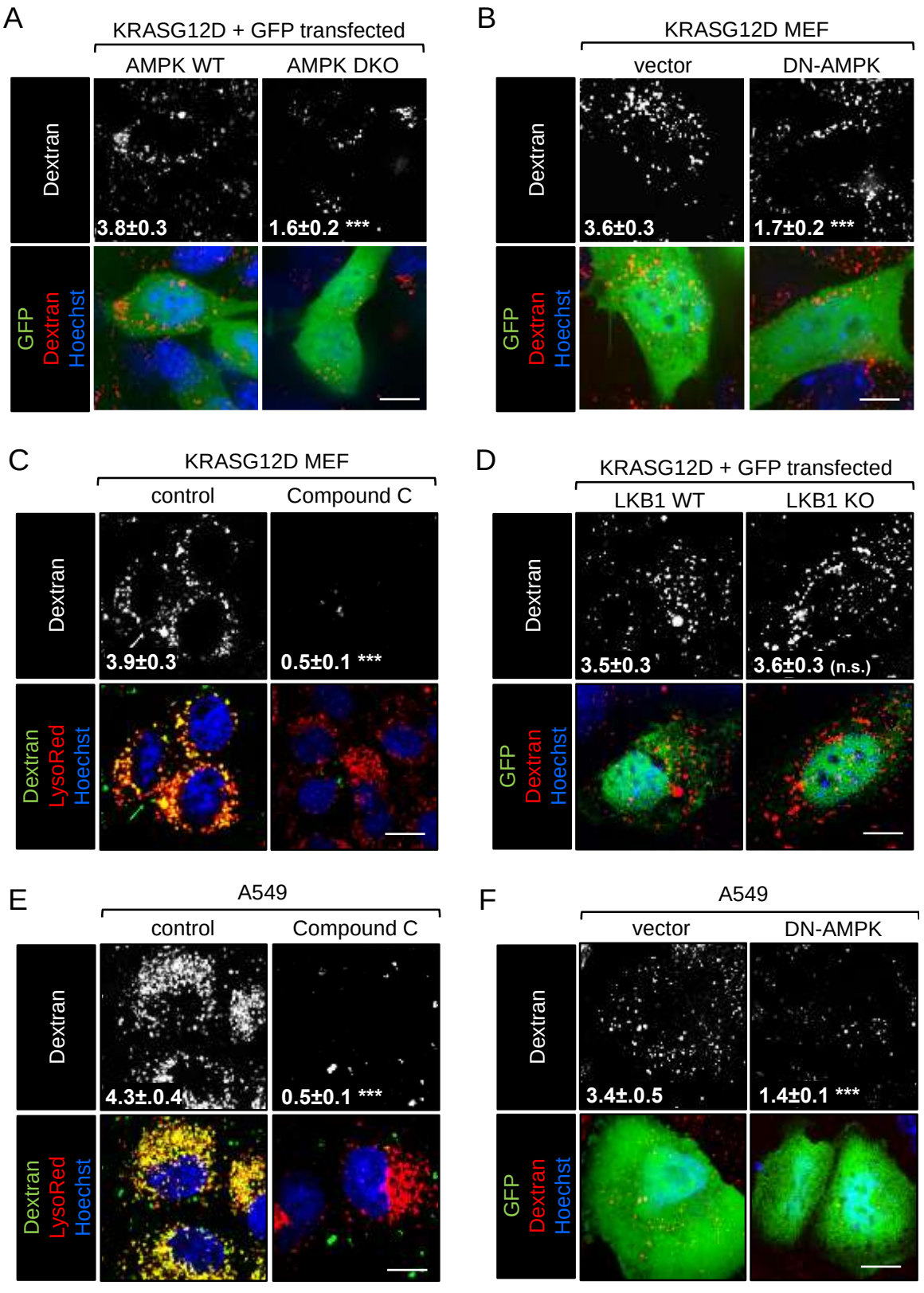
A
KRASG12D + GFP transfected
AMPK WT
AMPK DKO
Dextran
3.8±0.3
1.6±0.2 ***
GFP
Dextran
Hoechst
B
KRASG12D MEF
vector
DN-AMPK
Dextran
3.6±0.3
1.7±0.2 ***
GFP
Dextran
Hoechst
C
KRASG12D MEF
control
Compound C
Dextran
3.9±0.3
0.5±0.1 ***
Dextran
LysoRed
Hoechst
D
KRASG12D + GFP transfected
LKB1 WT
LKB1 KO
Dextran
3.5±0.3
3.6±0.3 (n.s.)
GFP
Dextran
Hoechst
E
A549
control
Compound C
Dextran
4.3±.0.4
0.5±0.1 ***
Dextran
LysoRed
Hoechst
F
A549
vector
DN-AMPK
Dextran
3.4±.0.5
1.4±0.1 ***
GFP
Dextran
Hoechst

Figure 2.3. AMPK activity is necessary for KRAS-driven macropinocytosis. **A)** Dextran uptake in GFP-positive AMPK WT or DKO MEFs 48 h after co-transfection with KRAS G12D and GFP plasmids. **B)** Dextran uptake in GFP-positive KRAS G12D MEFs 72 h after transfection with plasmids expressing GFP or DN-AMPK-IRES-GFP. **C)** Dextran uptake in KRAS G12D MEFs ± Compound C (10 μM). **D)** As in (A) but in LKB1 WT or KO MEF. **E)** Dextran uptake in A549 ($LKB1^{-/-}$, KRAS G12S) ± Compound C (10 μM). **F)** As in (B) but in A549 cells. Scale bars, 20 μm. All experiments were performed in complete medium. Dextran index ± SEM indicated in white with statistics relative to untreated, vector, or wildtype control; ≥ 25 cells were examined. Using a paired, two-tailed t test, ***, P ≤ 0.001; n.s., not significant.

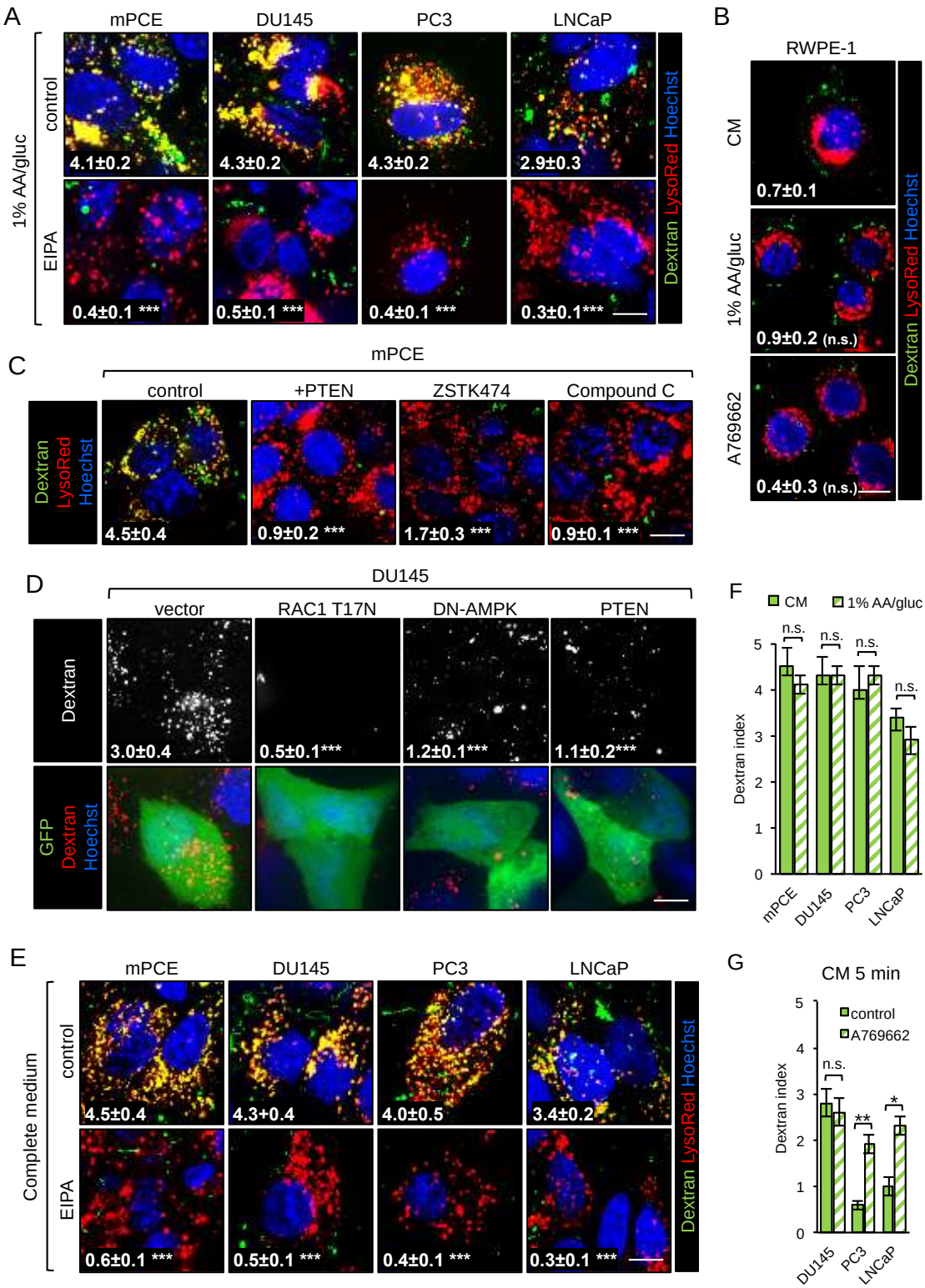
A
mPCE
DU145
PC3
LNCaP
1% AA/gluc
control
EIPA
4.1±0.2
4.3±0.2
4.3±0.2
2.9±0.3
0.4±0.1 ***
0.5±0.1 ***
0.4±0.1 ***
0.3±0.1***
Dextran LysoRed Hoechst
B
RWPE-1
CM
1% AA/gluc
A769662
0.7±0.1
0.9±0.2 (n.s.)
0.4±0.3 (n.s.)
Dextran LysoRed Hoechst
C
mPCE
control
+PTEN
ZSTK474
Compound C
Dextran LysoRed Hoechst
4.5±0.4
0.9±0.2 ***
1.7±0.3 ***
0.9±0.1 ***
D
DU145
vector
RAC1 T17N
DN-AMPK
PTEN
Dextran
GFP Dextran Hoechst
3.0±0.4
0.5±0.1***
1.2±0.1***
1.1±0.2***
F
CM
1% AA/gluc
Dextran index
n.s.
mPCE
DU145
PC3
LNCaP
E
mPCE
DU145
PC3
LNCaP
Complete medium
control
EIPA
4.5±0.4
4.3+0.4
4.0±0.5
3.4±0.2
0.6±0.1 ***
0.5±0.1 ***
0.4±0.1 ***
0.3±0.1 ***
Dextran LysoRed Hoechst
G
CM 5 min
control
A769662
Dextran index
n.s.
**
*
DU145
PC3
LNCaP

Figure 2.4. PTEN-deficient prostate cancer cells exhibit constitutive macropinocytosis. A) Dextran uptake in prostate cancer in 1% AA/gluc ± EIPA (50-75 μM). **B**) Dextran uptake in RWPE-1 cells in CM or 1% AA/gluc ± A769662 (50 μM). **C**) Dextran uptake in mPCE cells ± PTEN reconstitution or a 1 h pretreatment with the pan-PI3Ki ZSTK474 (200 nM) or Compound C (10 μM). **D**) Dextran uptake in GFP-positive DU145 cells 48 h after transfection with plasmids expressing GFP or GFP and RAC1 T17N, DN-AMPK, or wild type PTEN. **E,F**) Dextran uptake in prostate cancer cell lines in CM ± EIPA (50-75 μM), compared to results in 1% AA/gluc in (F). **G**) Dextran index in prostate cancer cells incubated with dextran for 5 min in CM ± A769662 (50 μM). All panels except (A) and part of (B) were conducted in complete medium. Scale bar, 20 μm. Dextran index in white, means ± SEM shown with statistics relative to control, CM, or vector; ≥ 25 cells were examined. Using a paired two-tailed t test, *, $P \leq 0.05$; **, $P \leq 0.01$; ***, $P \leq 0.001$; n.s., not significant. See also Supplementary Figure S6.

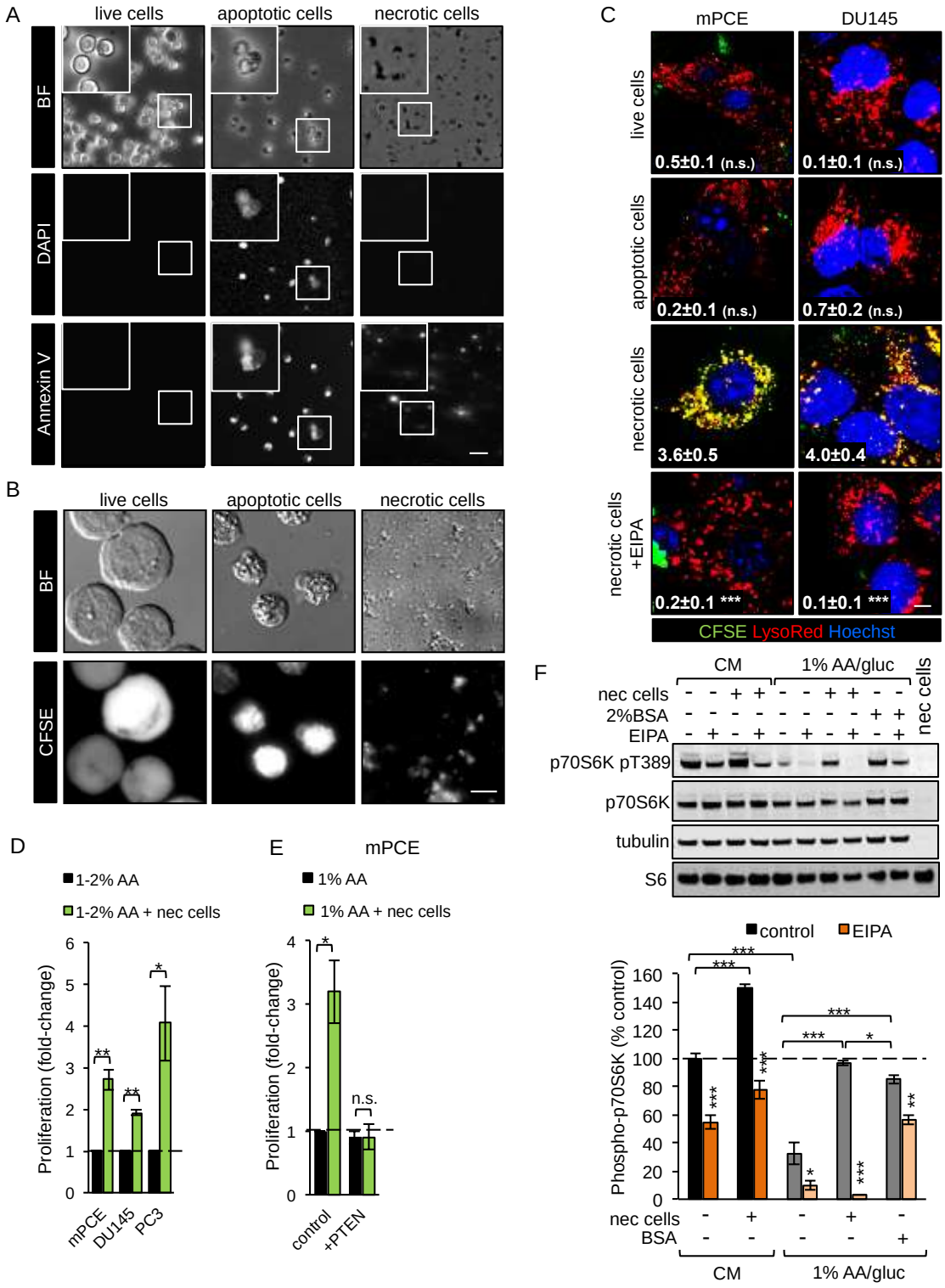
A
live cells
apoptotic cells
necrotic cells
BF
DAPI
Annexin V
B
live cells
apoptotic cells
necrotic cells
BF
CFSE
C
mPCE
DU145
live cells
apoptotic cells
necrotic cells
necrotic cells +EIPA
0.5±0.1 (n.s.)
0.1±0.1 (n.s.)
0.2±0.1 (n.s.)
0.7±0.2 (n.s.)
3.6±0.5
4.0±0.4
0.2±0.1 ***
0.1±0.1 ***
CFSE LysoRed Hoechst
D
1-2% AA
1-2% AA + nec cells
Proliferation (fold-change)
mPCE
DU145
PC3
E
mPCE
1% AA
1% AA + nec cells
Proliferation (fold-change)
n.s.
control
+PTEN
F
CM
1% AA/gluc
nec cells
2%BSA
EIPA
nec cells
p70S6K pT389
p70S6K
tubulin
S6
control
EIPA
Phospho-p70S6K (% control)
nec cells
BSA
CM
1% AA/gluc

Figure 2.5. PTEN-deficient prostate cancer cells consume necrotic debris via macropinocytosis to fuel growth. A) FL5.12 cells were killed by IL-3 withdrawal for 24 h at low density density (25,000 cells/ml) to produce apoptotic cells or 48 h at high density (100 million cells/ml) to trigger primary and secondary necrosis and stained as indicated. **B**) CFSE-labeled FL5.12 cells were killed as in (A). Statistics comparing necrotic cells ± EIPA. **C**) Prostate cancer cells were fed 1 million live, apoptotic, or necrotic CFSE-labeled FL5.12 cells or cell equivalents for 1 h prior to imaging. Where indicated, EIPA (50 μM) was added 1 h prior to necrotic cells; statistics test control versus EIPA. **D**) Prostate cancer cell proliferation after 72 h in 1% (mPCE, PC3) or 2% (DU145) AA medium ± necrotic debris (0.1% protein). DU145 cells did not proliferate in 1% AA medium. **E**) mPCE cells treated as in (D) ± PTEN reconstitution. In (D) and (E), results are expressed relative to the low nutrient control. **F**) mTORC1 signaling in mPCE cells after 4 h in CM or 1% AA/gluc ± necrotic cells (0.05% protein), 2% BSA, and/or EIPA (75 μM) as indicated. The far right lane is necrotic cells only. Scale bars, 10 μm. Means ± SEM shown, n ≥ 3 in all panels. Using a paired, two-tailed t test, *, $P \leq 0.05$; **, $P \leq 0.01$; ***, $P \leq 0.001$; n.s., not significant. Tukey's method was used to correct for multiple comparisons in (F). Uptake index indicated in white in (C); ≥ 25 cells were examined. See also Supplementary Figure S7-8.

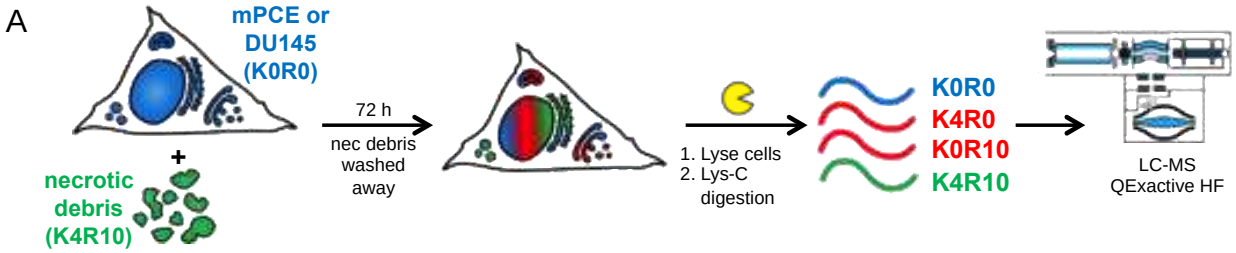

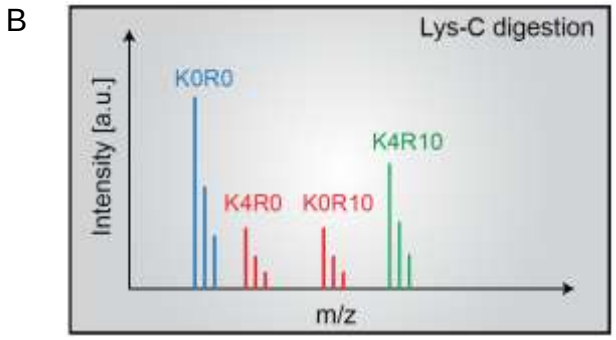

K0R0	MP-independent biomass
K4R0 K0R10	Biomass synthesized from MP
K4R10	Biomass synthesized from MP + engulfed necrotic debris

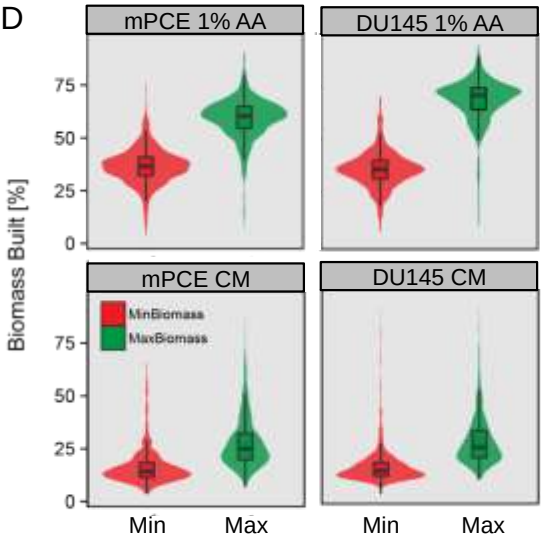

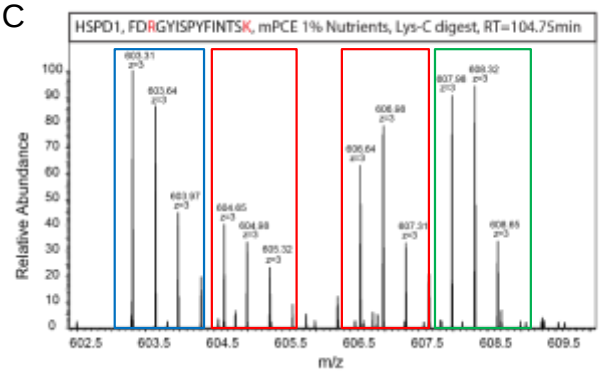

E

1% AA	% of protein biomass derived from macropinocytosis	
	Min.	Max.
mPCE	37%	60%
DU145	35%	71%

Complete medium	% of protein biomass derived from macropinocytosis	
	Min.	Max.
mPCE	15%	25%
DU145	14%	25%

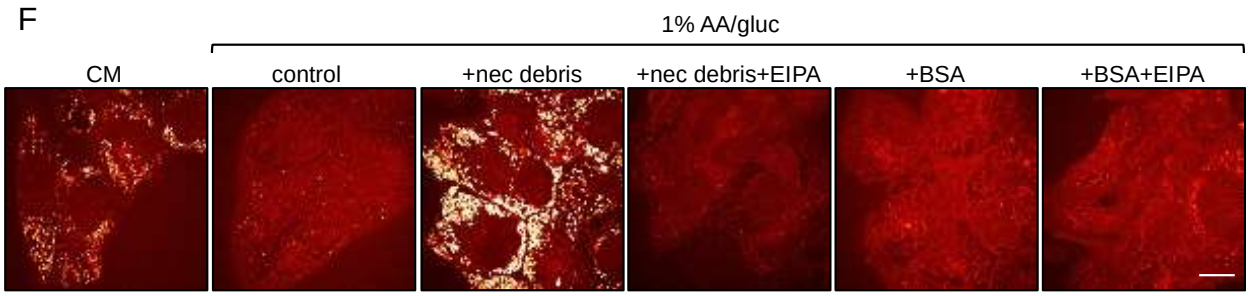

Figure 2.6. Necrotic debris consumed by macropinocytosis is used to build biomass. A) Proteomics workflow. Unlabeled mouse mPCE or human DU145 prostate cancer cells were fed K4R10-labeled necrotic FL5.12 cells for 72 h in 1% AA or CM, washed with PBS 3 times, then digested with Lys-C for LC-MS peptide analysis. **B**) Hypothetical predicted mass spectra of one peptide from the experiment in (A). Light peaks (blue) do not contain lysine or arginine derived from macropinocytosed proteins. Medium peaks (red) correspond to newly synthesized protein containing both unlabeled (MP independent) and labeled (MP dependent) lysine and arginine. Heavy peaks (green) correspond to newly synthesized peptides containing both heavy labeled lysine and arginine (MP dependent) or peptides from engulfed undigested necrotic debris. **C**) Actual peptide spectra of a triply charged peptide (amino acid sequence FDRGYISPYFNTSK from the HSPD1 protein) from Lys-C digested mPCE cells fed necrotic debris. **D,E)** Maximum and minimum protein biomass derived from macropinocytosed debris calculated as depicted graphically using violin plots (D) or described in the text and tabulated in (E). **F**) DU145 cells were cultured for 24 h in 1% AA/gluc ± necrotic debris, 2% BSA, ± EIPA (50 µM) then lipid droplets were imaged by CARS. Scale bar, 20 µm. See also Supplementary Figure S9.

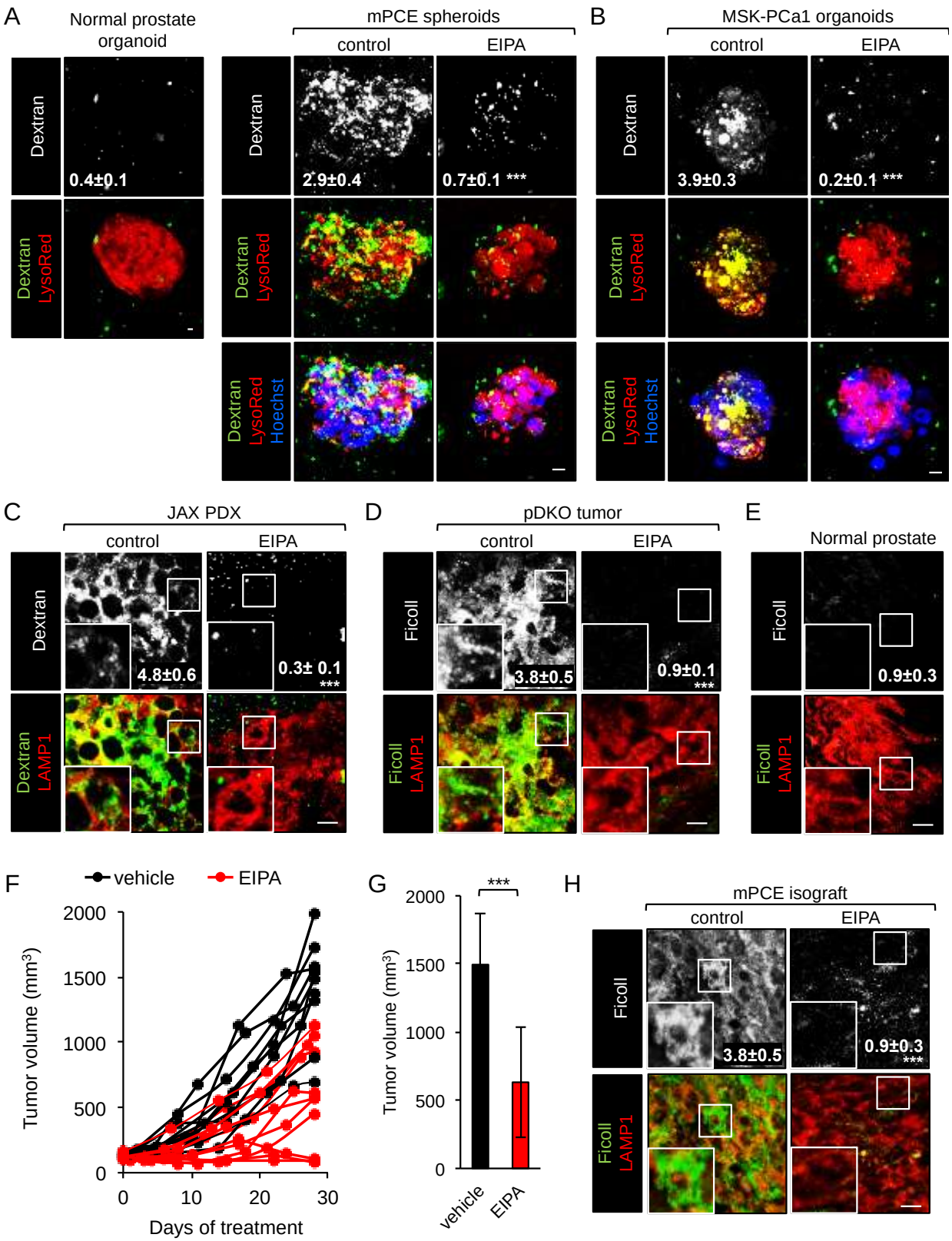
A
Normal prostate organoid
mPCE spheroids
control
EIPA
Dextran
0.4±0.1
2.9±0.4
0.7±0.1 ***
Dextran LysoRed
Dextran LysoRed Hoechst
B
MSK-PCa1 organoids
control
EIPA
3.9±0.3
0.2±0.1 ***
C
JAX PDX
control
EIPA
4.8±0.6
0.3± 0.1 ***
Dextran LAMP1
D
pDKO tumor
control
EIPA
Ficoll
3.8±0.5
0.9±0.1 ***
Ficoll LAMP1
E
Normal prostate
0.9±0.3
F
vehicle
EIPA
Tumor volume (mm3)
2000
1500
1000
500
0
0
10
20
30
Days of treatment
G
***
Tumor volume (mm3)
vehicle
EIPA
H
mPCE isograft
control
EIPA
3.8±0.5
0.9±0.3 ***

Figure 2.7. Prostate cancer cells exhibit macropinocytosis in 3D and *in vivo*. A,B) Dextran uptake in organoid cultures generated from prostate epithelial cells from C57BL/6 or *Pten*$^{flox/flox}$*;tp53*$^{flox/flox}$*;PB-Cre4* mice (A) or PTEN- and p53-deficient MSK-PCa1 metastatic human CRPC organoids (B). In (A), mouse prostate organoid media (55) or mPCE medium (67)containing 5% growth factor reduced Matrigel was utilized. In (B), human prostate organoid medium was utilized (56). **C**) Dextran uptake (2 mg intratumorally) in subcutaneous PTEN- and p53-deficient JAX PDX TM00298 tumors ± EIPA (10 mg/kg i.p.). **D,E**) 70 kD FITC-Ficoll (250 mg/kg i.v.) uptake in autochthonous tumors in *Pten*$^{flox/flox}$*;tp53*$^{flox/flox}$*;PB-Cre4* mice ± EIPA (10 mg/kg i.p.) (D) or normal prostate in C57BL/6 mice (E). **F,G**) Tumor volume in C57BL/6 mice bearing subcutaneous mPCE isografts after 28 d of treatment with vehicle or EIPA (7.5 mg/kg s.c. every other day) once tumors reached 100 mm^3. In G, means ± SD shown, n = 10-11. Using an unpaired, two-tailed t test, ***, $P \leq 0.001$. **H**) FITC-Ficoll (250 mg/kg i.v.) uptake in tumors in mice in (F,G) 2 h after treatment with vehicle or EIPA. Dextran or Ficoll index (mean ± SEM) shown in white; statistics not performed for normal prostate, otherwise are relative to control. Scale bar, 20 μm. See also Supplementary Figure S10-11.

REFERENCES

1. Selwan EM, Finicle BT, Kim SM, Edinger AL. Attacking the supply wagons to starve cancer cells to death. *FEBS Lett*. 2016; **590**: 885-907.
2. Weis SM, Cheresh DA. Tumor angiogenesis: molecular pathways and therapeutic targets. *Nat Med*. 2011; **17**: 1359-70.
3. Kerr MC, Teasdale RD. Defining macropinocytosis. *Traffic*. 2009; **10**: 364-71.
4. Lim JP, Gleeson PA. Macropinocytosis: an endocytic pathway for internalising large gulps. *Immunology and cell biology*. 2011; **89**: 836-43.
5. Swanson JA. Shaping cups into phagosomes and macropinosomes. *Nat Rev Mol Cell Biol*. 2008; **9**: 639-49.
6. Commisso C, Davidson SM, Soydaner-Azeloglu RG, Parker SJ, Kamphorst JJ, Hackett S, et al. Macropinocytosis of protein is an amino acid supply route in Ras-transformed cells. *Nature*. 2013; **497**: 633-7.
7. Palm W, Park Y, Wright K, Pavlova NN, Tuveson DA, Thompson CB. The Utilization of Extracellular Proteins as Nutrients Is Suppressed by mTORC1. *Cell*. 2015; **162**: 259-70.
8. Kamphorst JJ, Nofal M, Commisso C, Hackett SR, Lu W, Grabocka E, et al. Human pancreatic cancer tumors are nutrient poor and tumor cells actively scavenge extracellular protein. *Cancer Res*. 2015; **75**: 544-53.
9. Davidson SM, Jonas O, Keibler MA, Hou HW, Luengo A, Mayers JR, et al. Direct evidence for cancer-cell-autonomous extracellular protein catabolism in pancreatic tumors. *Nat Med*. 2017; **23**: 235-41.
10. Ridley AJ, Paterson HF, Johnston CL, Diekmann D, Hall A. The small GTP-binding protein rac regulates growth factor-induced membrane ruffling. *Cell*. 1992; **70**: 401-10.
11. Dharmawardhane S, Schurmann A, Sells MA, Chernoff J, Schmid SL, Bokoch GM. Regulation of macropinocytosis by p21-activated kinase-1. *Mol Biol Cell*. 2000; **11**: 3341-52.
12. Amyere M, Payrastre B, Krause U, Van Der Smissen P, Veithen A, Courtoy PJ. Constitutive macropinocytosis in oncogene-transformed fibroblasts depends on sequential permanent activation of phosphoinositide 3-kinase and phospholipase C. *Mol Biol Cell*. 2000; **11**: 3453-67.
13. Araki N, Johnson MT, Swanson JA. A role for phosphoinositide 3-kinase in the completion of macropinocytosis and phagocytosis by macrophages. *J Cell Biol*. 1996; **135**: 1249-60.
14. Fruman DA, Rommel C. PI3K and cancer: lessons, challenges and opportunities. *Nat Rev Drug Discov*. 2014; **13**: 140-56.
15. Dillon LM, Miller TW. Therapeutic targeting of cancers with loss of PTEN function. *Current drug targets*. 2014; **15**: 65-79.
16. Phin S, Moore MW, Cotter PD. Genomic Rearrangements of PTEN in Prostate Cancer. *Frontiers in oncology*. 2013; **3**: 240.
17. Shen MM, Abate-Shen C. Molecular genetics of prostate cancer: new prospects for old challenges. *Genes Dev*. 2010; **24**: 1967-2000.
18. Kim SM, Roy SG, Chen B, Nguyen TM, McMonigle RJ, McCracken AN, et al. Targeting cancer metabolism by simultaneously disrupting parallel nutrient access pathways. *J Clin Invest*. 2016; **126**: 4088-102.

19. Egami Y, Taguchi T, Maekawa M, Arai H, Araki N. Small GTPases and phosphoinositides in the regulatory mechanisms of macropinosome formation and maturation. *Frontiers in physiology*. 2014; **5**: 374.
20. Commisso C, Flinn RJ, Bar-Sagi D. Determining the macropinocytic index of cells through a quantitative image-based assay. *Nat Protoc*. 2014; **9**: 182-92.
21. Koivusalo M, Welch C, Hayashi H, Scott CC, Kim M, Alexander T, et al. Amiloride inhibits macropinocytosis by lowering submembranous pH and preventing Rac1 and Cdc42 signaling. *J Cell Biol*. 2010; **188**: 547-63.
22. Matthews H, Ranson M, Kelso MJ. Anti-tumour/metastasis effects of the potassium-sparing diuretic amiloride: an orally active anti-cancer drug waiting for its call-of-duty? *Int J Cancer*. 2011; **129**: 2051-61.
23. Gekle M, Freudinger R, Mildenberger S. Inhibition of Na+-H+ exchanger-3 interferes with apical receptor-mediated endocytosis via vesicle fusion. *J Physiol*. 2001; **531**: 619-29.
24. West MA, Bretscher MS, Watts C. Distinct endocytotic pathways in epidermal growth factor-stimulated human carcinoma A431 cells. *J Cell Biol*. 1989; **109**: 2731-9.
25. Hardie DG, Schaffer BE, Brunet A. AMPK: An Energy-Sensing Pathway with Multiple Inputs and Outputs. *Trends Cell Biol*. 2016; **26**: 190-201.
26. Kondratowicz AS, Hunt CL, Davey RA, Cherry S, Maury WJ. AMP-activated protein kinase is required for the macropinocytic internalization of ebolavirus. *J Virol*. 2013; **87**: 746-55.
27. Moser TS, Jones RG, Thompson CB, Coyne CB, Cherry S. A kinome RNAi screen identified AMPK as promoting poxvirus entry through the control of actin dynamics. *PLoS pathogens*. 2010; **6**: e1000954.
28. Laderoute KR, Amin K, Calaoagan JM, Knapp M, Le T, Orduna J, et al. 5'-AMP-activated protein kinase (AMPK) is induced by low-oxygen and glucose deprivation conditions found in solid-tumor microenvironments. *Mol Cell Biol*. 2006; **26**: 5336-47.
29. Palm W, Araki J, King B, DeMatteo RG, Thompson CB. Critical role for PI3-kinase in regulating the use of proteins as an amino acid source. *Proc Natl Acad Sci U S A*. 2017; **114**: E8628-E36.
30. Egan DF, Shackelford DB, Mihaylova MM, Gelino S, Kohnz RA, Mair W, et al. Phosphorylation of ULK1 (hATG1) by AMP-activated protein kinase connects energy sensing to mitophagy. *Science*. 2011; **331**: 456-61.
31. Gwinn DM, Shackelford DB, Egan DF, Mihaylova MM, Mery A, Vasquez DS, et al. AMPK phosphorylation of raptor mediates a metabolic checkpoint. *Mol Cell*. 2008; **30**: 214-26.
32. Kim J, Kundu M, Viollet B, Guan KL. AMPK and mTOR regulate autophagy through direct phosphorylation of Ulk1. *Nat Cell Biol*. 2011; **13**: 132-41.
33. Levy JMM, Towers CG, Thorburn A. Targeting autophagy in cancer. *Nat Rev Cancer*. 2017; **17**: 528-42.
34. Bae HB, Zmijewski JW, Deshane JS, Tadie JM, Chaplin DD, Takashima S, et al. AMP-activated protein kinase enhances the phagocytic ability of macrophages and neutrophils. *Faseb J*. 2011; **25**: 4358-68.

35. Hinde E, Digman MA, Hahn KM, Gratton E. Millisecond spatiotemporal dynamics of FRET biosensors by the pair correlation function and the phasor approach to FLIM. *Proc Natl Acad Sci U S A*. 2013; **110**: 135-40.
36. Fujii M, Kawai K, Egami Y, Araki N. Dissecting the roles of Rac1 activation and deactivation in macropinocytosis using microscopic photo-manipulation. *Scientific reports*. 2013; **3**: 2385.
37. Ji H, Ramsey MR, Hayes DN, Fan C, McNamara K, Kozlowski P, et al. LKB1 modulates lung cancer differentiation and metastasis. *Nature*. 2007; **448**: 807-10.
38. Shackelford DB, Shaw RJ. The LKB1-AMPK pathway: metabolism and growth control in tumour suppression. *Nat Rev Cancer*. 2009; **9**: 563-75.
39. Chen Z, Trotman LC, Shaffer D, Lin HK, Dotan ZA, Niki M, et al. Crucial role of p53-dependent cellular senescence in suppression of Pten-deficient tumorigenesis. *Nature*. 2005; **436**: 725-30.
40. Khan AS, Frigo DE. A spatiotemporal hypothesis for the regulation, role, and targeting of AMPK in prostate cancer. *Nature reviews Urology*. 2017; **14**: 164-80.
41. Merlot AM, Kalinowski DS, Richardson DR. Unraveling the mysteries of serum albumin-more than just a serum protein. *Frontiers in physiology*. 2014; **5**: 299.
42. Gkogkou C, Frangia K, Saif MW, Trigidou R, Syrigos K. Necrosis and apoptotic index as prognostic factors in non-small cell lung carcinoma: a review. *SpringerPlus*. 2014; **3**: 120.
43. Hiraoka N, Ino Y, Sekine S, Tsuda H, Shimada K, Kosuge T, et al. Tumour necrosis is a postoperative prognostic marker for pancreatic cancer patients with a high interobserver reproducibility in histological evaluation. *Br J Cancer*. 2010; **103**: 1057-65.
44. Pichler M, Hutterer GC, Chromecki TF, Jesche J, Kampel-Kettner K, Rehak P, et al. Histologic tumor necrosis is an independent prognostic indicator for clear cell and papillary renal cell carcinoma. *Am J Clin Pathol*. 2012; **137**: 283-9.
45. Ali TZ, Epstein JI. Basal cell carcinoma of the prostate: a clinicopathologic study of 29 cases. *The American journal of surgical pathology*. 2007; **31**: 697-705.
46. Magers M, Kunju LP, Wu A. Intraductal Carcinoma of the Prostate: Morphologic Features, Differential Diagnoses, Significance, and Reporting Practices. *Archives of pathology & laboratory medicine*. 2015; **139**: 1234-41.
47. Humphrey PA. Gleason grading and prognostic factors in carcinoma of the prostate. *Modern pathology : an official journal of the United States and Canadian Academy of Pathology, Inc*. 2004; **17**: 292-306.
48. Caruso RA, Branca G, Fedele F, Irato E, Finocchiaro G, Parisi A, et al. Mechanisms of coagulative necrosis in malignant epithelial tumors (Review). *Oncology letters*. 2014; **8**: 1397-402.
49. Green DR, Oguin TH, Martinez J. The clearance of dying cells: table for two. *Cell Death Differ*. 2016; **23**: 915-26.
50. Overholtzer M, Mailleux AA, Mouneimne G, Normand G, Schnitt SJ, King RW, et al. A nonapoptotic cell death process, entosis, that occurs by cell-in-cell invasion. *Cell*. 2007; **131**: 966-79.
51. Wu X, Daniels G, Lee P, Monaco ME. Lipid metabolism in prostate cancer. *American journal of clinical and experimental urology*. 2014; **2**: 111-20.

52. Yue S, Li J, Lee SY, Lee HJ, Shao T, Song B, et al. Cholesteryl ester accumulation induced by PTEN loss and PI3K/AKT activation underlies human prostate cancer aggressiveness. *Cell Metab*. 2014; **19**: 393-406.
53. Kaini RR, Sillerud LO, Zhaorigetu S, Hu CA. Autophagy regulates lipolysis and cell survival through lipid droplet degradation in androgen-sensitive prostate cancer cells. *The Prostate*. 2012; **72**: 1412-22.
54. Rambold AS, Cohen S, Lippincott-Schwartz J. Fatty acid trafficking in starved cells: regulation by lipid droplet lipolysis, autophagy, and mitochondrial fusion dynamics. *Dev Cell*. 2015; **32**: 678-92.
55. Chua CW, Shibata M, Lei M, Toivanen R, Barlow L, Shen M. Culture of mouse prostate organoids. *Protoc Exch*. 2014.
56. Gao D, Vela I, Sboner A, Iaquinta PJ, Karthaus WR, Gopalan A, et al. Organoid cultures derived from patients with advanced prostate cancer. *Cell*. 2014; **159**: 176-87.
57. Hotte SJ, Saad F. Current management of castrate-resistant prostate cancer. *Current oncology*. 2010; **17 Suppl 2**: S72-9.
58. Nussbaum N, George DJ, Abernethy AP, Dolan CM, Oestreicher N, Flanders S, et al. Patient experience in the treatment of metastatic castration-resistant prostate cancer: state of the science. *Prostate cancer and prostatic diseases*. 2016; **19**: 111-
59. Lee YM, Lee JO, Jung JH, Kim JH, Park SH, Park JM, et al. Retinoic acid leads to cytoskeletal rearrangement through AMPK-Rac1 and stimulates glucose uptake through AMPK-p38 MAPK in skeletal muscle cells. *J Biol Chem*. 2008; **283**: 33969-74.
60. Obenauer JC, Cantley LC, Yaffe MB. Scansite 2.0: Proteome-wide prediction of cell signaling interactions using short sequence motifs. *Nucleic Acids Res*. 2003; **31**: 3635-41.
61. Saito Y, Chapple RH, Lin A, Kitano A, Nakada D. AMPK Protects Leukemia-Initiating Cells in Myeloid Leukemias from Metabolic Stress in the Bone Marrow. *Cell stem cell*. 2015; **17**: 585-96.
62. Zadra G, Batista JL, Loda M. Dissecting the Dual Role of AMPK in Cancer: From Experimental to Human Studies. *Molecular cancer research : MCR*. 2015; **13**: 1059-72.
63. Liang J, Mills GB. AMPK: a contextual oncogene or tumor suppressor? *Cancer Res*. 2013; **73**: 2929-35.
64. White E. Deconvoluting the context-dependent role for autophagy in cancer. *Nat Rev Cancer*. 2012; **12**: 401-10.
65. Kuraishy A, Karin M, Grivennikov SI. Tumor promotion via injury- and death-induced inflammation. *Immunity*. 2011; **35**: 467-77.
66. Suhalim JL, Chung CY, Lilledahl MB, Lim RS, Levi M, Tromberg BJ, et al. Characterization of cholesterol crystals in atherosclerotic plaques using stimulated Raman scattering and second-harmonic generation microscopy. *Biophys J*. 2012; **102**: 1988-95.
67. Jiao J, Wang S, Qiao R, Vivanco I, Watson PA, Sawyers CL, et al. Murine cell lines derived from Pten null prostate cancer show the critical role of PTEN in hormone refractory prostate cancer development. *Cancer Res*. 2007; **67**: 6083-91.

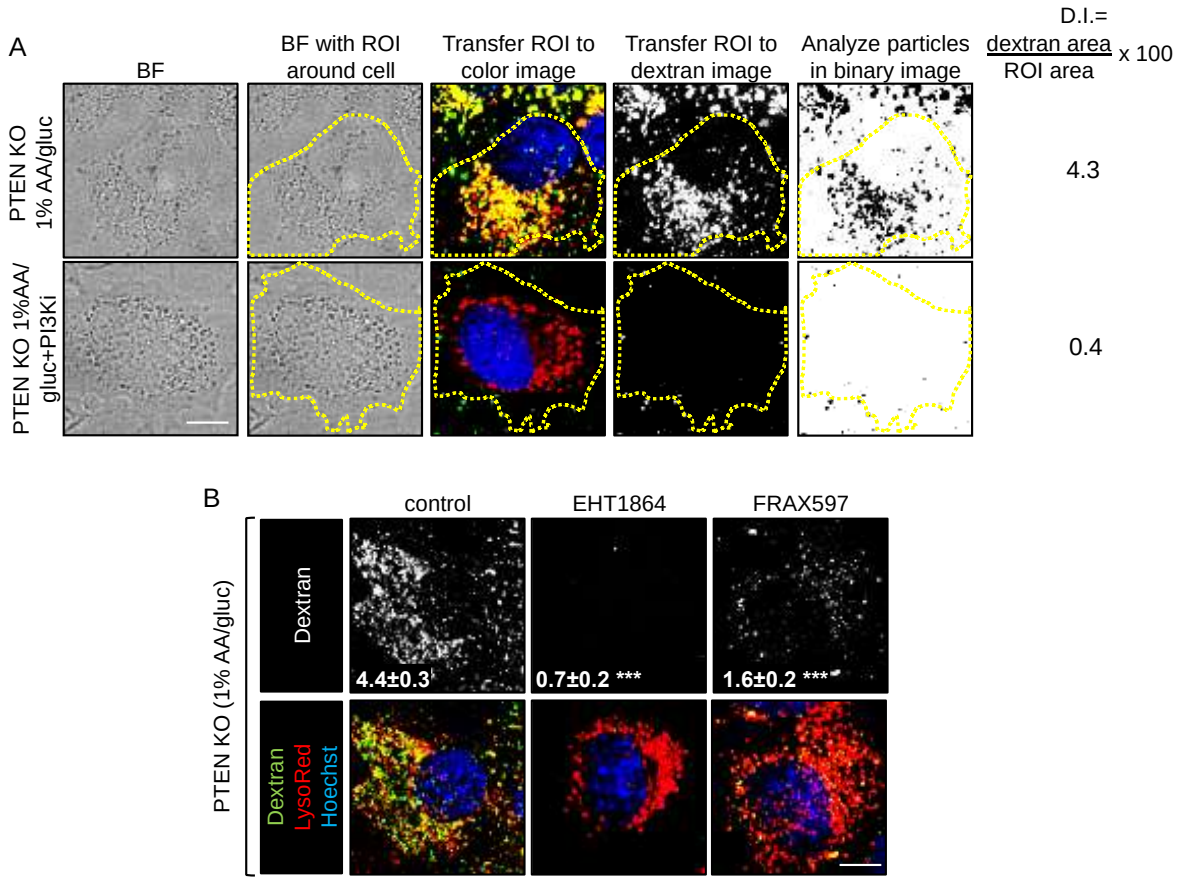

Supplementary Figure S2.1, related to Figure 2.1. PTEN-deficient MEFs exhibit macropinocytosis under nutrient stress. A) Dextran uptake quantification workflow; see Supplemental Methods for additional information. BF, brightfield; ROI, region of interest; D.I, dextran index. **B**) Dextran uptake in PTEN KO MEFs in 1% AA/gluc pre- treated with RAC1 inhibitor EHT1684 (50 µM) or PAK inhibitor FRAX597 (10 µM) for 2 h.

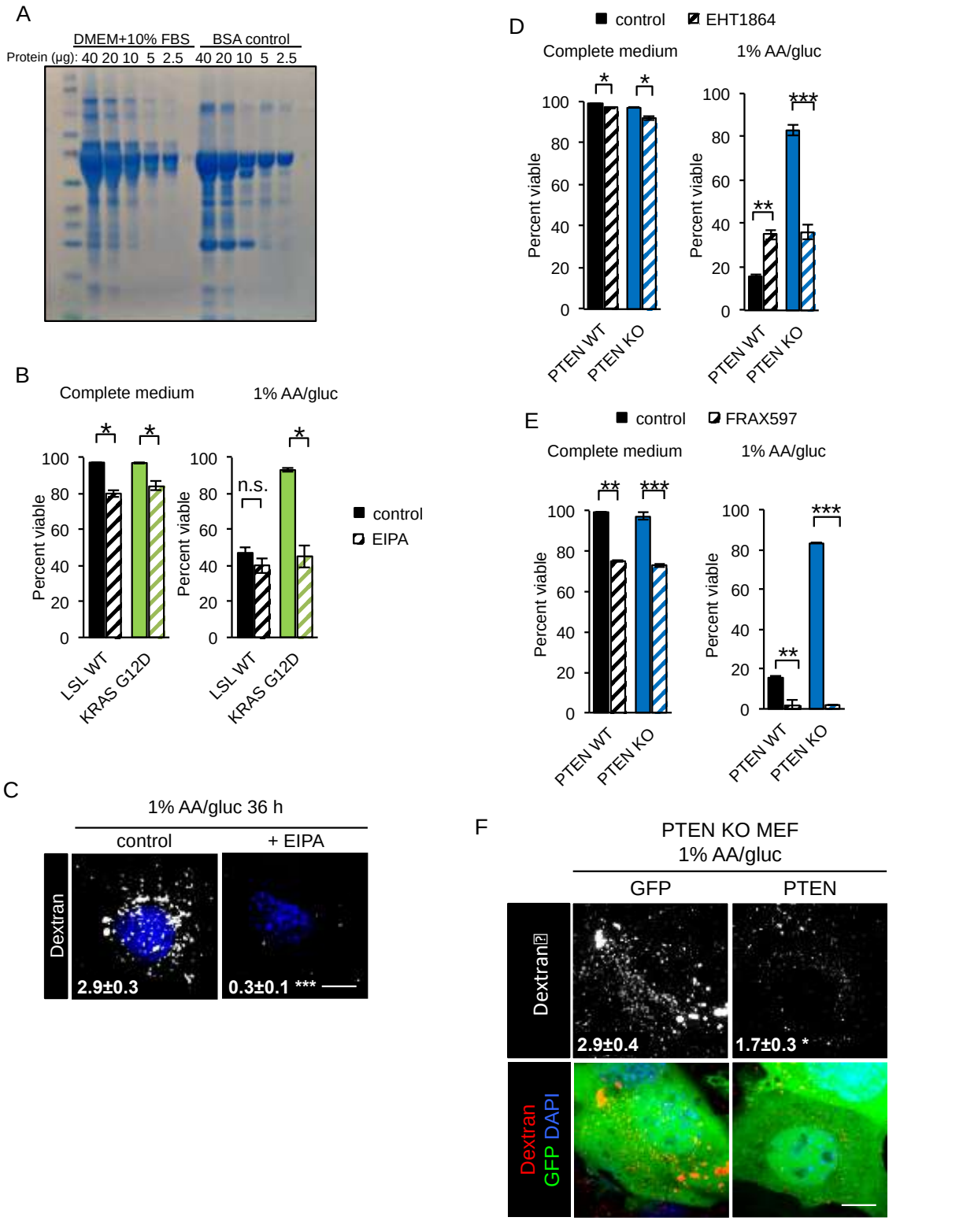

Supplementary Figure S2

Supplementary Figure S2.2, related to Figure 2.1. PTEN-deficient cells use macropinocytosis to consume albumin and survive nutrient stress. A) The indicated protein equivalents of complete medium (DMEM with 10% serum) or BSA were evaluated by SDS-PAGE and Coomassie staining. **B**) Viability of LSL WT or KRAS G12D MEF after 48 h in complete medium or 1% AA/gluc ± EIPA (25 µM). **C**) Dextran uptake in PTEN KO MEFs in 1% AA/gluc after 36 h ± EIPA (25 µM). **D,E**) Viability of PTEN WT or KO MEF after 48 h in complete medium or 1% AA/gluc ± EHT1864 (25 µM) (D) or FRAX597 (10 µM) (E). **F**) Dextran uptake in GFP-positive PTEN KO MEFs transfected with GFP or GFP and PTEN in 1% AA/gluc. Scale bars, 20 µm. Dextran index ± SEM indicated in white. n ≥ 3 in panels B**,** D, and E. For imaging ≥ 25 cells were examined. Using a paired, two-tailed t test, *, $P \leq 0.05$; **, $P \leq 0.01$; ***, $P \leq 0.001$, n.s. not significant.

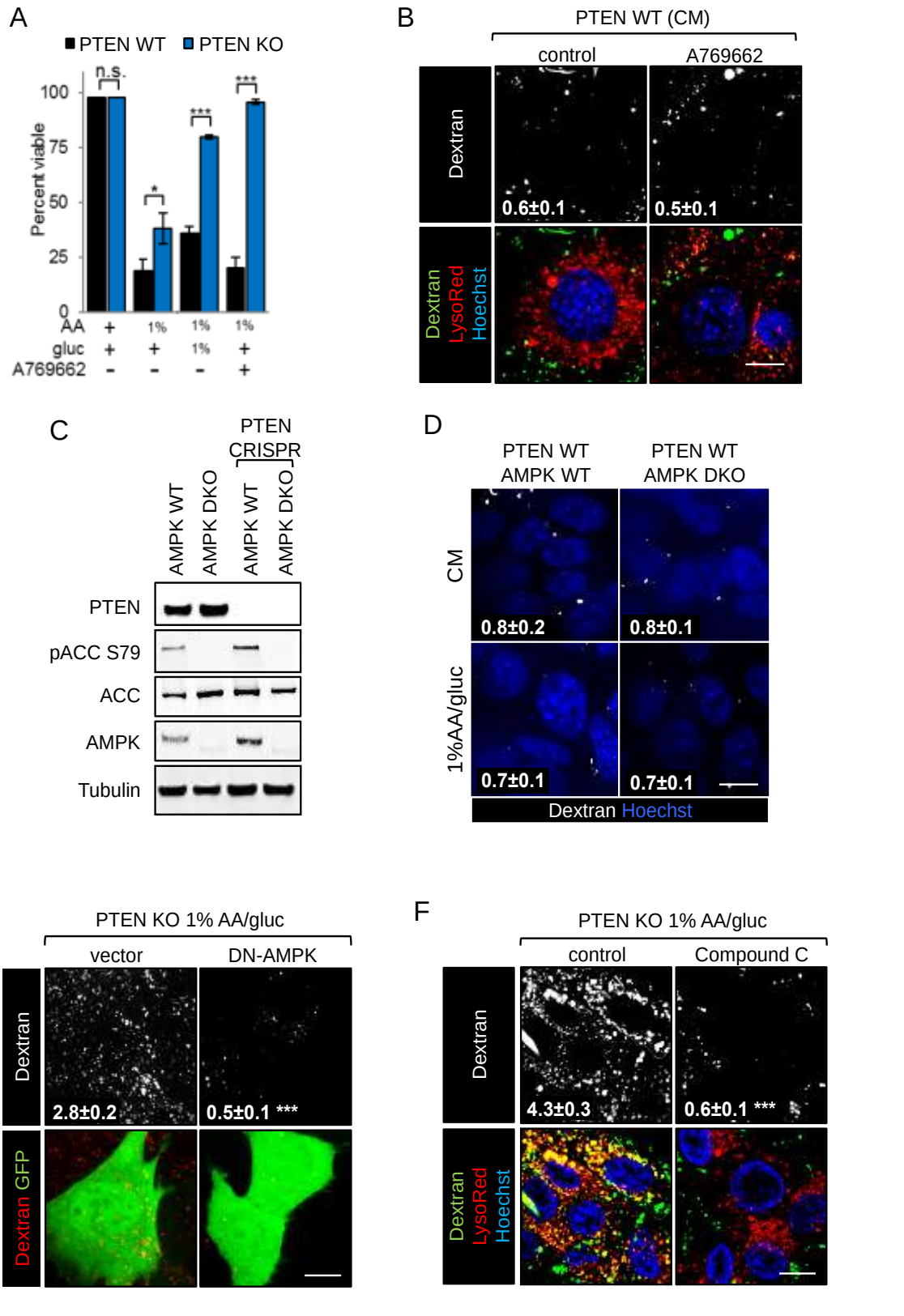

Supplementary Figure S3

Supplementary Figure S2.3, related to Figure 2.2. A) Viability of PTEN WT or KO MEFs after 72 h in the indicated media ± A769662 (10 μM). **B**) Dextran uptake in PTEN WT MEFs in CM ± A769662 (50 μM). **C**) Western blot of AMPK WT and DKO MEFs following CRISPR/Cas9-mediated PTEN deletion. **D**) Dextran uptake in AMPK WT or DKO MEFs with WT PTEN in CM or 1% AA/gluc. **E**) Dextran uptake in GFP-positive PTEN KO MEFs expressing GFP or dominant-negative AMPK (DN-AMPK) and GFP in 1% AA/gluc. **F**) Dextran uptake in PTEN KO MEFs in 1% AA/gluc ± Compound C (10 μM). Scale bars, 20 μm. Means ± SEM shown, n ≥ 3 in panel A. Dextran index ± SEM indicated in white. For imaging ≥ 25 cells were examined. Using a paired, two-tailed t test, *, $P \leq 0.05$; **, $P \leq 0.01$; ***, $P \leq 0.001$, n.s. not significant.

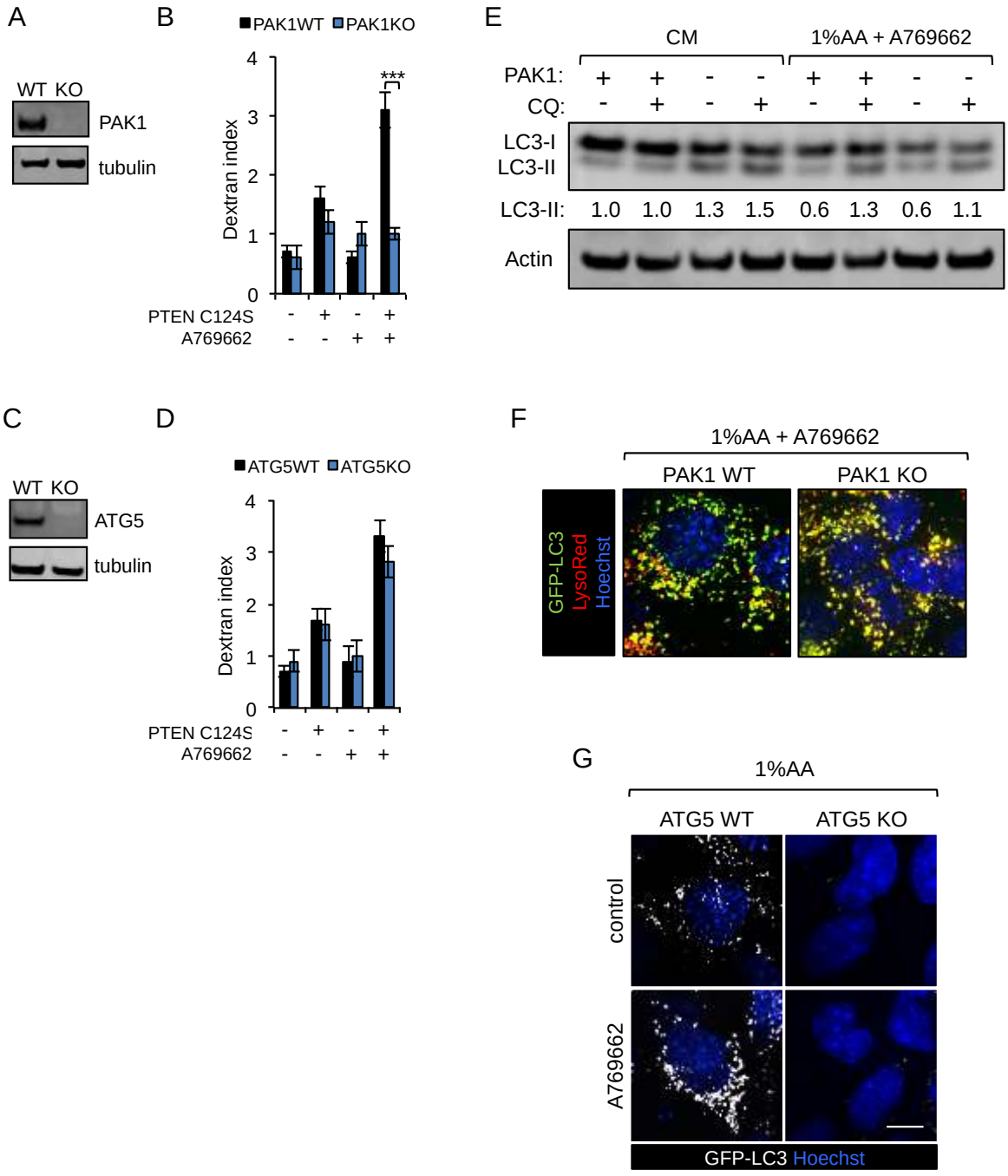

Supplementary Figure S4

Supplementary Figure S2.4, related to Figure 2.2. PAK1 is necessary for macropinocytosis but not autophagy while ATG5 is necessary for autophagy but not macropinocytosis. A) Western blot in PAK1 WT and KO MEFs. **B**) Dextran uptake in PAK1 WT or KO MEFs ± PTEN C124S in 1% AA ± A769662 (50 µM). **C**) Western blot in ATG5 WT and KO MEFs. **D**) Dextran uptake in ATG5 WT or KO MEFs ± PTEN C124S in 1% AA ± A769662 (50 µM). **E**) Western blot of PAK1 WT or KO MEFs after 1 h in the indicated medium ± A769662 (50 µM) ± chloroquine (CQ, 25 µM). LC3-II was quantified using LICOR software. **F**) GFP-LC3 and Lysotracker Red in PAK1 WT or KO cells maintained in 1% AA + A769662 (50 µM) for 3 h. **G**) GFP-LC3 in ATG5 WT or KO MEFs maintained in the indicated medium + A769662 (50 µM) for 3 h. Scale bars, 20 µm. In panels B and D, means ± SEM shown, ≥ 25 cells were examined. Using a paired, two-tailed t test, ***, $P \leq 0.001$.

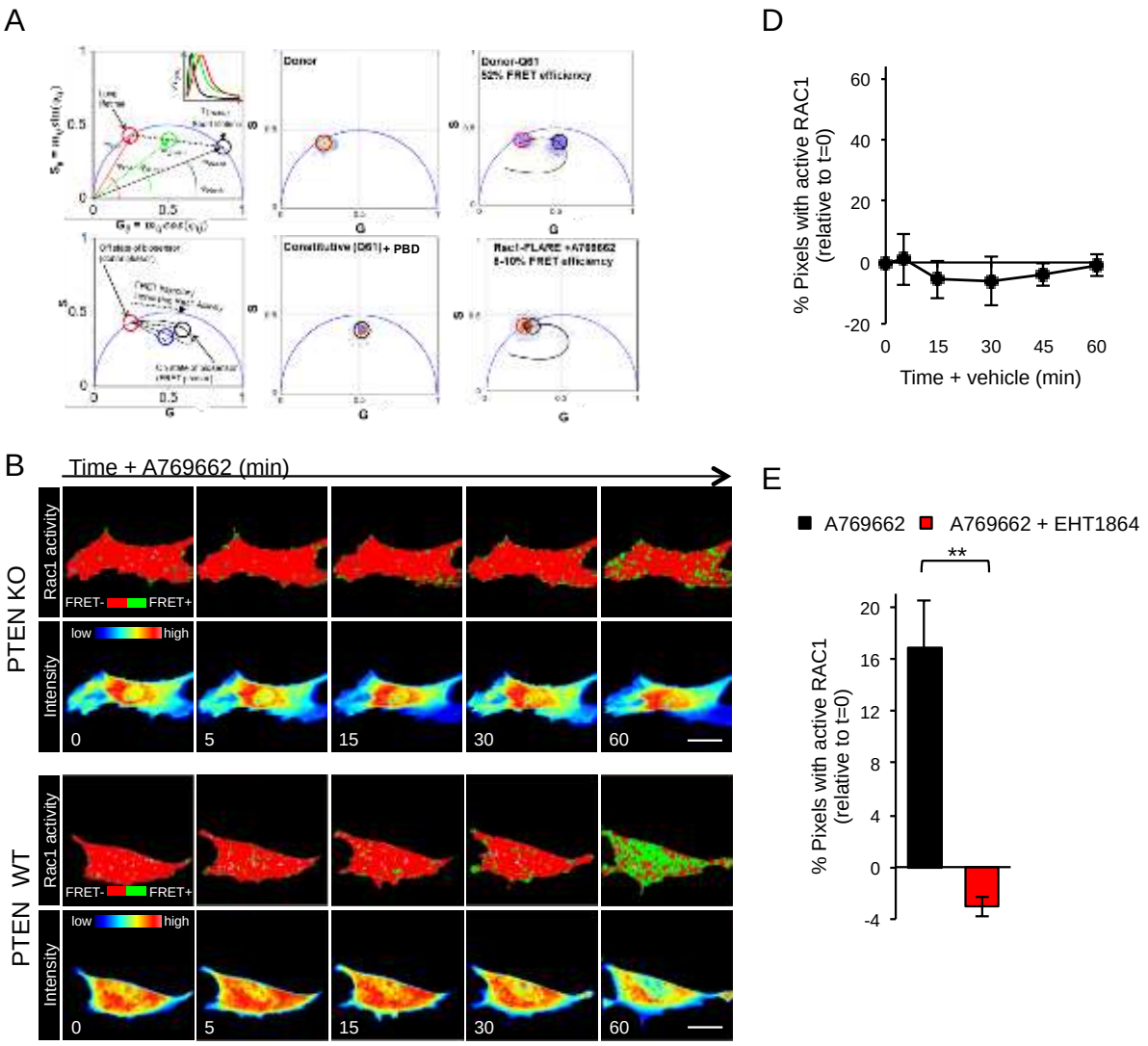

Supplementary Figure S5

Supplementary Figure S5, Related to Figure 2.2. Analysis of RAC1 biosensor activation by A769662 in MEFs. A) Phasor plot analysis of RAC1 biosensor activity in PTEN KO MEFs. Left top: Phasor plot representation of two simulated fluorescence lifetime decays. Left bottom: FRET analysis represented on the phasor plot. Red cursor indicates the off-state of the inactive RAC1 biosensor (unquenched donor), black cursor indicates maximal on-state of constitutively-active RAC1 biosensor (quenched donor), and blue cursor indicates the position of cellular autofluorescence. From these positions on the phasor plot, the theoretical FRET trajectory of RAC1 biosensor was identified (curved black line). Tracking the FRET trajectory allows for translation of the lifetime shift to FRET efficiency. Middle: Positions of the unquenched donor (top) or quenched donor (bottom) on the phasor plot. Right: FRET efficiency calculated by the trajectory of donor to constitutively-active RAC1 biosensor (top) and FRET efficiency of the RAC1 FLARE biosensor upon the addition of A769662 (bottom). **B)** RAC1 activation in PTEN KO and WT MEFs over time after addition of A769662 (50 µM). Top: Pseudo-color representation of RAC1 activity (FLIM-FRET). Bottom: RAC1 biosensor intensity. The field of view is 74.6 µm x 74.6 µm. Scale bars, 20 µm. **C)** Western blot showing kinetics of AMPK activation in PTEN WT or KO cells treated with A769662 (50 µM). **D)** PTEN KO MEFs were transfected with FLARE RAC1 constructs and imaged by FLIMFRET. Cells were treated with medium containing DMSO vehicle and imaged at 5, 15, 30, 45, and 60 minutes following addition. The amount of pixels that contain active RAC1 are plotted as a percentage of the total pixels of the cell. (n=3). **E)** PTEN KO MEFs were transfected with FLARE RAC1 constructs and imaged by FLIM-FRET. Following addition of A769662 for 60 minutes, the RAC1 inhibitor EHT1864 was added to block FRET. After 15 minutes with EHT1864 (50 µM), cells were imaged. The amount of pixels that contain active RAC1 are plotted as a percentage of total pixels of the cell. Mean ± SEM shown; **, $P \leq 0.01$ with an unpaired t test (A769662: n=7; A769662 + EHT1864: n=3).

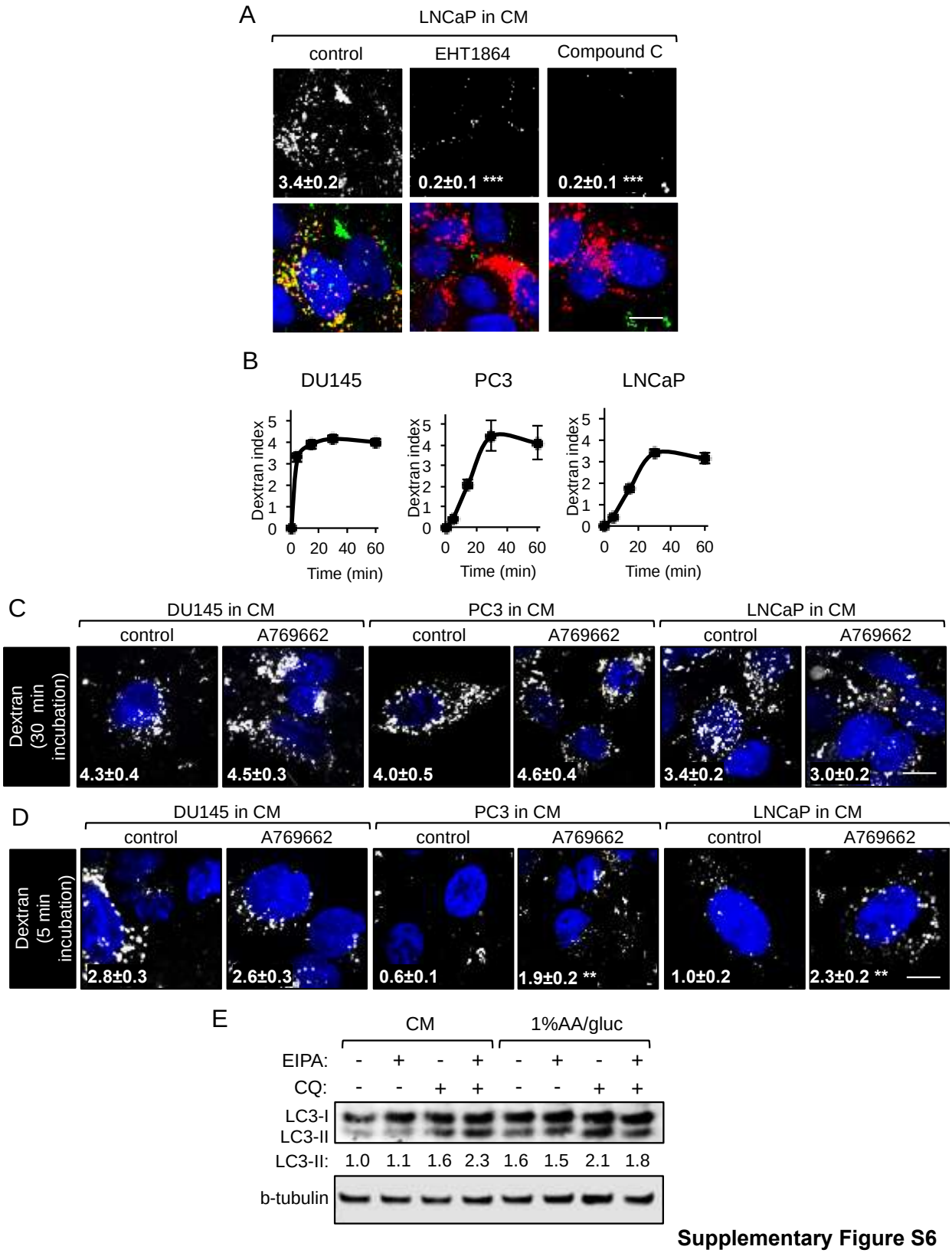

Supplementary Figure S6

Supplementary Figure S2.6, related to Figure 2.2. AMPK promotes macropinocytosis in prostate cancer. A) Dextran uptake in LNCaP cells in CM ± pre-treatment (2 h) with EHT1864 (50 µM). **B**) Prostate cancer cells were pulsed with dextran for the indicated intervals (0, 5, 15, 30 and 60 min) and dextran uptake quantified. In each cell line, steady state was reached by 30 min. **E,F**) Dextran uptake in prostate cancer cells in complete medium ± A769662 (50 µM) after 30 min (E) or 5 (F) min incubation with dextran. Mean ± SEM shown. Scale bars, 20 µM. Dextran index indicated in white in images. ≥ 25 cells were examined except for (F) where 15 cells evaluated. G) Western blot PC3 cells after 1 h in the indicated medium ± chloroquine (CQ, 25 µM). LC3-II was quantified using LICOR software.

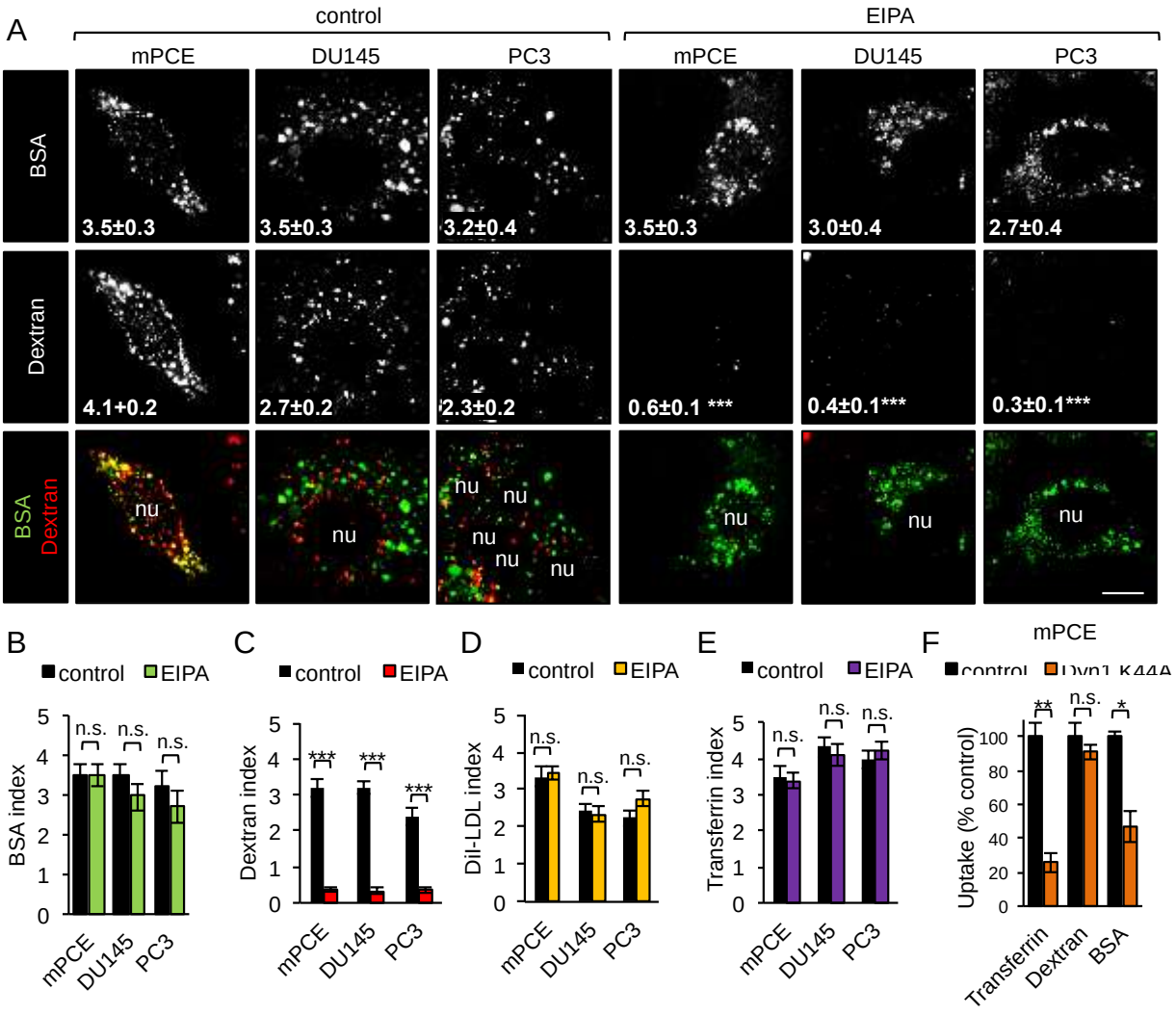

Supplementary Figure S2.7, related to Figure 2.2. AMPK promotes macropinocytosis in prostate cancer. A) Alexa 488 BSA or Texas Red dextran uptake in prostate cancer cells ± EIPA (50-75 μM). **B,C)** Quantification of (A). **D)** Dil-LDL uptake ± EIPA (50-75 μM). **E)** Transferrin-488 uptake ± EIPA (50-75 μM). **F)** BSA, dextran, and transferrin uptake in mPCE cells ± DN dynamin1 (Dyn1 K44A). Nu, nucleus. Dextran or BSA Index shown in white. Scale bar 20 μm. Means ± SEM shown, ≥ 15 cells were examined. Using paired two-tailed t test, *, P ≤ 0.05; **, P ≤ 0.01; ***, P ≤ 0.001; n.s., not significant.

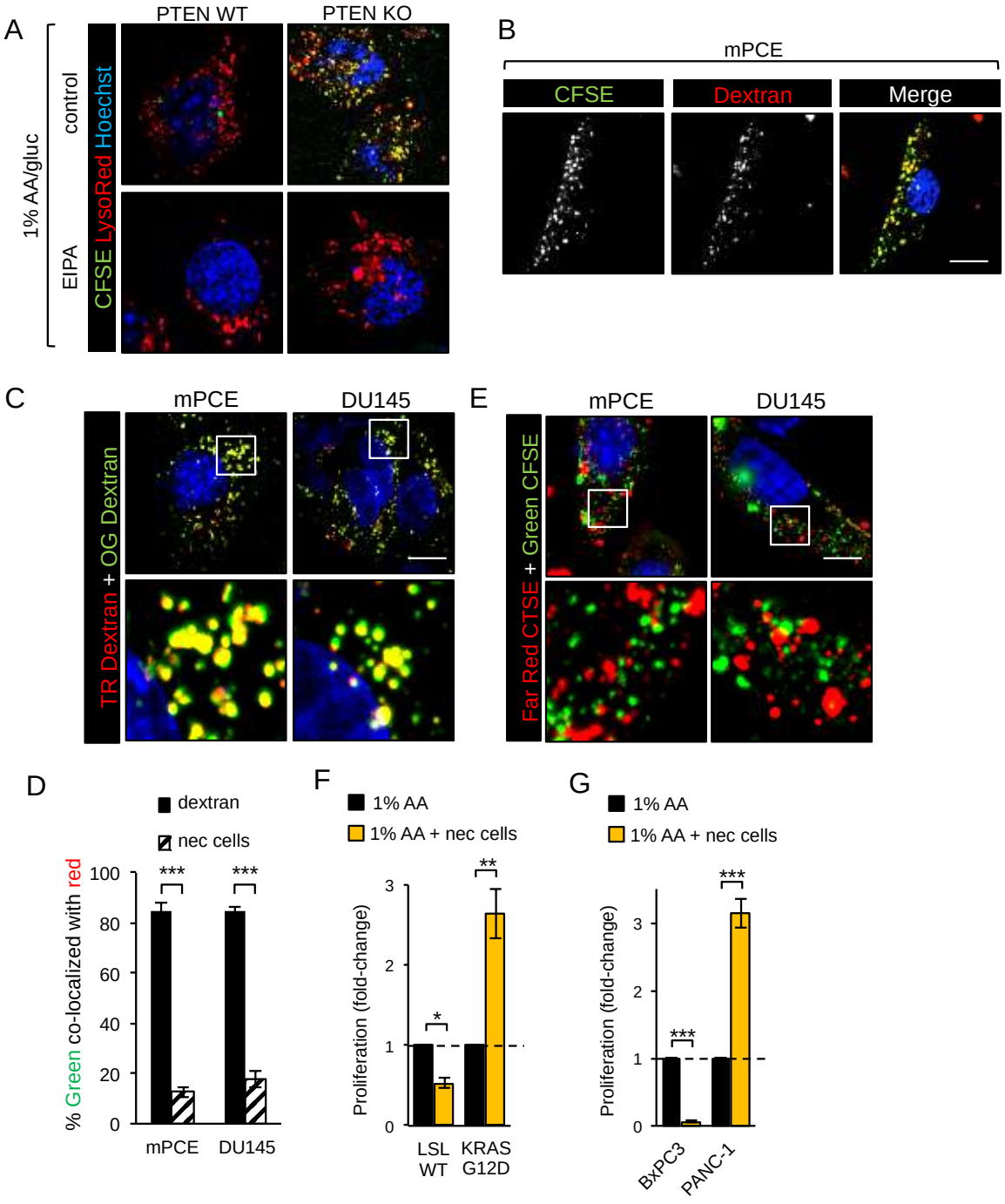

Supplementary Figure S8

Supplementary Figure S2.8, related to Figure 2.5. Necrotic debris is taken up through macropinocytosis in prostate cancer cells. A) CFSE-labeled necrotic cell debris uptake in PTEN WT and KO MEFs in 1% AA/gluc ± EIPA (50 μM). **B**) Green CFSE-labeled necrotic cell debris and Texas Red Dextran uptake in mPCE cells in CM. **C**) Texas Red- and Oregon Green-dextran were added together to mPCE prostate cancer cells in CM and uptake measured after 30 min. **D**) As in (B) except Far Red CTSE- and green CFSE-labeled necrotic cell debris were added instead of dextran. **E**) Quantification of green pixels co-localized with red pixels within cells in (C and D). **F**) Proliferation of control LSL or KRAS G12D MEF after 72 h in 1% AA/gluc ± necrotic debris (0.1% protein). **G**) Proliferation of BxPC3 or PANC-1 cells after 96 h in 1% AA ± necrotic debris (0.1% protein). Scale bars, 20 μm. n ≥ 3 in panels F,G**.** For imaging ≥ 25 cells were examined. Using a paired, two-tailed t test, *, $P \leq 0.05$; **, $P \leq 0.01$; ***, $P \leq 0.001$.

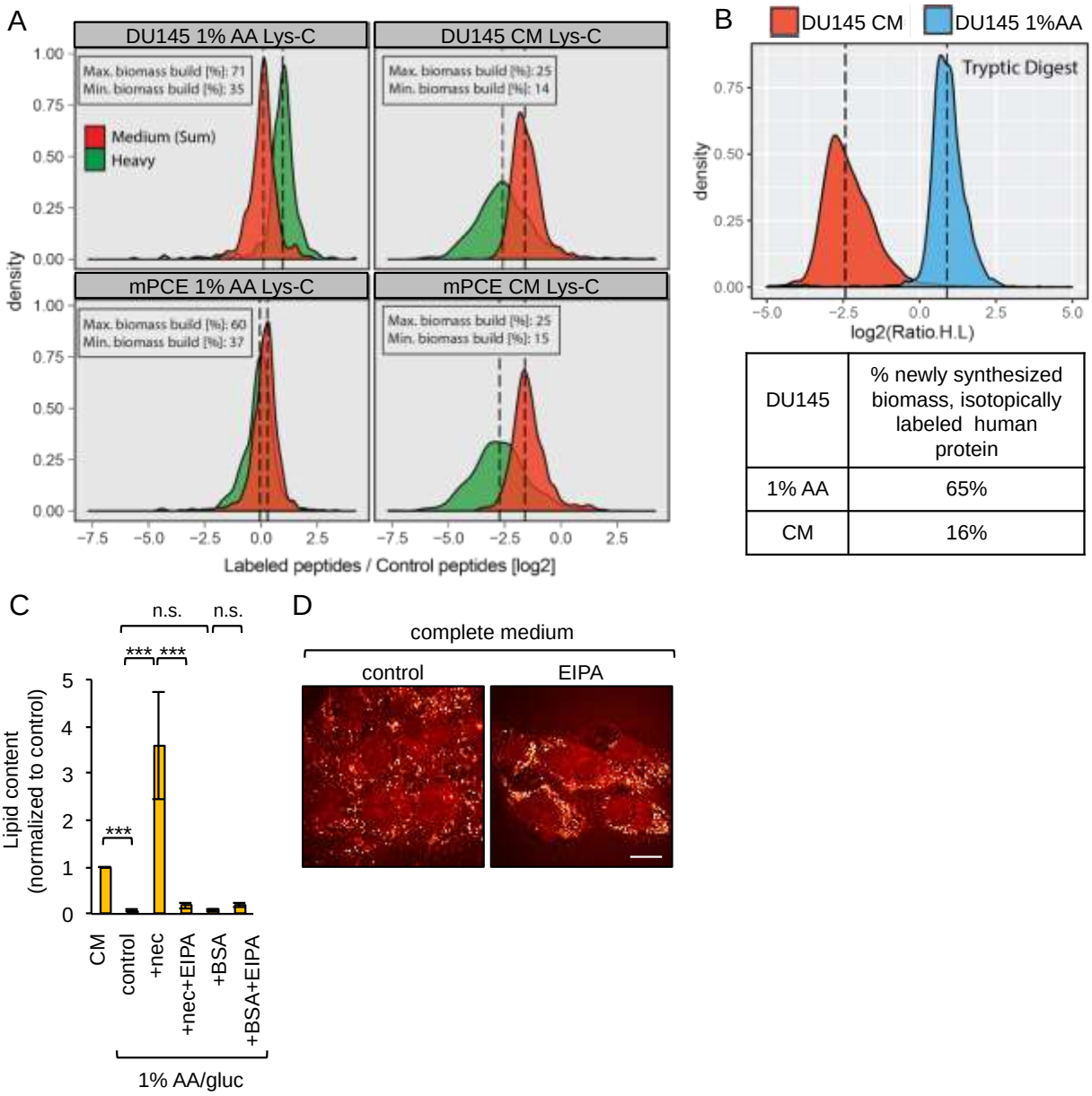

DU145	% newly synthesized biomass, isotopically labeled human protein
1% AA	65%
CM	16%

Supplementary Figure S2.9, related to Figure 6. Macropinocytosis is used to build biomass. A) Measured ratio distributions resulting from Lys-C digests that were used to calculate median biomass in Figures 6D-E. Distribution represents counts versus log2 fold change of peptide ratios measured for medium (red, sum of K4R0 and K0R10 mixed peak ratios) or heavy peptides (green, K4R10) in Lys-C digests. **B)** Tryptic digests of human DU145 cells were used to confirm Lys-C results (Figures 6D-E). Distributions depict SILAC ratios measured in peptides arising from proteins unique to humans in an Andromeda search. The incorporation of isotopically labeled amino acids into 65% of the human peptides in 1% AA medium and 16% in CM is consistent with biomass build estimates using Lys-C digestion. **C)** Quantification of lipid droplets detected by CARS in Figure 6F. **D)** DU145 cells were cultured in complete medium ± 50

μM EIPA for 24 h and fixed with 4% PFA. Lipid droplets were imaged by CARS. ≥ 25 cells were examined. Using a paired, two-tailed t test, *, P ≤ 0.05; **, P ≤ 0.01; ***, P ≤ 0.001, n.s. not significant. Tukey's test was used to correct for multiple comparisons in (C). Scale bar, 20 μm.

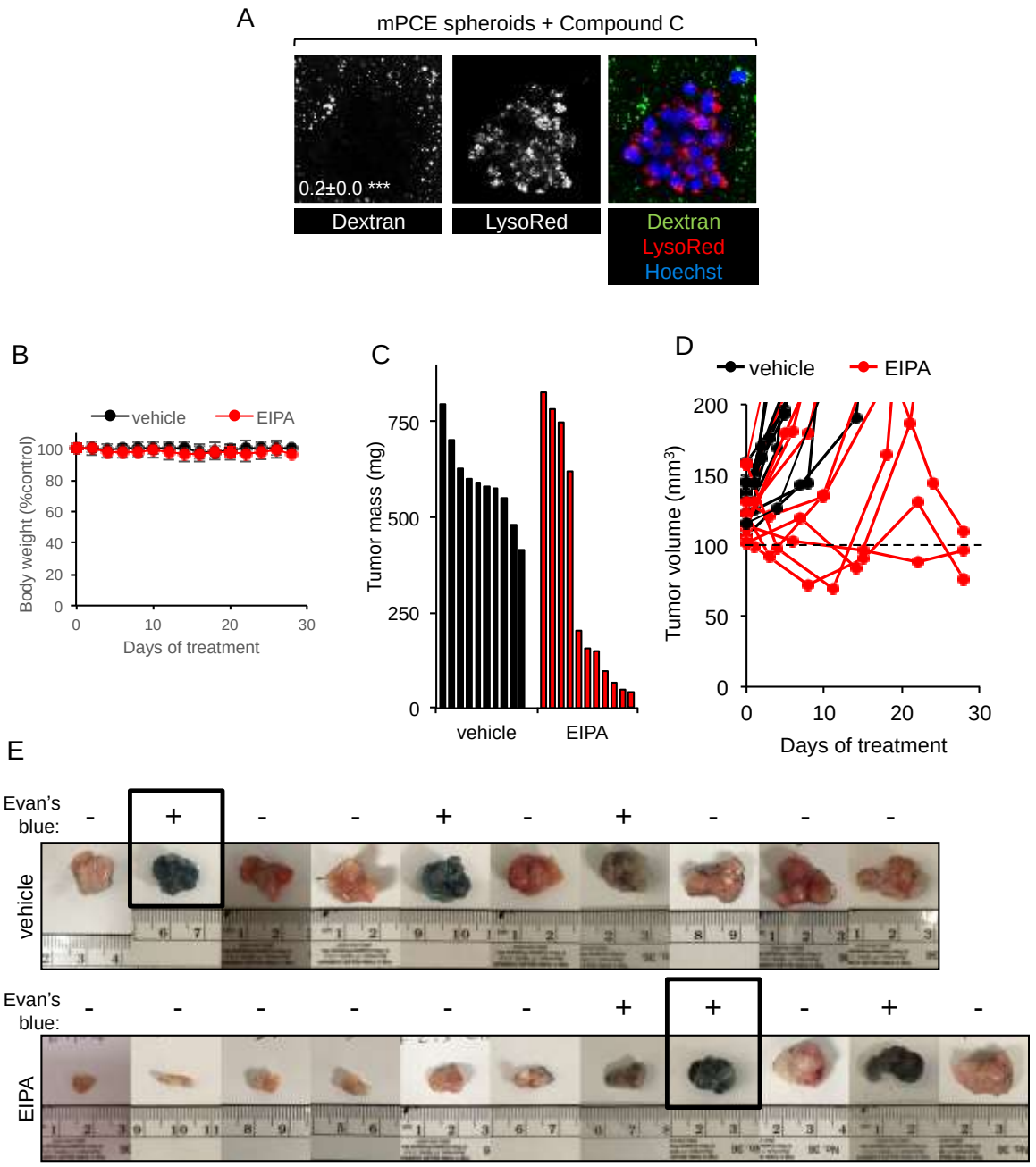

Supplementary Figure S10

Supplementary Figure S2.10: Inhibiting macropinocytosis reduces prostate tumor growth, Related to Figure 7. A) Dextran uptake in mouse prostate tumor organoids ± Compound C (20 μM). **B-D**) Body weight (B), tumor weight at sacrifice (C), or tumor volume measured with calipers (D) in C57BL/6 mice with subcutaneous mPCE isograft tumors treated with vehicle (1% DMSO in PBS) or EIPA (7.5 mg/kg) subcutaneously every other day once tumors reached 100 mm^3. Panel (D) is the same as Figure 7F but displayed with a Y-axis that allows discrimination of tumor regressions. **E**) mPCE isograft tumors excised from mice in (B-D). Tumors that are blue were from mice intravenously co-injected with FITC-Ficoll and Evan's blue dye prior to sacrifice. Evan's blue dye was used to confirm successful i.v. injection of Ficoll and delivery to tumors even in mice where EIPA blocked tumor cell macropinocytosis. Boxed images indicate tumor samples used in Figure 2.7H.

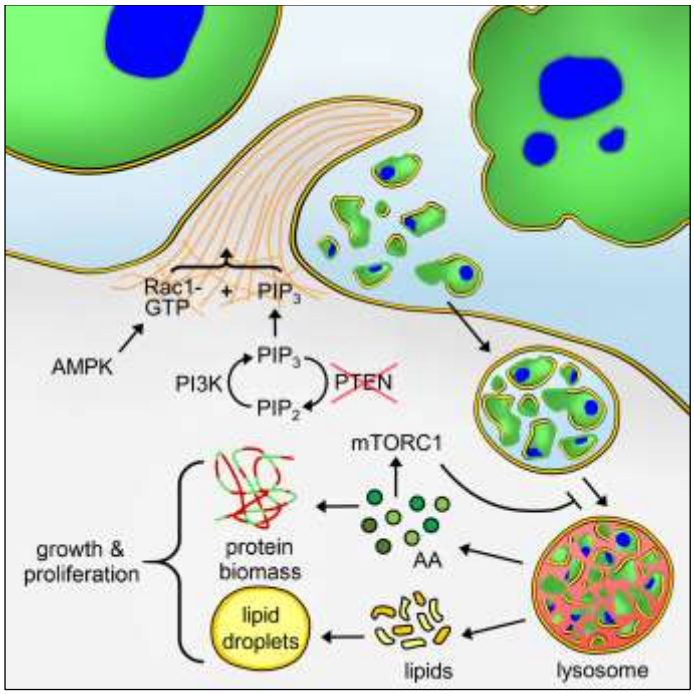

Supplementary Figure S2.11. Model Figure. PTEN-deficiency induces AMPK-dependent macropinocytosis that allows the conversion of necrotic debris into amino acids and lipids used to drive growth. Intact cells are too large to enter but extracellular proteins may also be engulfed.

CHAPTER 3

Macropinocytosis supports mammary tumor growth and confers resistance to therapies targeting cancer anabolism

Contributions:

The study was conceived by ALE and me. Experiments were designed by me and ALE. All experiments were carried out by me. Data were analyzed and interpreted by me and ALE. Manuscript was prepared by me and ALE.

Macropinocytosis confers resistance to therapies targeting cancer anabolism

Vaishali Jayashankar and Aimee L. Edinger

Department of Developmental and Cell Biology, University of California Irvine, Irvine, CA 92697

[*Keywords:* macropinocytosis, necrocytosis, PI3 kinase, PTEN, KRAS, cancer metabolism, necrosis, breast cancer, nutrient scavenging, click chemistry, drug resistance, fatty acid synthase, nucleotide synthesis, radiation, doxorubicin, 5-FU, and gemcitabine]

Corresponding author:

Aimee L. Edinger
2128 Natural Sciences I
University of California, Irvine
Irvine, CA 92697
aedinger@uci.edu

ABSTRACT

KRAS-driven pancreas and PTEN-deficient prostate tumors use macropinocytosis to scavenge extracellular proteins and proliferate in amino acid-deficient media. Here we show that breast cancer cell lines with activating mutations in KRAS or the PI3K pathway use macropinocytosis to proliferate under multiple forms of nutrient stress. A click chemistry-based flux assay revealed that macropinocytosis of dead cell debris provides not just amino acids, but also sugars, fatty acids, and nucleotides that can support biosynthesis. In fact, macropinocytic breast and prostate cancer cells became resistant to fatty acid synthesis inhibition when supplemented with necrotic debris consistent with their ability to recover palmitate, the product of fatty acid synthase. Strikingly, supplementation with necrotic debris conferred near complete resistance to multiple standard-of-care chemotherapies that inhibit and/or create dependence on nucleotide biosynthesis provided that cells were macropinocytic. These findings imply that macropinocytosis plays a much larger role in tumor anabolism than previously appreciated and define a novel mechanism for therapeutic resistance.

INTRODUCTION

Because oncogenic mutations constitutively drive anabolism, cancer cells require continuous access to extracellular nutrients for their survival [1]. At the same time, nutrient delivery to tumor cells is limited by abnormal, leaky vasculature and high interstitial pressure that collapses blood vessels, further compromising perfusion. These limitations make tumor cells reliant on the catabolic process of autophagy [2]. While macroscopic tumor growth depends on autophagy because it keeps tumor cells alive, tumor cell catabolism produces atrophy, not growth. For nutrient-deprived tumor cells to proliferate, they must complement nutrient recycling via autophagy with the scavenging of macromolecules from the microenvironment [1]. Because scavenged nutrients are derived from extrinsic, rather than intrinsic, macromolecules, they can support proliferation as well as survival [3]. Macropinocytosis is one scavenging strategy [1]. Macropinosomes form when plasma membrane ruffles close on themselves and pinch off, producing large, uncoated intracellular vesicles encapsulating extracellular proteins, fluid, and small particles. Oncogenic mutations in RAS or activation of the phosphoinositide 3-kinase (PI3 kinase) pathway can drive macropinocytosis [3-5]. The RAC1 activation required for ruffling can occur via phosphatidylinositol-(3,4,5)-trisphosphate (PIP_3) dependent guanine nucleotide exchange factors [6], downstream of AMP-sensitive kinase (AMPK) [3], or through alternative mechanisms. PIP_3 is also required for macropinosome closure [7]. Pancreas and prostate cancers bearing oncogenic mutations in KRAS or PTEN, respectively, use amino acids derived from engulfed extracellular proteins to proliferate in nutrient-limiting environments [3, 4, 8-10]. PI3 kinase pathway mutations are also common in breast cancer [11]. While macropinocytosis

has not yet been described in this cancer class, breast tumors would likely benefit from macropinocytosis. Desmoplasia, excessive fibrosis that limits perfusion, creates a selective pressure that would favor the outgrowth of breast cancer cells that are capable of nutrient scavenging [12]. Necrosis is a common feature of invasive breast cancer; breast tumor growth often outstrips the vasculature leaving tumor cells nutrient-limited [13]. Necrotic cell debris consumed via macropinocytosis could sustain protein synthesis in poorly perfused areas where extracellular amino acids would be limiting [3].

Many standard-of-care chemotherapeutics kill tumor cells by creating nutrient stress [14]. Some of these agents target enzymes required for de novo nucleotide synthesis, while others cause DNA damage that increases the demand for nucleotides for DNA repair [15]. Autophagy can supply cells with recycled nucleotides and confers resistance to both chemotherapy and radiation [16, 17]. By providing amino acids, macropinocytosis might also confer resistance to therapies that increase the demand for nucleotides by fueling de novo nucleotide synthesis pathways. If macropinocytic cells could produce nucleotides directly from scavenged DNA, even greater protection might be observed because the energetic cost of nucleotide synthesis would be avoided. Necrocytosis, the macropinocytosis of necrotic cell debris, could in principle supply the end-products of all biosynthetic pathways. Because nutrients supplied by necrocytosis would be derived from cell-extrinsic sources rather than catabolism, they could support not only survival, but even allow proliferation in cells exposed to chemotherapies that target metabolism. Here we demonstrate that breast cancer cell lines with oncogenic mutations that activate KRAS or the PI3K pathway can use macropinocytosis to fuel proliferation in

nutrient-limiting conditions. Moreover, macropinocytic breast cancer cells that are able to scavenge not just amino acids, but also sugars, lipids, and nucleotides from necrotic cell debris exhibited dramatic resistance to a range of therapies targeting the metabolic dependencies of cancer cells.

RESULTS

Macropinocytosis supports anabolism in amino acid-deprived breast cancer cells

To determine whether breast cancer cells with activating mutations in KRAS and PIK3CA or the loss of PTEN are macropinocytic, 70 kD dextran uptake was measured in a panel of breast cancer cell lines. Because nutrient stress is required to induce macropinocytosis in some cells [3], experiments were conducted in both complete and nutrient-deficient medium containing 1% the normal level of amino acids and glucose (1% AA/gluc). To confirm that dextran uptake occurred via macropinocytosis, 5-[N-ethyl-N-isopropyl] amiloride (EIPA), an Na^+/H^+ exchanger (NHE) inhibitor that blocks macropinocytosis but not receptor-mediated endocytosis [3, 18], was used to block dextran uptake. Immortalized but non-transformed hTERT-HME1 mammary epithelial cells and MCF10A cells did not exhibit macropinocytosis in complete medium, but dextran uptake was stimulated by nutrient deprivation (Fig. 3.1a and Supplementary Fig. 3.1a). Similar to pancreas, bladder, and lung cancer cell lines with KRAS mutations [3, 4], KRAS-mutant MDA-MB-231 breast cancer cells were robustly macropinocytic in complete medium (Fig. 3.1a and Supplementary Fig. 3.1a). MCF-7 and T-47D cells with $PIK3CA^{E545K}$ and $PIK3CA^{H1047R}$ mutations, respectively, also efficiently took up high molecular weight dextran in both complete and 1% AA/gluc medium. Hs578T breast cancer cells carry a

mutation in the PI3K regulatory subunit p85α, PIK3R1, that leads to hyper-activation of the PI3K pathway. Like MCF-7 and T-47D cells, Hs578T cells exhibited constitutive macropinocytosis. PTEN-null BT-459 breast cancer cells exhibited constitutive macropinocytosis similar to PTEN-deficient prostate cancer cells [3] (Fig. 3.1a and Supplementary Fig. 3.1a). In contrast, PTEN-null HCC1569 cells did not exhibit macropinocytosis even under nutrient stress, although they were capable of performing macropinocytosis when stimulated with phorbol 12-myristate 13-acetate (PMA), an inducer of robust macropinocytosis in multiple cell types (Fig. 3.1a and Supplementary Fig. 3.1a, b). 4T1 murine mammary carcinoma cells, a commonly used model for triple-negative breast cancer [19, 20], were also evaluated. While not macropinocytic in complete medium, glucose restriction or directly activating AMPK with A769662 stimulated macropinocytosis in 4T1 cells (Fig. 3.1a and Supplementary Fig. 3.1a,c). EIPA-sensitive 70 kD FITC-Ficoll uptake was observed in orthotopic, syngeneic 4T1 tumors in female BALB/c mice indicating that the level of AMPK activation in tumors is sufficient to trigger macropinocytosis (Fig. 3.1b). Together, these results suggest that many breast tumors are macropinocytic.

Prostate and pancreas cancer cell lines can support proliferation in amino acid-limiting conditions with macropinocytosis [3, 4, 9]. In most of these studies, albumin is provided as a macropinocytic fuel source as it is one of the most abundant extracellular proteins in tumors. However, physiological levels of bovine serum albumin (BSA, 5%) did not support the proliferation of constitutively macropinocytic MCF-7 or T-47D cells or non-macropinocytic HCC1569 cells in medium containing 1% of the normal amount of amino

acids (1% AA, Fig. 3.1c). BSA can only provide amino acids in proportion to their presence in its primary sequence, a ratio that may not be ideal to support global protein synthesis. Necrotic cell debris is also consumed by macropinocytosis. Upon digestion in the lysosome, dead cell fragments will provide amino acids at the ratio they are present in cellular proteins. As expected, breast cancer cells were able to consume necrotic, but not apoptotic or live, CFSE-labeled cells (Fig. 3.1d-f), a process we have termed necrocytosis [3]. Necrotic cell debris supported the proliferation of macropinocytic (MCF-7 and T-47D) breast cancer cells in 1% AA medium even when provided at a 25-fold lower concentration than BSA (0.2% protein, Fig. 3.1c). Non-macropinocytic HCC1569 cells did not benefit from supplementation with necrotic debris. Moreover, apoptotic cells, which are too large to be consumed by macropinocytosis, did not support the proliferation of macropinocytic MCF-7 breast cancer cells under the same conditions (Fig. 3.1f,g). These studies confirm that the rate of macropinocytic flux in amino acid-limited breast cancer cells is sufficient to support proliferation, that necrotic cell debris is a superior fuel source compared to albumin, and that the nutrients contained in necrotic debris are only accessible to macropinocytic cells.

Using click chemistry to measure protein flux through macropinocytosis

For macropinocytosed proteins to support protein synthesis in a nutrient-deprived cell, four processing steps are required: uptake, trafficking to the lysosome, lysosomal proteolysis, and export of the monomeric amino acids to the cytosol [1]. The transfer of isotopically-labeled amino acids from the necrotic cells' proteome into the macropinocytic cells' proteome requires that each of these steps is completed and is

therefore a holistic measurement of macropinocytic flux [3]. Although highly specific and quantitative, this approach requires relatively expensive labeling medium and proteomics capabilities that are not readily accessible to all laboratories. Copper-catalyzed azido-alkyne cycloaddition, a common form of “click” chemistry [21], offers an alternative strategy for measuring macropinocytic flux (Fig. 3.2a). A “clickable” alkynyl form of methionine, homopropargylglycine (HPG), is commercially available, inexpensive, and readily incorporated into proteins [22]. HPG can be followed using azido-modified reagents. For example, HPG derived from necrocytosed proteins can be visualized in the macropinocytic cell proteome by microscopy after clicking on azido-biotin and staining with Alexa488-streptavidin.

To validate this new strategy for measuring macropinocytic flux, HPG-labeled FL5.12 murine hematopoetic cells were generated (Fig. 3.2b). FL5.12 cells are ideally suited for creating labeled, necrotic debris due to their rapid growth (doubling time of 12 h) and their strict dependence on exogenous IL-3 for survival which allows for the induction of apoptosis and secondary necrosis without the application of noxious chemicals. As expected, adding free HPG to amino acid-deprived MCF-7 (macropinocytic) or HCC1569 (non-macropinocytic) cells also resulted in robust labeling of cytosolic and nuclear proteins (Fig. 3.2c). In contrast, when HPG was provided in the form of labeled necrotic debris, only macropinocytic MCF-7 cells were labeled. At 1 h, HPG labeling was confined to macropinosome-like structures distributed throughout the cytosol (Fig. 3.2d). Confirming that necrotic debris was consumed via macropinocytosis, the HPG-positive structures in MCF7 cells were eliminated by EIPA, and no HPG labeling was

observed in non-macropinocytic HCC1569 cells incubated with HPG-labeled necrotic debris (Fig. 3.2d-f). After 24 h, the HPG signal in MCF-7 cells was distributed throughout the nucleus and cytosol, producing a pattern similar to that seen in MCF-7 cells labeled with free HPG (Fig. 3.2c, g). Blocking macropinocytosis with EIPA prevented the transfer of HPG from necrotic cell debris into the macropinocytic MCF-7 proteome (Fig. 3.2g, h). Blocking protein synthesis with cycloheximide resulted in a diffuse cytosolic staining pattern in MCF-7 cells fed HPG-labeled necrotic debris confirming that new protein synthesis was required for HPG labeling of nuclear and cytosolic proteins in macropinocytic cells. Non-macropinocytic HCC1569 breast cancer cells did not incorporate HPG from necrotic debris even when the incubation period was extended to 24 h (Fig. 3.2h, i). In summary, a clickable amino acid tracer can be used to monitor macropinocytic flux and confirmed that nutrient-deprived, macropinocytic breast cancer cells can fuel new protein synthesis with proteins scavenged from dead cell corpses.

Necrocytosis provides access to carbohydrates

Several studies have demonstrated that amino acids can be scavenged from macropinocytosed proteins [3, 4, 8, 9, 23]. However, necrotic cell debris contains all of the building blocks necessary to produce a new cell provided that each macromolecule can be broken down in the lysosome and the subunits exported to the cytosol. Cancer cells import and oxidize glucose to generate ATP, but glucose is also funneled into the hexosamine biosynthesis pathway to produce N-acetylglucosamine (GlcNAc) required for protein O-GlcNAcylation reactions [24]. To assess whether GlcNAc, and potentially

other carbohydrates, can be scavenged via necrocytosis, FL5.12 cells were labeled with a clickable, alkynyl form of GlcNAc, tetraacylated N-(4-pentynoyl)-glucosamine (Ac_4GlcNAl) (Fig. 3.3a, [25]). The acetyl groups on Ac_4GlcNAl increase the membrane permeability of this unnatural sugar but are removed by carboxyesterases in the cytosol, generating the monosaccharide. FL5.12, MCF-7, and HCC1569 cells all labeled efficiently with free Ac_4GlcNAl, producing labeling patterns consistent with the wide range of membrane, cytosolic, and nuclear proteins that undergo O-GlcNAcylation (Fig. 3.3a, b, [26]). Macropinocytic MCF-7 breast cancer cells, but not non-macropinocytic HCC1569 cells, were able to recover GlcNAl from labeled necrotic cell debris, producing a staining pattern similar to that observed upon free Ac_4GlcNAl addition (Fig. 3.3b-e). Blocking macropinocytosis with EIPA significantly reduced GlcNAl flux from necrotic debris into MCF-7 cells (Fig. 3.3c, d). As EIPA completely blocked HPG incorporation from labeled necrotic debris under similar experimental conditions (Fig. 3.2g, h), MCF-7 cells may secrete enzymes that liberate free GlcNAl from necrotic debris. As non-macropinocytic HCC1569 breast cancer cells did not label when incubated with GlcNAl-labeled necrotic cell debris (Fig. 3.3d, e), enzymes that release free GlcNAl are not present in the necrotic debris itself. The ability to scavenge carbohydrates may contribute to the ability of macropinocytic MCF-7 and T-47D, but not non-macropinocytic HCC1569, cells to proliferate in low glucose medium (1% AA/gluc) in the presence of necrotic debris (Fig. 3.3f). In summary, GlcNAc can be scavenged from necrotic material via macropinocytosis.

Necrocytosis relieves dependence on fatty acid synthesis

While necrocytosis preserves lipid droplets in nutrient-restricted prostate cancer cells [3], it is not clear whether lipids can be directly scavenged from cell corpses or whether scavenging of other nutrients simply reduces ATP demand and, consequently, lipid catabolism in the macropinocytic cell. To directly monitor lipid flux from necrotic cell debris into macropinocytic breast cancer cells, FL5.12 cells were labeled with alkynyl palmitate, a fatty acid used for fatty acid oxidation, post-translational protein modifications, and to build cell membranes [27]. FL5.12, MCF-7, and HCC1569 cells labeled efficiently with free alkynyl palmitate (Fig. 3.4a, b). Similar to results with HPG and GlcNAl (Fig. 3.2 and 3.3), macropinocytic MCF-7, but not non-macropinocytic HCC1569, breast cancer cells recovered alkynyl palmitate from labeled necrotic debris (Fig. 3.4c, d and Supplementary Fig. 3.2). Inhibiting macropinocytosis with EIPA eliminated labeling in MCF-7 cells confirming that macropinocytosis was required. Thus, necrocytosis can provide macropinocytic breast cancer cells with palmitate and likely other fatty acids. Fatty acid synthesis is critical for tumor cell growth [14]. Fatty acid synthase (FASN) is over-expressed in some breast tumors [28], and FASN inhibition limits breast tumor growth [29, 30]. As macropinocytic breast cancers can scavenge the product of FASN, palmitate, from necrotic cell debris (Fig. 3.4c, d), necrocytosis may reduce dependence on FASN and sensitivity to FASN inhibitors. The FASN inhibitor GSK2194069 [31] killed MCF-7 cells and slowed the proliferation of HCC1569 breast cancer cells (Fig. 3.4e, f). Consistent with the proposal that palmitate scavenging would reduce dependence on FASN, supplementation with necrotic cell debris rescued macropinocytic MCF-7, but not non-macropinocytic HCC1569, breast cancer cells from GSK2194069. Prostate cancers both over-express FASN [32, 33] and depend on fatty acid

uptake [34]; blocking either process limits prostate cancer cell growth and survival. PTEN-deficient prostate cancers (e.g. LNCaP) are macropinocytic [3], while PTEN-replete 22Rv1 prostate cancer cells are not (Fig. 3.4g). Both LNCaP and 22Rv1 prostate cancer cells died when exposed to the FASN inhibitor GSK2194069 (Fig. 3.4h, i). Similar to results with breast cancer cells, macropinocytic LNCaP cells, but not non-macropinocytic 22Rv1 cells, were rescued by supplementation with necrotic cell debris. These results demonstrate that necrocytosis provides fatty acids and affords resistance to therapeutics that limit lipid biosynthesis.

Necrocytosis affords resistance to therapies that increase dependence on nucleotide synthesis

Nucleotide synthesis represents a metabolic bottleneck for rapidly proliferating cancer cells [14]. Amino acids derived from macropinocytosed proteins could be used to support nucleotide synthesis. Alternatively, scavenging nucleotides via necrocytosis would avoid energetically-demanding biosynthesis. When the alkynyl thymidine analog 5-ethynyl-2-deoxyuridine (EdU) [35] was added to the culture medium, it was readily incorporated into the genomic DNA of FL5.12, MCF-7, and HCC1569 cells as expected (Fig. 3.5a, b). Akin to results obtained with HPG, GlcNAl, and alkynyl palmitate, macropinocytic MCF-7 cells, but not non-macropinocytic HCC1569 cells, were able to recover EdU from necrotic cell debris (Fig. 3.5c-e). Blocking macropinocytosis with EIPA prevented the transfer of EdU from necrotic cell debris to MCF-7 cells, again implicating macropinocytosis in this process. Blocking DNA replication with hydroxyurea [36] also eliminated the nuclear EdU signal in MCF-7 cells, confirming that EdU was incorporated

into genomic DNA. In sum, macropinocytic cells can recover nucleotides directly from necrotic debris.

Many conventional cancer therapies target nucleotide biosynthesis directly or indirectly [37, 38]. Agents such as 5-FU and gemcitabine block nucleotide biosynthesis, while DNA damaging agents increase dependence on nucleotide synthesis necessary to support DNA repair. Many different solid tumors initially respond to genotoxic chemotherapies, but resistance frequently develops. Metabolic adaptations include the up-regulation of de novo nucleotide synthesis pathways, nutrient import, and recycling via autophagy [15, 17, 39]. By providing breast cancer cells with scavenged nucleotides (Fig. 3.5), necrocytosis may also contribute to resistance to standard-of-care therapies that deplete nucleotide pools. Breast cancer is often treated with the pyrimidine analog 5-fluorouracil (5-FU) that inhibits thymidylate synthase [40]. MCF-7 cells died when treated with 5-FU while HCC1569 cells stopped proliferating (Fig. 3.6a, b). Supplementation with necrotic cell debris afforded striking protection to 5-FU-treated macropinocytic MCF-7 cells, restoring proliferation to the level seen in untreated cells. As necrotic cell debris did not protect HCC1569 cells, the debris is not simply reducing toxicity by sequestering 5-FU. Like 5-FU, gemcitabine blocks nucleotide synthesis, but in this case by inhibiting ribonucleotide reductase [40]. Gemcitabine is a standard-of-care treatment for pancreas cancer, a tumor type that is frequently macropinocytic. Gemcitabine killed both macropinocytic PANC-1 and non-macropinocytic BxPC3 cells (Fig. 3.6c, d). Supplementation with necrotic cell debris fully restored proliferation in PANC-1 cells while failing to benefit BxPC3 cells that are incapable of necrocytosis [3] (Fig. 3.6c, d).

The ability of necrocytosis to protect from DNA damaging agents was next evaluated. Doxorubicin and cisplatin stimulated macropinocytosis in contextually macropinocytic 4T1 cells (Fig. 3.7a). These agents are known to stimulate ROS which can stimulate AMPK activation. ROS was sufficient to stimulate macropinocytosis in an AMPK dependent manner (Fig. 3.7b). The topoisomerase inhibitor doxorubicin also induces DNA damage [43]. Doxorubicin triggered cell death in MCF-7, MDA-MB-231, and HCC1569 breast cancer cells (Fig. 3.7c). Necrotic cell debris prevented death in both of the macropinocytic cell lines, MCF-7 and MDA-MB-231, while non-macropinocytic HCC1569 cells remained fully sensitive to doxorubicin. Radiation has been reported to increase AMPK activation [41, 42], and γ-irradiation stimulated macropinocytosis in 4T1 cells even though they were maintained in complete medium (Fig. 3.7d). While the human breast cancer cell lines MCF-7, MDA-MB-231, and HCC1569 were resistant to γ-irradiation (not shown), murine 4T1 mammary carcinoma cells were sensitive (Fig. 3.7e). Supplementation with necrotic cell debris supported proliferation in irradiated 4T1 breast cancer cells in a manner reversed by the macropinocytosis inhibitor EIPA (Fig. 3.7e). The cytotoxic chemotherapeutic commonly used in prostate cancer, docetaxel, is a microtubule-stabilizing agent that does not kill via metabolic stress. Consistent with this, necrocytosis did not protect macropinocytic LNCaP cells from docetaxel-induced death (Supplementary Fig. 3.3b, c). Together, these findings demonstrate that necrocytosis can render cancer cells resistant to a variety of metabolic cancer therapies by providing the end products of biosynthesis.

DISCUSSION

Many cancer cells are likely macropinocytic. Activation of the RAS and PI3 kinase pathways is common across cancer classes and has been shown to drive macropinocytosis in pancreas, lung, colorectal, bladder, prostate, and now breast cancer cells [3, 4, 44, 45] (Fig. 3.1a). Importantly, the rate of macropinocytic flux in breast cancer cells is sufficient to support proliferation in nutrient-limiting conditions provided that necrotic corpses are supplied as fuel (Figs. 3.1c and 3.3f). Albumin can support the proliferation of some macropinocytic cells in low glutamine or when non-essential amino acids are limiting [4, 10], but was not sufficient to support breast cancer cell proliferation in media generally deficient in amino acids (Fig. 3.1c). As necrotic cell debris supported proliferation in amino acid- and glucose-deficient medium even when provided at a 25-fold lower concentration than albumin (Fig. 3.1c and Fig 3.3f), necrotic cell debris is likely to be an important macropinocytic fuel in tumors. Tumor growth represents the sum of tumor cell death and birth; dead cells are present throughout tumors, not just in large, necrotic foci [46]. In some cases, triggering apoptosis paradoxically promotes tumorigenesis, stimulating the proliferation of neighboring cells. This death-driven proliferation may stem from a combination of inflammatory signals and necrocytosis when apoptotic cells undergo secondary necrosis. Similarly, co-injection of dead cells with viable 4T1 cells accelerates their proliferation in subcutaneous tumor models [47]; these dead cells may fuel the proliferation of their viable neighbors. In poorly perfused areas of the tumor, macroscopic necrosis would represent a banquet for macropinocytic tumor cells. Most solid tumors, including breast cancers, contain necrotic areas, and evidence of tumor necrosis correlates with poor prognosis [13, 48-50]. In summary, necrotic

cell debris is a high-value macropinocytic fuel that likely makes an important contribution to tumor anabolism and helps to explain paradoxical observations that cell death drives tumor growth.

Prior to this report, macropinocytosis had only been documented to provide amino acids [3-5, 8-10, 44, 51]. While necrocytosis can maintain lipid droplet content in amino acid-deprived prostate cancer cells [3], whether this occurred because protein scavenging decreased the need for lipid droplet catabolism or because necrotic cell debris supplied lipids was unclear. Click chemistry-based flux analysis now shows that many macromolecules, not just amino acids, can be recovered via necrocytosis. Extracellular proteins are often glycosylated, and thus many macropinocytosed proteins would carry sugars that could be recycled. Carbohydrate scavenging (Fig. 3.3d) could spare glucose that would otherwise be required for glycosylation and stimulate pro-growth signal transduction and transcription. For example, GlcNAc synthesis is important for the expression of growth factor receptors that are critical for breast cancer cell proliferation and survival [52, 53]. The fatty acid palmitate was also scavenged from necrotic cell debris via macropinocytosis (Fig. 3.4c, d). Palmitate can be oxidized, used for membrane synthesis, or support signaling in growing cancer cells. Fatty acid synthesis is particularly important in breast and prostate cancer cells, and fatty acids synthase inhibitors are in clinical trials [29, 54]. The effectiveness of the fatty acid synthase inhibitor GSK2194069 against breast and prostate cancer cells was significantly compromised if macropinocytic cells had access to necrotic cell debris (Fig. 3.4e-i); if palmitate can be scavenged from the tumor microenvironment, cells will no longer need to synthesize it

with fatty acid synthase. In sum, necrocytosis is likely to decrease the effectiveness of many different therapies targeting tumor anabolism by providing the end products of biosynthesis. Pairing these drugs with macropinocytosis inhibitors may increase the depth of the response and limit the development of resistance.

Therapeutic resistance remains a major obstacle in combating cancer. In keeping with the results presented here (Fig. 3.6), patients with tumors bearing PIK3CA or KRAS mutations or with decreased PTEN activity are more likely to be resistant to chemotherapy [55-58]. There is also a strong link between tumor necrosis and therapeutic resistance across tumor classes. Necrosis would facilitate the scavenging DNA fragments reducing dependence on nucleotide biosynthesis pathways that are a known therapeutic liability [14, 15, 59, 60]. It is particularly striking that the nucleotide synthesis inhibitors 5-FU and gemcitabine failed to even limit proliferation if cells were able to perform necrocytosis (Fig. 3.6a-d). This result is consistent with recent reports that deoxycytidine release from macrophages also limits the effectiveness of gemcitabine [61]. The effectiveness of genotoxic therapies such as doxorubicin and γ-irradiation that create dependence on de novo nucleotide synthesis pathways [15, 62] was also compromised by necrocytosis (Fig. 3.6 e-g). Genotoxic therapies and radiation are standard-of-care treatments for many cancer classes that are likely to be macropinocytic. Glioblastomas, a cancer class with a dismal long-term survival rate even with therapy, often have PTEN and PIK3CA mutations, AMPK activation, and large areas of necrosis at diagnosis [63, 64]. Both radiation and temozolomide, an alkylating agent, are first line treatments; necrocytosis may play an important role in

therapeutic resistance in glioblastoma patients. In summary, macropinocytosis inhibitors have the potential to produce significant gains in patient survival when used in combination with radiation and standard-of-care chemotherapy.

The contribution that macropinocytosis makes to cancer cell anabolism and therapeutic resistance has likely been unrecognized in part due to the conditions under which in vitro experiments are generally conducted. Standard tissue culture media are largely bereft of macropinocytic fuel, containing only limited amounts of albumin (0.3%), a suboptimal macropinocytic fuel even when supplemented to 17-fold higher levels (Figs. 3.1c and 3.3f). In contrast, the tumor microenvironment is rich in macromolecules and debris that are ripe for scavenging. Indeed, macropinocytosis may provide one explanation for discrepant results with metabolic inhibitors in vitro and in vivo (e.g. [65]). An additional translational implication of this study is that the clinical benefits of autophagy inhibitors that block lysosomal degradation (e.g. chloroquine derivatives [66, 67]) may be derived as much from blocking macropinocytic flux as from autophagy inhibition. If so, the biomarkers selected to identify sensitive patients and confirm therapeutic efficacy would need to be reconsidered. Given the accumulating evidence that many tumor classes are macropinocytic and the clear anabolic benefits of scavenging, it is very likely that macropinocytosis makes a major contribution to therapeutic resistance across cancer classes.

METHODS

Cell lines and cell culture

All cultured cells were maintained at 37°C in 5% CO_2. All media were supplemented with 10% standard fetal bovine serum and antibiotics unless otherwise stated. MDA-MB-231, MCF-7, T-47D, BT-549, Hs578T, HCC1569, hTERT-HME1 PANC-1, BxPC3 and LNCaP, cells were obtained from the ATCC. The 4T1 cell line was provided by Jennifer Prescher (UC Irvine). MCF-10A cells were supplied by Ben Ho Park (Johns Hopkins School of Medicine). 22Rv1 cells were provided by Ionis Pharmaceuticals (Carlsbad, CA). hTERT-HME1 were cultured without serum in MEGM base medium supplemented additives provided in the MEGM™ BulletKit™ medium. MCF-10A cells were cultured in DMEM/F12 Ham's Mixture without phenol red and supplemented with 5% horse serum, EGF (20 ng/ml), insulin (10 µg/ml), hydrocortisone (0.5 mg/ml), cholera toxin (100 ng/ml), 1% penicillin and streptomycin. MDA-MB-231 and PANC-1 cells were cultured in DMEM media with L-glutamine, 4.5 g/L glucose and without sodium pyruvate and supplemented with 1% sodium pyruvate. MCF-7 cells were cultured in RPMI supplemented with 1% L-glutamine. LNCaP, HCC1569, 22Rv1 and BxPC3 cells were cultured in RPMI-ATCC modified medium. T-47D and BT-549 cells were cultured in RPMI-ATCC modified medium with 0.2 units/ml or 0.023 IU/ml bovine insulin, respectively. 4T1 were cultured in DMEM media with L-glutamine, 4.5 g/L glucose and without sodium pyruvate. Hs578T were cultured in the same medium as 4T1 but supplemented with 15% FBS and 0.01 µg/ml insulin. FL5.12 cells were maintained in RPMI 1640 medium supplemented with 10 mM HEPES, 55 µM β-mercaptoethanol, antibiotics, 2 mM L-glutamine, and 500 pg/ml murine rIL-3. All cells

were passaged for ≤ 3 wk at which point low-passage vials were thawed. *Mycoplasma* testing was performed using the VENOR GeM PCR kit every 4-6 months for all cell lines. 4T1 cells were cured of *Mycoplasma* by culturing in ciprofloxacin for 8 wk (confirmed by PCR).

Dextran uptake assays

Cells were seeded into 8-chamber slides (Cellvis, cat# C8-1.5H-N) 12-16 h before uptake assays. Cells were subjected to nutrient stress for 16 h prior to dextran uptake assays. MEM or RPMI containing 1% of the normal amount of amino acids and/or glucose (1% AA or 1% AA/gluc medium) was produced by preparing DMEM or RPMI lacking amino acids and/or glucose from chemical components and mixing it 99:1 with complete medium. Cells were incubated with 70 kD Oregon Green fluorescent dextran (1 mg/mL) or 70 kD Texas Red fluorescent dextran (1 mg/mL) and Hoechst 33342 (1:1,000) for 30 min, washed three times with PBS, and fresh culture medium added. Drug pre-treatment and concentrations were as follows: EIPA, 50 μM, 1.5 h pre-treatment; PMA, 250 nM, co-treatment with dextran uptake assays; A769662, 50 μM, 1.5 h pre-treatment. Dextran uptake assays were performed 2 h after irradiation (2 Gy).

Generation and uptake of necrotic cell debris and apoptotic cells

Apoptotic and necrotic cells were prepared as described previously [3]. Briefly, apoptotic FL5.12 cells were generated by withdrawing IL-3 from cells maintained at a density of 1 million/ml. Necrotic cell debris was collected after 72 h of IL-3 withdrawal where cells were maintained at 10 million/ml. Where indicated, FL5.12 cells were labeled with 5 μM

CFSE at 500,000 cells/ml in PBS containing 1% FBS and 500 pg/ml IL-3 for 30 min. One million necrotic or apoptotic CFSE-labeled cell equivalents were spun down in a microfuge at 13,000 rpm at 4°C for 10 min, the supernatant discarded, and the pelleted debris added to nutrient-deprived (1% AA/gluc for 16 h) macropinocytic breast cancer cells for 1 h. Where indicated, breast cancer cells were pre-treated with 50 μM EIPA for 1.5 h. Cells were imaged live in fresh culture medium after 4-6 washes with PBS to completely remove any remnants of apoptotic or necrotic cells.

Proliferation assays

Cells at 60% confluence (12-16 h after seeding in a 24 well plate) were washed twice with PBS then incubated in 1% AA or 1% AA/gluc medium and supplemented with 10 million necrotic cell equivalents (0.2% protein), 10 million apoptotic cell equivalents (1% protein), or 5% fatty acid free bovine serum albumin. The degree of nutrient stress was selected based on nutrient titration experiments demonstrating a 50% reduction in cell viability at 48 h. For proliferation assays in Figs. 4 and 6, cells were treated when 30% confluent (12-16 h after seeding in a 24 well plate) with: FASN inhibitor GSK2194069 (20 μM), 5-FU (30 μM), gemcitabine (20 μM), docetaxel (5 μM), or doxorubicin (1 μM) or subjected to γ-irradiation (5 Gy). Treated cells were provided with 10 million necrotic cell equivalents (0.2% protein) or left un-supplemented. Cell proliferation was determined by flow cytometry by recording the number of cells that excluded vital dye (DAPI (1 mg/mL) or PI (1 mg/mL)) over a fixed collection interval (30 sec). Representative bright field images were obtained before cells were processed for flow cytometry.

Flux analysis using click chemistry

FL5.12 cells were labeled with 100 μM L-homopropargylglycine hydrochloride (HPG), 500 μM alkynyl palmitic acid (alk-PA), 100 μM N-(4-pentynoyl)-glucosamine tetraacylated (Ac_4GlcNAl), or 1 mM EdU for 24 h at a density of 10 million/ml. HPG labeling was performed in methionine-free medium and alkynyl palmitic acid labeling was conducted in medium containing 10% charcoal stripped serum. Necrosis was induced in labeled cells as described above. MCF-7 or HCC1569 (70% confluence in 8 chamber slides) were maintained in 1% AA for 16 h before 1 million cell equivalents of alkyne-labeled necrotic debris was added for 24-48 h. Cells were washed 3-5 times with PBS, fixed in 4% paraformaldehyde (10 min, RT), washed twice with PBS, permeablized and blocked (10% FBS and 0.3% Triton-X100 in PBS for 30 min rocking at RT), and washed twice with PBS. The click reaction (copper catalyzed cycloaddition) was performed using 100 μM Tris [(1-benzyl-1H-1,2,3-triazol-4-yl)methyl] amine TBTA, 1 mM sodium ascorbate (made fresh each time), 100 μM $CuS0_4$ and 0.5 mM biotin-azide in 100 μl blocking solution for 1 h at 30°C. After 3 washes with PBS, cells were incubated for 1 h with Alexa488-streptavidin (1:1,000 in blocking solution), stained with DAPI (1 mg/ml in PBS) for 10 min, washed, and imaged in PBS. Drug concentrations and pre-treatments were as follows: cycloheximide, 50 mg/mL (4 h); hydroxyurea, 10 mM, (4 h); or EIPA, 50 μM (1.5 h).

In vivo experiments

All experiments conducted in mice were performed in accordance with the Institutional Animal Care and Use Committee of University of California, Irvine. To produce

orthotopic tumors, 1 x 10^4 4T1 cells in 100 µl PBS were injected into the 4^{th} mammary fat pad of 3-4 week old female BALB/c mice. Twenty-three days later (tumor volume ≤ 1,100 mm^3), 70 kD FITC-FICOLL (1 mg dissolved in 1% Evan's Blue Dye in saline) was injected intratumorally 1 h after intraperitoneal (i.p.) injection of vehicle (DMSO) or 10 mg/kg EIPA. Mice were sacrificed 1 h after Ficoll injection and tumors were excised and frozen in OCT. Cryosections (5-8/tumor) were fixed in 4% paraformaldehyde, stained with 1 mg/mL DAPI in PBS, washed twice with PBS, and mounted using Vectashield mounting medium.

Image analysis

Images were collected on either a Yokogawa spinning disk confocal using a 100X oil objective (dextran and CFSE labeled FL5.12 uptake assays) or 40X water objective with 1.5X magnification (click chemistry and in vivo Ficoll uptake) or a Nikon Eclipse-TI inverted microscope (bright field only). All live imaging (dextran or CFSE labeled FL5.12 uptake assays) was performed at 37°C. Z-stacks were collected with step size of 0.5 microns and 8-10 stacks were obtained from 20-40 independent fields. Microscope acquisition settings were held constant within each experiment and determined for each experiment using positive and negative controls. All image processing and analysis was performed using Image J software (version 2.0, NIH). Maximum projections of z-stacks are shown in the figures; rolling ball background subtraction was applied. Dextran and CFSE-necrotic or -apoptotic cell uptake was quantified using the "analyze particles" function to determine the ratio of total particle area to total cell area as described previously [3, 68].

Statistical analysis

Significance was determined using a two-tailed unpaired t test or a two-way ANOVA or one-way ANOVA where multiple groups were compared; Tukey's method or Dunnet's test, respectively, was used to correct for multiple comparisons. Mean ± SEM is shown unless otherwise indicated. *, P≤0.05; **, P≤0.01; ***, P≤0.001; ns, not significant.

ACKNOWLEDGEMENTS

The authors thank Ben Ho Park (Johns Hopkins School of Medicine), Jenn Prescher, and Ionis Pharmaceuticals for generously providing MCF-10A cells, 4T1 cells or 22Rv1 cells, respectively. We thank John Cooper (Washington University) for providing all the reagents used to study CARMIL1. We thank David Fruman, Brendan Finicle, Seong Kim, Tricia Nguyen, Archna Ravi, and Alison McCracken for valuable discussions. We thank Elizabeth Selwan for aiding with γ-irradiation. This work was supported by grants to ALE from the NIH (R01 GM089919), CDMRP (W81XWH-15-1-0010), University of California Cancer Research Coordinating Committee (CRR-17-426826), and UCI Applied Innovation.

AUTHOR CONTRIBUTIONS

The study was conceived by VJ and ALE. Experiments were designed by VJ and ALE. Experiments were carried out by VJ. Data were analyzed and interpreted by VJ and ALE. Manuscript was prepared by VJ and ALE.

DECLARATION OF INTERESTS

ALE is an inventor on patent application 15/760199 which includes molecules that, among other activities, inhibit macropinocytic flux.

Fig. 1

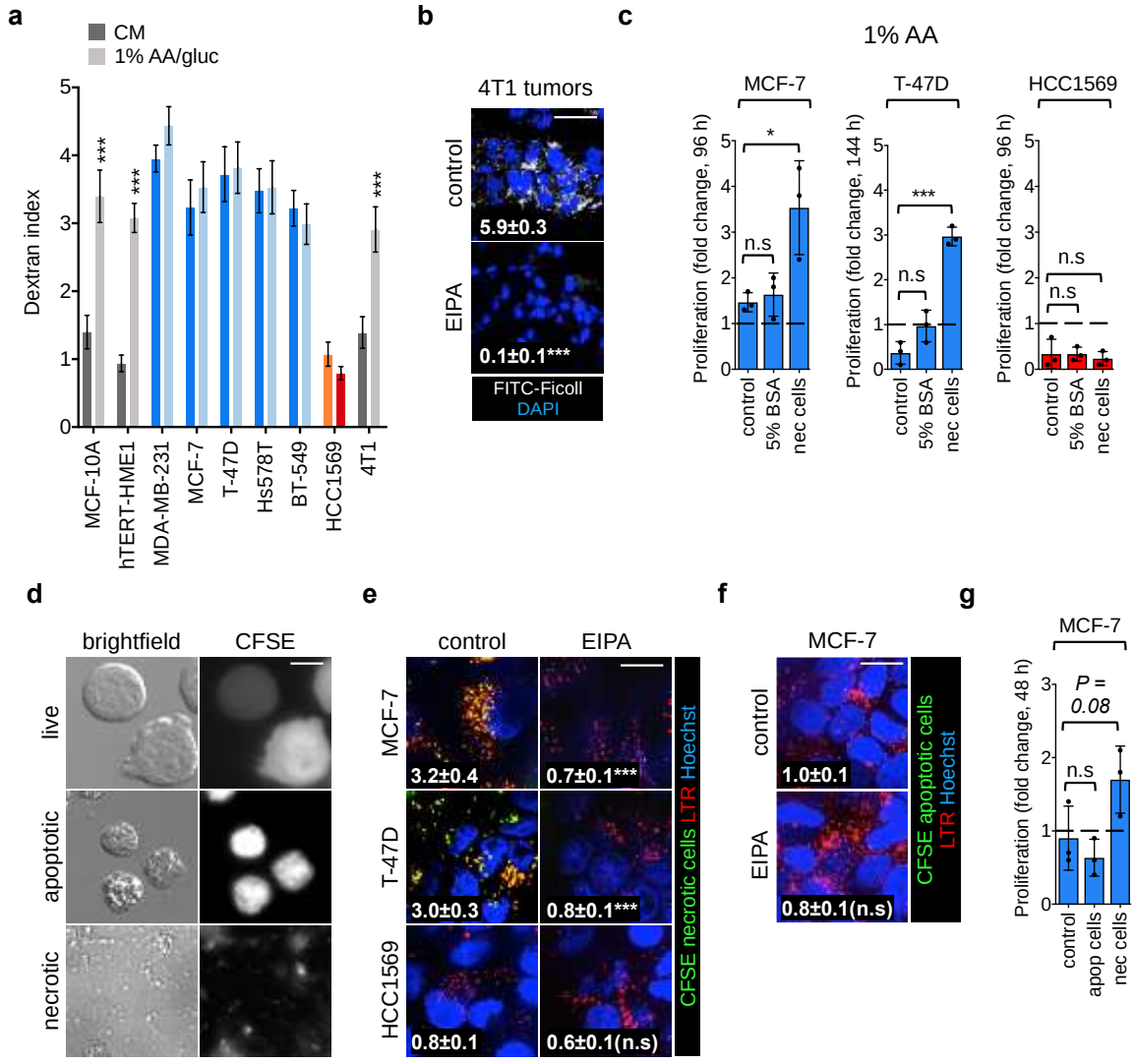
a
CM
1% AA/gluc
Dextran index
MCF-10A
hTERT-HME1
MDA-MB-231
MCF-7
T-47D
Hs578T
BT-549
HCC1569
4T1
b
4T1 tumors
control
EIPA
5.9±0.3
0.1±0.1***
FITC-Ficoll
DAPI
c
1% AA
MCF-7
T-47D
HCC1569
Proliferation (fold change, 96 h)
Proliferation (fold change, 144 h)
n.s
control
5% BSA
nec cells
d
brightfield
CFSE
live
apoptotic
necrotic
e
control
EIPA
MCF-7
T-47D
HCC1569
3.2±0.4
0.7±0.1***
3.0±0.3
0.8±0.1***
0.8±0.1
0.6±0.1(n.s)
CFSE necrotic cells LTR Hoechst
f
MCF-7
control
EIPA
1.0±0.1
0.8±0.1(n.s)
CFSE apoptotic cells
LTR Hoechst
g
MCF-7
P = 0.08
Proliferation (fold change, 48 h)
control
apop cells
nec cells

Figure 3.1. Macropinocytosis supports proliferation in amino acid-deprived breast cancer cells. a Dextran index in complete medium (CM) or 1% AA/gluc medium in the indicated breast cancer cell lines. Grey bars represent contextually macropinocytic cell lines, blue bars represent constitutively macropinocytic cell lines, and red bars represent non-macropinocytic cell lines. Mean ± SEM shown. Using a two-way ANOVA with Tukey's method to correct for multiple comparisons**,** ***, $P \leq 0.001$, no asterisks indicates $P > 0.05$. **b** FITC-Ficoll uptake in orthotopic 4T1 tumors. Where indicated, EIPA (10 mg/kg) was administered 1 h before Ficoll. Fifteen fields were evaluated from 4-6 tumor sections; Ficoll field index ± SEM shown in white. Using an unpaired, two-tailed t test**,** ***, $P \leq 0.001$. **c** Proliferation of macropinocytic MCF-7 and T-47D cells or non-macropinocytic HCC1569 cells in 1% AA medium ± fatty acid-free albumin (5%) or necrotic debris (0.2% protein). Mean ± SD, n=3. Using a one-way ANOVA and Dunnett's test to correct for multiple comparisons, *, $P \leq 0.05$; ***, $P \leq 0.001$, n.s., not significant. **d** IL-3 was withdrawn from CFSE-labeled FL5.12 cells for 24 h at low density (25,000 cells/ml) to produce apoptotic cells or 48 h at high density (100 million cells/ml) to produce necrotic cell debris. Scale bar, 10 µm. **e** The indicated cell lines were maintained in 1% AA/gluc ± EIPA (50 µM) and supplemented with CFSE-labeled necrotic debris. **f** MCF-7 cells maintained in 1%AA/gluc ± EIPA (50 µM) and supplemented with CFSE-labeled apoptotic FL5.12 cells. For **e,f**, in white, percent of cell area positive for CFSE (mean ± SEM). Using a one-way ANOVA and Dunnett's test to correct for multiple comparisons, ***, $P \leq 0.001$, n.s., not significant. **g** MCF-7 cell proliferation in 1% AA ± apoptotic cells (1% protein) or necrotic cell debris (0.2% protein). Proliferation evaluated at 48 h to avoid secondary necrosis of apoptotic cells. Mean ± SD, n=3. Using a one-way ANOVA and Dunnett's test to correct for multiple comparisons, n.s., not significant. In **a**,**e,** and **f**, 50-100 cells from 2-3 independent experiments were evaluated. Scale bars, 20 µm**.**

Fig. 2

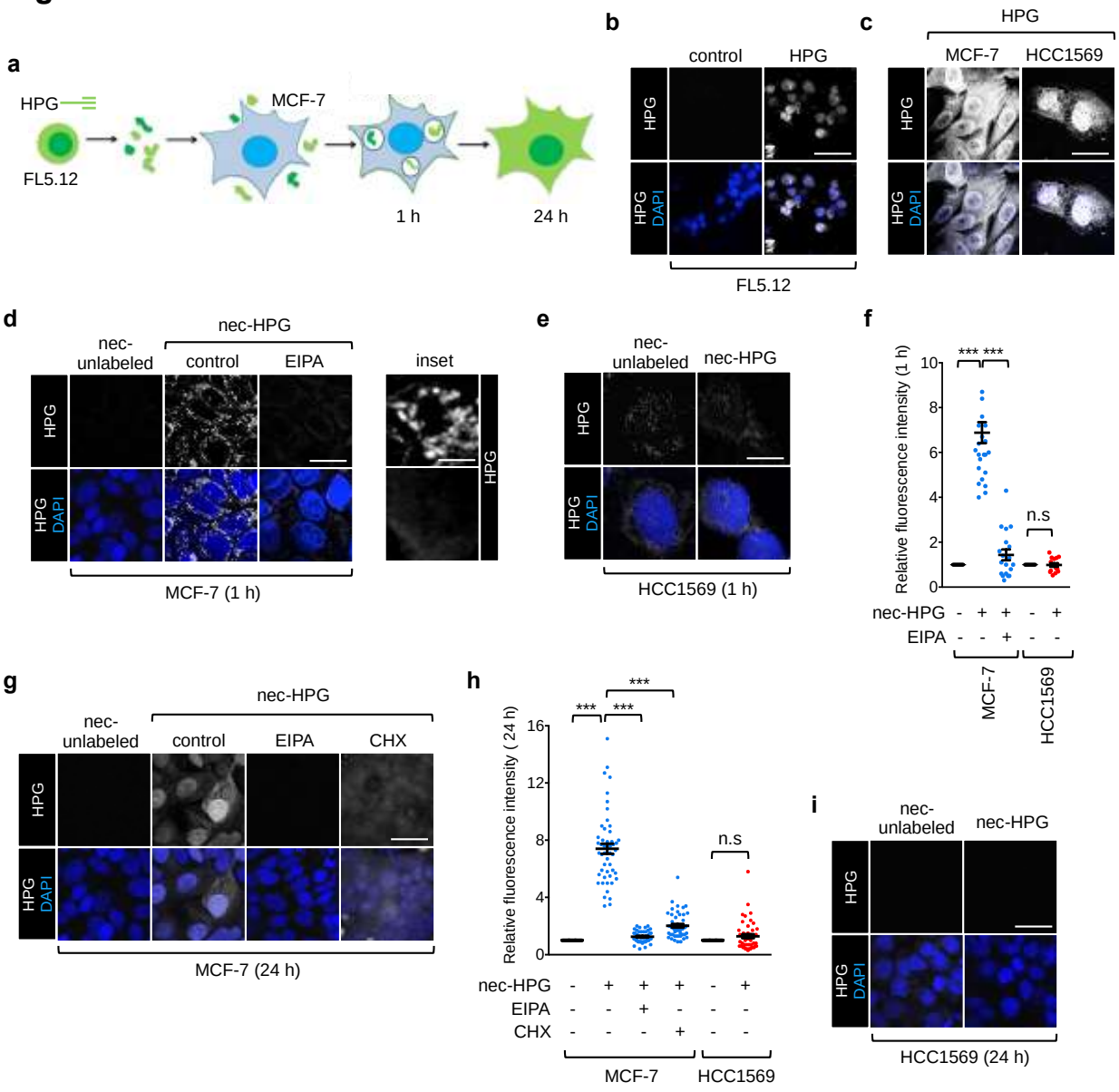

Figure 3.2. Measurement of macropinocytic protein flux in breast cancer cells. a Assay schematic. FL5.12 cells were labeled with L-homopropargylglycine (HPG) prior to the induction of necrosis. Macropinocytic MCF-7 cells were supplemented with HPG-labeled necrotic debris for 1 h or 24 h. HPG incorporation into the MCF-7 cell proteome was detected with clickable biotin-azide followed by Alexa488-streptavidin. **b** FL5.12 cells were labeled with HPG (100 μM) for 24 h in complete medium (CM); HPG was detected with biotin-azide and strepavidin-488. **c** MCF-7 or HCC1569 cells labeled as in (**b**) but in 1% AA medium. **d,e** MCF-7 (**d**) or HCC1569 (**e**) cells in 1% AA medium were supplemented with unlabeled or HPG-labeled necrotic cell debris (nec-HPG) for 1 h ± 50 μM EIPA. **f** Integrated fluorescence intensity per cell in (**d,e**) normalized to cells fed

unlabeled necrotic debris. A total of 50 cells from 1-3 independent experiments were examined; mean ± SEM shown. Using a one-way ANOVA and Tukey's method to correct for multiple comparisons, ***, $P \leq 0.001$, n.s., not significant. **g** MCF-7 cells were supplemented with necrotic cell debris as in (**d**) but for 24 h ± 50 μM EIPA or ± 50 μg/ml cycloheximide. **h** Integrated fluorescence intensity per cell from (**g,i**) normalized to cells fed unlabeled necrotic debris. **i** HCC1569 cells were supplemented with necrotic cell debris as in (**e**) but for 24 h. Scale bars, 20 μm.

Fig. 3

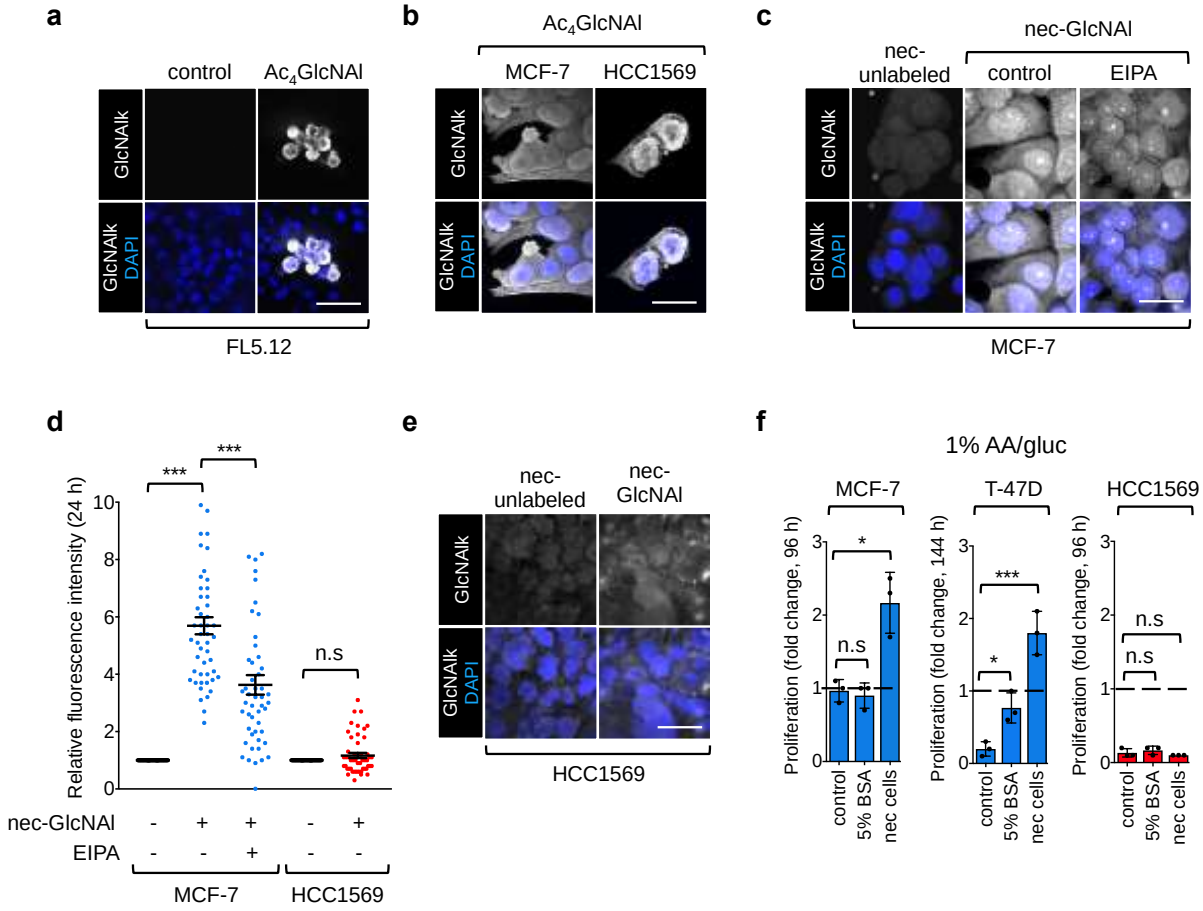
a
control
Ac4GlcNAl
GlcNAlk
GlcNAlk DAPI
FL5.12
b
Ac4GlcNAl
MCF-7
HCC1569
GlcNAlk
GlcNAlk DAPI
c
nec-GlcNAl
nec-unlabeled
control
EIPA
GlcNAlk
GlcNAlk DAPI
MCF-7
d
Relative fluorescence intensity (24 h)
***
***
n.s
nec-GlcNAl
EIPA
MCF-7
HCC1569
e
nec-unlabeled
nec-GlcNAl
GlcNAlk
GlcNAlk DAPI
HCC1569
f
1% AA/gluc
MCF-7
T-47D
HCC1569
Proliferation (fold change, 96 h)
Proliferation (fold change, 144 h)
control
5% BSA
nec cells
n.s

Figure 3.3: Macropinocytic breast cancer cells scavenge sugars via necrocytosis. **a** FL5.12 cells labeled with Ac_4GlcNAl (100 μM) in complete medium for 24 h; GlcNAl detected with biotin-azide and Alexa488-streptavidin. **b** MCF-7 and HCC1569 cells were labeled as in (**a**) but in 1% AA medium. **c** Macropinocytic MCF-7 cells ± 50 μM EIPA maintained in 1% AA medium for 24 h with unlabeled or GlcNAl-labeled necrotic cell debris (nec-GlcNAl). **d** Integrated fluorescence intensity per cell in (**c**,**e**) normalized to cells fed unlabeled necrotic cell debris. A total of 50 cells were examined from 1-3 independent experiments; mean ± SEM shown. Using a one-way ANOVA and Tukey's method to correct for multiple comparisons, ***, $P \leq 0.001$, n.s., not significant. **e** As in (**c**), but with non-macropinocytic HCC1569 cells. **f** Proliferation of macropinocytic MCF-7 and T-47D cells or non-macropinocytic HCC1569 cells in 1% AA/gluc medium supplemented with fatty acid-free albumin (5%) or necrotic debris (0.2% protein). Means ± SD, n=3. Using a one-way ANOVA and Dunnett's test to correct for multiple comparisons, *, $P \leq 0.05$; ***, $P \leq 0.001$, n.s., not significant. Scale bars, 20 μm.

Fig. 4

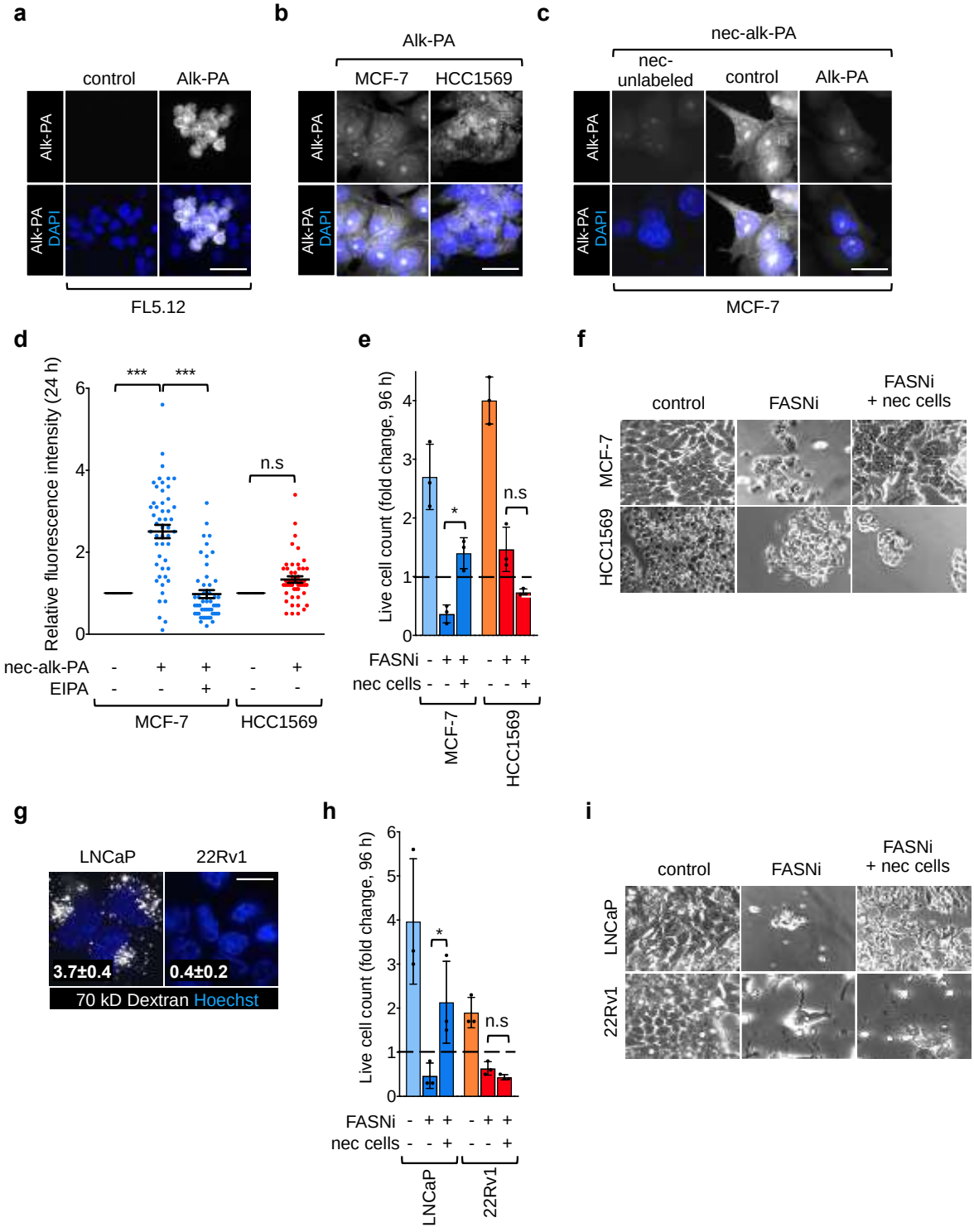
a
control
Alk-PA
Alk-PA
Alk-PA DAPI
FL5.12
b
Alk-PA
MCF-7
HCC1569
c
nec-alk-PA
nec-unlabeled
control
Alk-PA
MCF-7
d
Relative fluorescence intensity (24 h)
***
***
n.s
nec-alk-PA
EIPA
MCF-7
HCC1569
e
Live cell count (fold change, 96 h)
*
n.s
FASNi
nec cells
MCF-7
HCC1569
f
control
FASNi
FASNi + nec cells
MCF-7
HCC1569
g
LNCaP
22Rv1
3.7±0.4
0.4±0.2
70 kD Dextran Hoechst
h
Live cell count (fold change, 96 h)
*
n.s
FASNi
nec cells
LNCaP
22Rv1
i
control
FASNi
FASNi + nec cells
LNCaP
22Rv1

Figure 3.4. Necrocytosis supplies fatty acids and confers resistance to fatty acid synthase inhibition. a FL5.12 cells labeled with alkynyl-PA (500 μM) in complete medium for 24 h; alk-PA detected with biotin-azide and Alexa488-streptavidin. **b** MCF-7 and HCC1569 cells labeled as in (**a**) but in 1% AA medium. **c** Macropinocytic MCF-7 cells maintained in 1% AA medium for 24 h ± 50 μM EIPA supplemented with unlabeled or alk-PA-labeled necrotic cell debris (nec-alk-PA). **d** Integrated fluorescence intensity per cell in (**c**, **Supplementary Fig. 2**) normalized to cells fed unlabeled necrotic cell debris. A total of 50 cells were quantified from 1-3 independent experiments; mean ± SEM shown. Using a one-way ANOVA and Tukey's method to correct for multiple comparisons, ***, $P \leq 0.001$, n.s., not significant. **e** Proliferation of macropinocytic MCF-7 or non-macropinocytic HCC1569 cells ± 20 μM FASNi (GSK 2194069) ± necrotic debris (0.2% protein) at 96 h. **f** Representative bright field images for proliferation assay in (**e**). **g** 70kD dextran uptake in LNCaP or 22Rv1 prostate cancer cells. Dextran index ± SEM shown in white. A total of 50 cells were quantified from 1-3 independent experiments; mean ± SEM shown. **h** Proliferation of macropinocytic LNCaP cells or non-macropinocytic 22Rv1 cells ± 20 μM FASNi (GSK 2194069) ± necrotic debris (0.2% protein) at 96 h. **i** Representative bright field images for proliferation assay in (**h**). For **e,h**, means ± SD, n=3. Using a one-way ANOVA and Dunnett's test to correct for multiple comparisons, *, $P \leq 0.05$; ***, $P \leq 0.001$, n.s., not significant. Scale bars, 20 μm.

Fig. 5

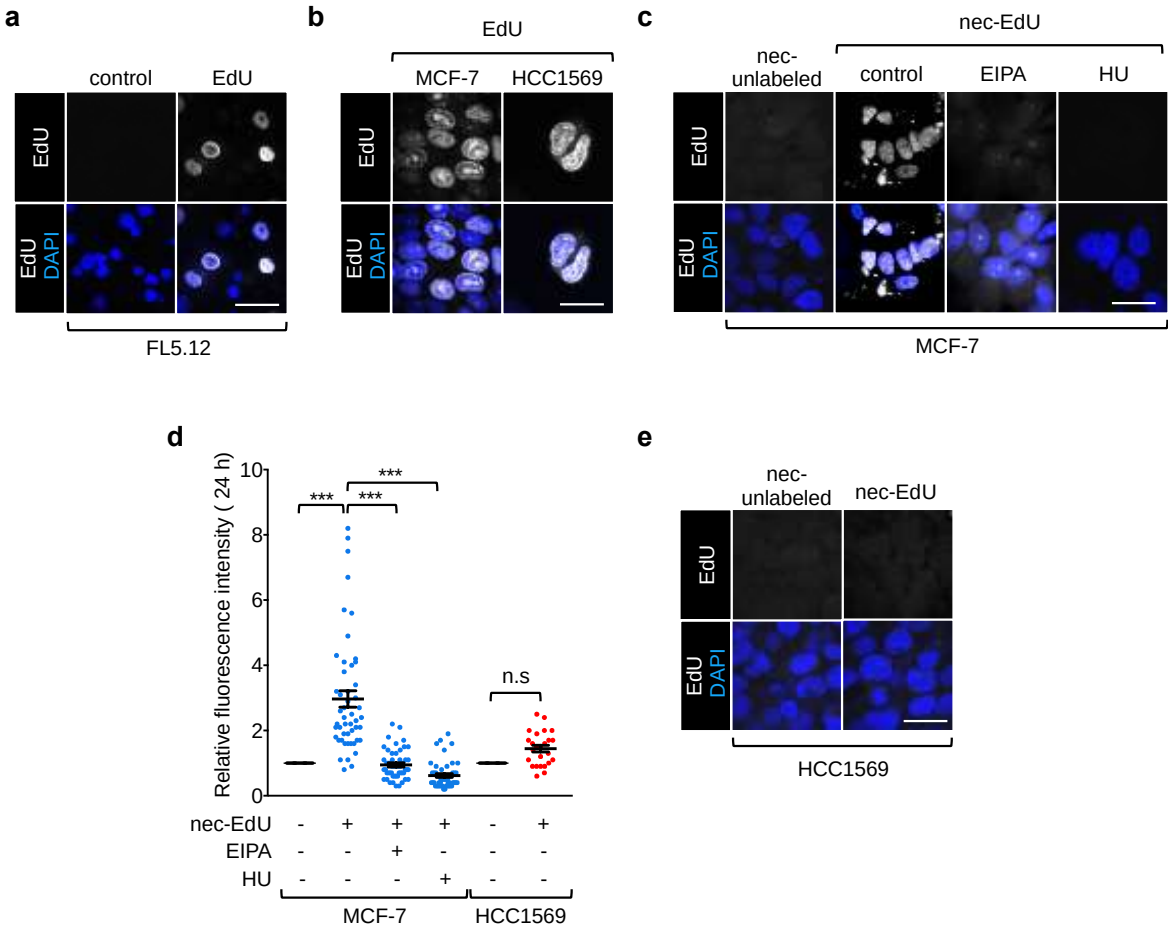

Figure 3.5. Necrocytosis provides nucleotides. a FL5.12 cells labeled with EdU (1 mM) in complete medium; EdU detected with biotin-azide and Alexa488- streptavidin. **b** MCF-7 and HCC1569 cells labeled as in (**a**) but in 1% AA medium. **c** Macropinocytic MCF-7 cells ± 50 μM EIPA or 10 mM hydroxyurea (HU) were maintained in 1% AA medium for 48 h and supplemented with unlabeled or EdU-labeled necrotic cell debris (nec-EdU). **d** Integrated fluorescence intensity per cell in (**c,e**) normalized to cells fed unlabeled necrotic cell debris. A total of 50 cells were quantified from 1-3 independent experiments; mean ± SEM shown. Using a one-way ANOVA and Tukey's method to correct for multiple comparisons, ***, $P \leq 0.001$, n.s., not significant. **e** As in (**c**) but for non-macropinocytic HCC1569 cells. Scale bars, 20 μm.

Fig. 6

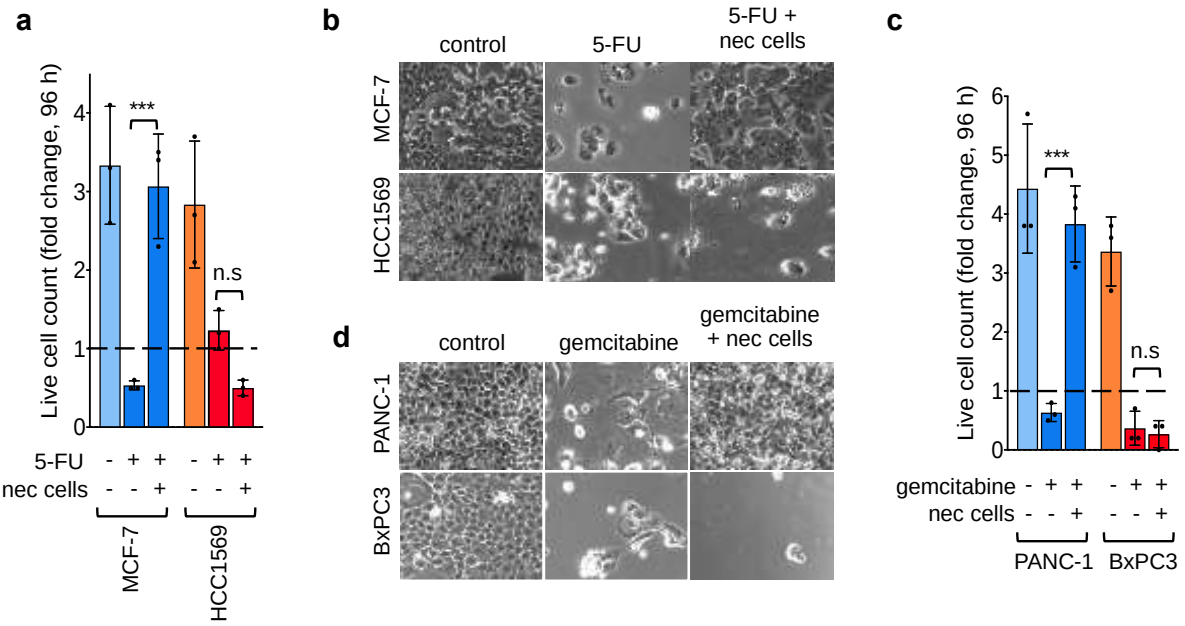

Figure 3.6. Necrocytosis confers resistance to nucleotide synthesis inhibitors. a Proliferation of macropinocytic MCF-7 or non-macropinocytic HCC1569 cells ± 30 μM 5-FU ± necrotic debris (0.2% protein) at 96 h. **b** Representative bright field images for proliferation assay in (**a**). **c** Proliferation of macropinocytic PANC-1 or non-macropinocytic BxPC-3 cells ± necrotic debris (0.2% protein) ± 20 μM gemcitabine at 96 h. **d** Representative bright field images for proliferation assay in (**c**). In **a and c,** means ± SD, n=3; Using a one-way ANOVA and Dunnett's test to correct for multiple comparisons, *, $P \leq 0.05$; ***, $P \leq 0.001$, n.s., not significant.

Fig. 7

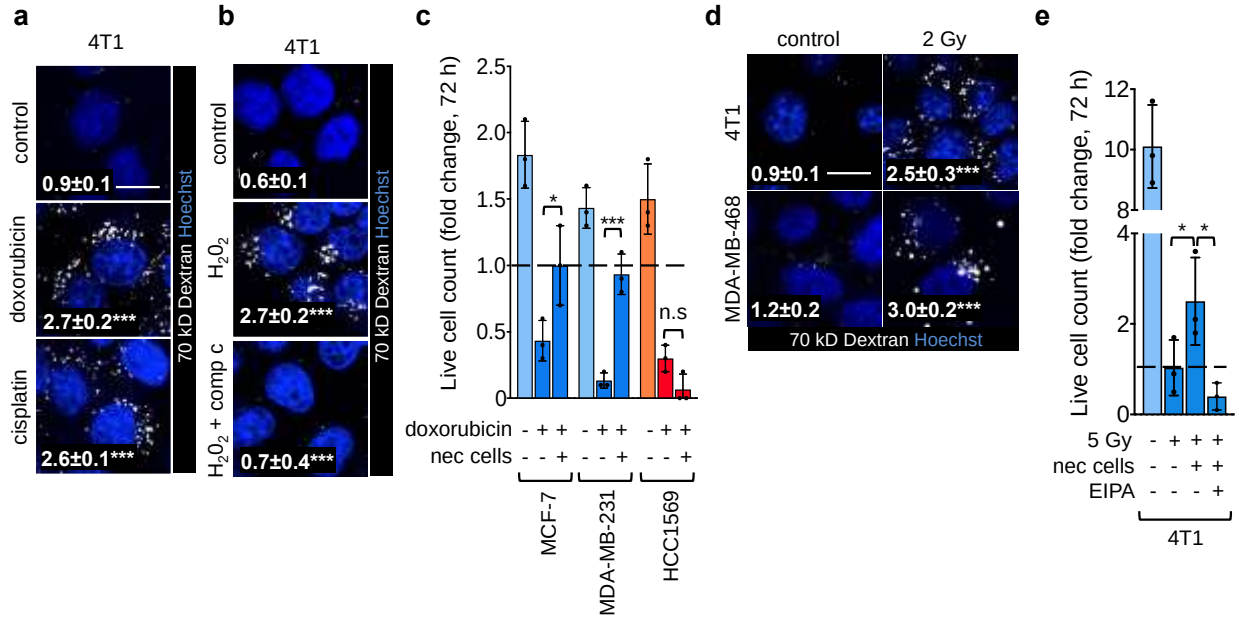

Figure 3.7. Standard of care therapies stimulate macropinocytosis which confers resistance to genotoxic agents. a Dextran uptake in 4T1 cells ± doxorubicin (250 nM) or cisplatin (1 μM). **b** Dextran uptake in 4T1 cells ± H_20_2 (500 μM) ± compound C (10 μM. **c** Proliferation of macropinocytic MCF-7 and MDA-MB-231 or non-macropinocytic HCC1569 cells ± 1 μM doxorubicin ± necrotic debris (0.2% protein) at 72 h.). **d** Dextran uptake in 4T1 or MDA-MB-468 cells ± 5 gy gamma irradiation. **e** Proliferation of 4T1 cells in CM subjected to 5 Gy of γ-irradiation ± nec cells and ± 10 μM EIPA at 72 h. Statistics compare dextran index in control and treated cells. In B-F, 30-100 cells examined in 2-3 independent experiments; mean ±SEM shown. In **c and e,** means ± SD, n=3; Using a one-way ANOVA and Dunnett's test to correct for multiple comparisons, *, $P \leq 0.05$; ***, $P \leq 0.001$, n.s., not significant.

Supplementary Fig. 1 - Related to Figure 1

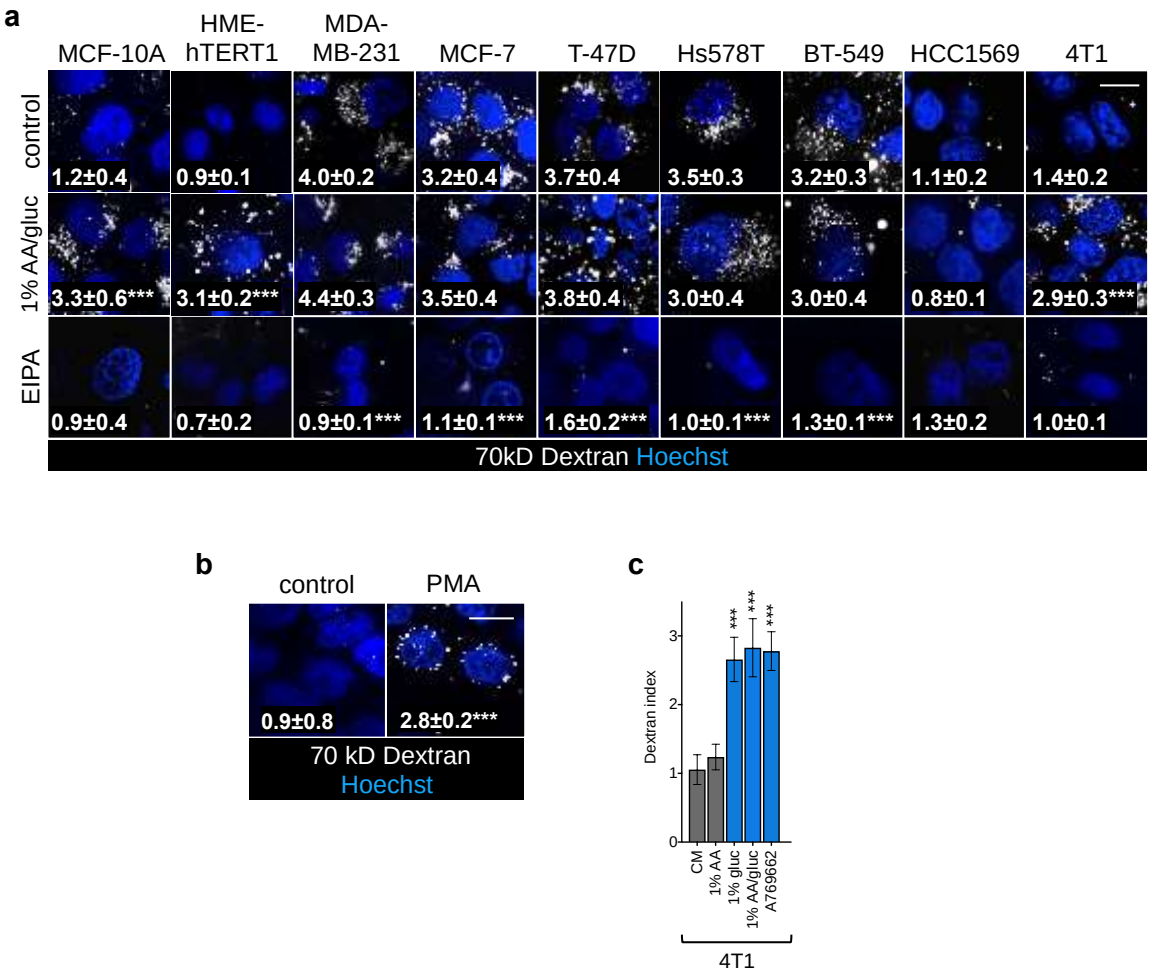

Figure S3.1. Standard of care therapies stimulate macropinocytosis which confers resistance to genotoxic agents. Breast cancer cells lines with activating mutations in KRAS or the PI3K pathway exhibit macropinocytosis. **a** 70 kD dextran uptake in CM ± EIPA (50 μM) or 1% AA/gluc medium in the indicated breast cancer cell lines. Representative images for dextran index in breast cancer cells shown in Fig. 3.1a. Statistics compare dextran index in CM and 1% AA/gluc (white asterisks) and CM ± EIPA (50 μM). Using a two-way ANOVA with Tukey's method to correct for multiple comparisons, ***, $P \leq 0.001$, n.s., not significant. **b** Dextran uptake in HCC1569 cells ± PMA (250 nM). Statistics compare dextran index in cells ± PMA. Using an unpaired, two-tailed t test, ***, $P \leq 0.001$. In a,b, dextran index shown in white (mean ± SEM); Scale bars, 20 μm. c Dextran index in 4T1 cells maintained in CM ± A769662 (50 μM), 1% AA, 1% gluc, or 1% AA/gluc medium as indicated. Using a two-way ANOVA with Dunnett's method to correct for multiple comparisons, ***, $P \leq 0.001$, n.s., not significant.

Supplementary Fig. 2 - Related to Figure 4

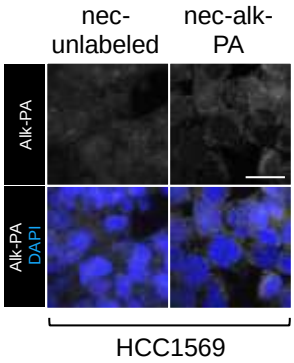

Figure S3.2. Standard of care therapies stimulate macropinocytosis which confers resistance to genotoxic agents. a Dextran uptake in 4T1 cells ± doxorubicin (250 nM) or cisplatin (1 μM). **b** Dextran uptake in 4T1 cells ± H_20_2 (500 μM) ± compound C (10 μM. **c** Proliferation of macropinocytic MCF-7 and MDA-MB-231 or non-macropinocytic HCC1569 cells ± 1 μM doxorubicin ± necrotic debris (0.2% protein) at 72 h.). **d** Dextran uptake in 4T1 or MDA-MB-468 cells ± 5 gy gamma irradiation. **e** Proliferation of 4T1 cells in CM subjected to 5 Gy of γ-irradiation ± nec cells and ± 10 μM EIPA at 72 h. Statistics compare dextran index in control and treated cells. In B-F, 30-100 cells examined in 2-3 independent experiments; mean ±SEM shown. In **c and e,** means ± SD, n=3; Using a one-way ANOVA and Dunnett's test to correct for multiple comparisons, *, $P \leq 0.05$; ***, $P \leq 0.001$, n.s., not significant.

Supplementary Fig. 3 - Related to Figure 6

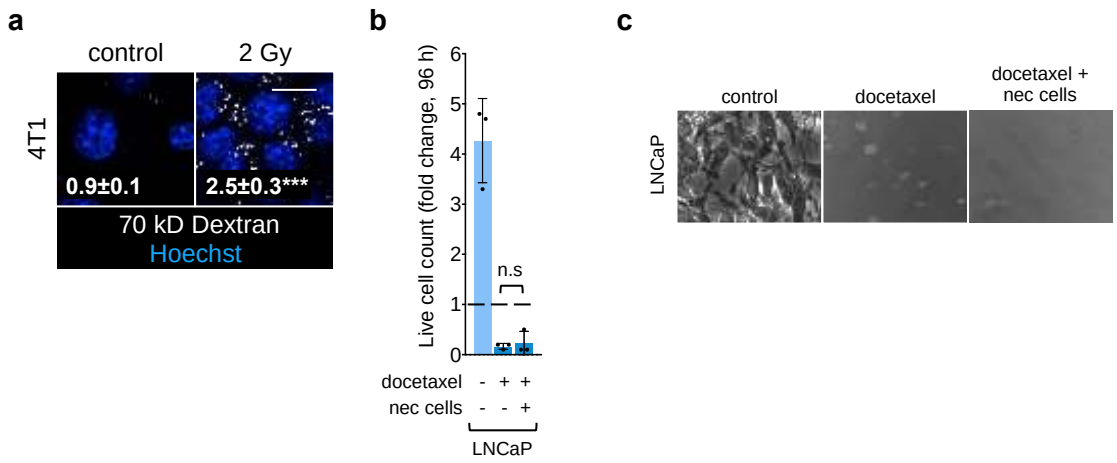

Figure S3.3. Contribution of necrocytosis to drug-resistance. a Dextran uptake in 4T1 cells 2 h after exposure to γ-irradiation (2 Gy). Statistics compare dextran index in control and irradiated cells. Dextran index shown in white (mean ± SEM); 50-100 cells from 2-3 independent experiments were evaluated. Using an unpaired, two-tailed t test, ***, $P \leq 0.001$. **b** Proliferation of macropinocytic LNCaP cells ± 5 μM docetaxel ± necrotic debris (0.2% protein) at 96 h. Means ± SD, n=3. Using a one-way ANOVA and Dunnett's test to correct for multiple comparisons, p>0.05, n.s., not significant. **c** Representative brightfield images for proliferation assay in (**b**).

REFERENCES

1. Finicle, B.T., Jayashankar, V. & Edinger, A.L. Nutrient scavenging in cancer. *Nat Rev Cancer* **18**, 619-633 (2018).
2. Kimmelman, A.C. & White, E. Autophagy and Tumor Metabolism. *Cell Metab* **25**, 1037-1043 (2017).
3. Kim, S.M. *et al.* PTEN Deficiency and AMPK Activation Promote Nutrient Scavenging and Anabolism in Prostate Cancer Cells. *Cancer discovery* **8**, 866-883 (2018).
4. Commisso, C. *et al.* Macropinocytosis of protein is an amino acid supply route in Ras-transformed cells. *Nature* **497**, 633-637 (2013).
5. Palm, W., Araki, J., King, B., DeMatteo, R.G. & Thompson, C.B. Critical role for PI3-kinase in regulating the use of proteins as an amino acid source. *Proc Natl Acad Sci U S A* **114**, E8628-E8636 (2017).
6. Amyere, M. *et al.* Constitutive macropinocytosis in oncogene-transformed fibroblasts depends on sequential permanent activation of phosphoinositide 3-kinase and phospholipase C. *Mol Biol Cell* **11**, 3453-3467 (2000).
7. Araki, N., Johnson, M.T. & Swanson, J.A. A role for phosphoinositide 3-kinase in the completion of macropinocytosis and phagocytosis by macrophages. *J Cell Biol* **135**, 1249-1260 (1996).
8. Davidson, S.M. *et al.* Direct evidence for cancer-cell-autonomous extracellular protein catabolism in pancreatic tumors. *Nat Med* **23**, 235-241 (2017).
9. Kamphorst, J.J. *et al.* Human pancreatic cancer tumors are nutrient poor and tumor cells actively scavenge extracellular protein. *Cancer Res* **75**, 544-553 (2015).
10. Palm, W. *et al.* The Utilization of Extracellular Proteins as Nutrients Is Suppressed by mTORC1. *Cell* **162**, 259-270 (2015).
11. Nik-Zainal, S. *et al.* Landscape of somatic mutations in 560 breast cancer whole-genome sequences. *Nature* **534**, 47-54 (2016).
12. Walker, R.A. The complexities of breast cancer desmoplasia. *Breast cancer research : BCR* **3**, 143-145 (2001).
13. Gilchrist, K.W., Gray, R., Fowble, B., Tormey, D.C. & Taylor, S.G.t. Tumor necrosis is a prognostic predictor for early recurrence and death in lymph node-positive breast cancer: a 10-year follow-up study of 728 Eastern Cooperative Oncology Group patients. *Journal of clinical oncology : official journal of the American Society of Clinical Oncology* **11**, 1929-1935 (1993).
14. Vander Heiden, M.G. & DeBerardinis, R.J. Understanding the Intersections between Metabolism and Cancer Biology. *Cell* **168**, 657-669 (2017).

15. Brown, K.K., Spinelli, J.B., Asara, J.M. & Toker, A. Adaptive Reprogramming of De Novo Pyrimidine Synthesis Is a Metabolic Vulnerability in Triple-Negative Breast Cancer. *Cancer discovery* **7**, 391-399 (2017).

16. Levy, J.M.M., Towers, C.G. & Thorburn, A. Targeting autophagy in cancer. *Nat Rev Cancer* **17**, 528-542 (2017).

17. Guo, J.Y. *et al.* Autophagy provides metabolic substrates to maintain energy charge and nucleotide pools in Ras-driven lung cancer cells. *Genes Dev* **30**, 1704-1717 (2016).

18. Koivusalo, M. *et al.* Amiloride inhibits macropinocytosis by lowering submembranous pH and preventing Rac1 and Cdc42 signaling. *J Cell Biol* **188**, 547-563 (2010).

19. Kaur, M., Gupta, B., Sinha, C. & Shende, S. A report on a case of accidental neck strangulation and its anesthetic concerns. *Anesthesia, essays and researches* **4**, 120-122 (2010).

20. Pulaski, B.A. & Ostrand-Rosenberg, S. Mouse 4T1 breast tumor model. *Current protocols in immunology / edited by John E. Coligan ... [et al.]* **Chapter 20**, Unit 20 22 (2001).

21. Horisawa, K. Specific and quantitative labeling of biomolecules using click chemistry. *Frontiers in physiology* **5**, 457 (2014).

22. Landgraf, P., Antileo, E.R., Schuman, E.M. & Dieterich, D.C. BONCAT: metabolic labeling, click chemistry, and affinity purification of newly synthesized proteomes. *Methods Mol Biol* **1266**, 199-215 (2015).

23. Hodakoski, C. *et al.* Rac-Mediated Macropinocytosis of Extracellular Protein Promotes Glucose Independence in Non-Small Cell Lung Cancer. *Cancers* **11** (2019).

24. Slawson, C., Copeland, R.J. & Hart, G.W. O-GlcNAc signaling: a metabolic link between diabetes and cancer? *Trends Biochem Sci* **35**, 547-555 (2010).

25. Vocadlo, D.J., Hang, H.C., Kim, E.J., Hanover, J.A. & Bertozzi, C.R. A chemical approach for identifying O-GlcNAc-modified proteins in cells. *Proc Natl Acad Sci U S A* **100**, 9116-9121 (2003).

26. Yang, X. & Qian, K. Protein O-GlcNAcylation: emerging mechanisms and functions. *Nat Rev Mol Cell Biol* **18**, 452-465 (2017).

27. Gao, X. & Hannoush, R.N. A Decade of Click Chemistry in Protein Palmitoylation: Impact on Discovery and New Biology. *Cell chemical biology* **25**, 236-246 (2018).

28. Menendez, J.A. & Lupu, R. Fatty acid synthase and the lipogenic phenotype in cancer pathogenesis. *Nat Rev Cancer* **7**, 763-777 (2007).

29. Alwarawrah, Y. *et al.* Fasnall, a Selective FASN Inhibitor, Shows Potent Anti-tumor Activity in the MMTV-Neu Model of HER2(+) Breast Cancer. *Cell chemical biology* **23**, 678-688 (2016).

30. Brenner, A.J. *et al.* Abstract P6-11-09: Heavily pre-treated breast cancer patients show promising responses in the first in human study of the first-In-class fatty acid synthase (FASN) inhibitor, TVB-2640 in combination with paclitaxel. *Cancer Res.* (2017).

31. Hardwicke, M.A. *et al.* A human fatty acid synthase inhibitor binds beta-ketoacyl reductase in the keto-substrate site. *Nat Chem Biol* **10**, 774-779 (2014).

32. Van de Sande, T. *et al.* High-level expression of fatty acid synthase in human prostate cancer tissues is linked to activation and nuclear localization of Akt/PKB. *J Pathol* **206**, 214-219 (2005).

33. Shah, U.S. *et al.* Fatty acid synthase gene overexpression and copy number gain in prostate adenocarcinoma. *Human pathology* **37**, 401-409 (2006).

34. Watt, M.J. *et al.* Suppressing fatty acid uptake has therapeutic effects in preclinical models of prostate cancer. *Science translational medicine* **11** (2019).

35. Salic, A. & Mitchison, T.J. A chemical method for fast and sensitive detection of DNA synthesis in vivo. *Proc Natl Acad Sci U S A* **105**, 2415-2420 (2008).

36. Koc, A., Wheeler, L.J., Mathews, C.K. & Merrill, G.F. Hydroxyurea arrests DNA replication by a mechanism that preserves basal dNTP pools. *J Biol Chem* **279**, 223-230 (2004).

37. Buj, R. & Aird, K.M. Deoxyribonucleotide Triphosphate Metabolism in Cancer and Metabolic Disease. *Frontiers in endocrinology* **9**, 177 (2018).

38. Christopherson, R.I., Lyons, S.D. & Wilson, P.K. Inhibitors of de novo nucleotide biosynthesis as drugs. *Accounts of chemical research* **35**, 961-971 (2002).

39. Shuvalov, O. *et al.* One-carbon metabolism and nucleotide biosynthesis as attractive targets for anticancer therapy. *Oncotarget* **8**, 23955-23977 (2017).

40. Parker, W.B. Enzymology of purine and pyrimidine antimetabolites used in the treatment of cancer. *Chemical reviews* **109**, 2880-2893 (2009).

41. Sanli, T. *et al.* Ionizing radiation activates AMP-activated kinase (AMPK): a target for radiosensitization of human cancer cells. *International journal of radiation oncology, biology, physics* **78**, 221-229 (2010).

42. Sanli, T. *et al.* Ionizing radiation regulates the expression of AMP-activated protein kinase (AMPK) in epithelial cancer cells: modulation of cellular signals regulating cell cycle and survival. *Radiotherapy and oncology : journal of the European Society for Therapeutic Radiology and Oncology* **102**, 459-465 (2012).

43. Tewey, K.M., Rowe, T.C., Yang, L., Halligan, B.D. & Liu, L.F. Adriamycin-induced DNA damage mediated by mammalian DNA topoisomerase II. *Science* **226**, 466-468 (1984).

44. Redelman-Sidi, G. *et al.* The Canonical Wnt Pathway Drives Macropinocytosis in Cancer. *Cancer Res* **78**, 4658-4670 (2018).

45. Tajiri, H. *et al.* Targeting Ras-Driven Cancer Cell Survival and Invasion through Selective Inhibition of DOCK1. *Cell reports* **19**, 969-980 (2017).

46. Labi, V. & Erlacher, M. How cell death shapes cancer. *Cell death & disease* **6**, e1675 (2015).

47. Huang, Q. *et al.* Caspase 3-mediated stimulation of tumor cell repopulation during cancer radiotherapy. *Nat Med* **17**, 860-866 (2011).

48. Richards, C.H. *et al.* Prognostic value of tumour necrosis and host inflammatory responses in colorectal cancer. *The British journal of surgery* **99**, 287-294 (2012).

49. Maiorano, E. *et al.* Prognostic and predictive impact of central necrosis and fibrosis in early breast cancer: results from two International Breast Cancer Study Group randomized trials of chemoendocrine adjuvant therapy. *Breast cancer research and treatment* **121**, 211-218 (2010).

50. Richards, C.H., Mohammed, Z., Qayyum, T., Horgan, P.G. & McMillan, D.C. The prognostic value of histological tumor necrosis in solid organ malignant disease: a systematic review. *Future oncology* **7**, 1223-1235 (2011).

51. Nofal, M., Zhang, K., Han, S. & Rabinowitz, J.D. mTOR Inhibition Restores Amino Acid Balance in Cells Dependent on Catabolism of Extracellular Protein. *Mol Cell* **67**, 936-946 e935 (2017).

52. Wellen, K.E. *et al.* The hexosamine biosynthetic pathway couples growth factor-induced glutamine uptake to glucose metabolism. *Genes Dev* **24**, 2784-2799 (2010).

53. Nahta, R., Hortobagyi, G.N. & Esteva, F.J. Growth factor receptors in breast cancer: potential for therapeutic intervention. *The oncologist* **8**, 5-17 (2003).

54. Jones, S.F. & Infante, J.R. Molecular Pathways: Fatty Acid Synthase. *Clin Cancer Res* **21**, 5434-5438 (2015).

55. Santarpia, M. *et al.* PIK3CA mutations and BRCA1 expression in breast cancer: potential biomarkers for chemoresistance. *Cancer investigation* **26**, 1044-1051 (2008).

56. Yuan, H. *et al.* Association of PIK3CA Mutation Status before and after Neoadjuvant Chemotherapy with Response to Chemotherapy in Women with Breast Cancer. *Clin Cancer Res* **21**, 4365-4372 (2015).

57. Steelman, L.S. *et al.* Suppression of PTEN function increases breast cancer chemotherapeutic drug resistance while conferring sensitivity to mTOR inhibitors. *Oncogene* **27**, 4086-4095 (2008).

58. Brown, K.K. & Toker, A. The phosphoinositide 3-kinase pathway and therapy resistance in cancer. *F1000prime reports* **7**, 13 (2015).

59. Galmarini, C.M., Mackey, J.R. & Dumontet, C. Nucleoside analogues and nucleobases in cancer treatment. *The lancet oncology* **3**, 415-424 (2002).

60. Valvezan, A.J. *et al.* mTORC1 Couples Nucleotide Synthesis to Nucleotide Demand Resulting in a Targetable Metabolic Vulnerability. *Cancer Cell* **32**, 624-638 e625 (2017).

61. Halbrook, C.J. *et al.* Macrophage-Released Pyrimidines Inhibit Gemcitabine Therapy in Pancreatic Cancer. *Cell Metab* (2019).

62. Franklin, D.A. *et al.* p53 coordinates DNA repair with nucleotide synthesis by suppressing PFKFB3 expression and promoting the pentose phosphate pathway. *Scientific reports* **6**, 38067 (2016).

63. Chhipa, R.R. *et al.* AMP kinase promotes glioblastoma bioenergetics and tumour growth. *Nature Cell Biology* **20**, 823-835 (2018).

64. Liu, S. *et al.* Relationship between necrotic patterns in glioblastoma and patient survival: fractal dimension and lacunarity analyses using magnetic resonance imaging. *Scientific reports* **7**, 8302 (2017).

65. Davidson, S.M. *et al.* Environment Impacts the Metabolic Dependencies of Ras-Driven Non-Small Cell Lung Cancer. *Cell Metab* **23**, 517-528 (2016).

66. Rebecca, V.W. *et al.* PPT1 Promotes Tumor Growth and Is the Molecular Target of Chloroquine Derivatives in Cancer. *Cancer discovery* **9**, 220-229 (2019).

67. Boone, B.A. *et al.* Safety and Biologic Response of Pre-operative Autophagy Inhibition in Combination with Gemcitabine in Patients with Pancreatic Adenocarcinoma. *Annals of surgical oncology* **22**, 4402-4410 (2015).

68. Commisso, C., Flinn, R.J. & Bar-Sagi, D. Determining the macropinocytic index of cells through a quantitative image-based assay. *Nat Protoc* **9**, 182-192 (2014).

CHAPTER 4

CONCLUSIONS

Macropinocytosis is a not just a KRAS phenotype, but a cancer phenotype

Classifying macropinocytosis as just a KRAS-driven metabolic adaptation has led to a gross underestimation of its contribution to tumor anabolism. Downstream of RAS, the lipid $PI(3,4,5)P_3$ (PIP_3) generated by class 1 PI3K triggers signaling cascades that control both actin organization and macropinosome closure[1]. Consistent with the central role of PIP_3 in macropinocytosis, prostate cancers with loss of function mutations in the PI3K antagonist PTEN exhibit macropinocytosis in vitro and in vivo (Fig. 2.1A and 2.4A). Breast cancers with mutations in PTEN, PI3K or KRAS also exhibit macropinocytosis (Fig. 3.1A). PI3K signaling is elevated in a wide spectrum of cancer classes; whether additional tumor classes with elevated PIP_3 production perform macropinocytosis requires further investigation. Constitutive Wnt, Src and Pkc signaling promotes macropinocytosis suggesting that multiple oncogenic mutations can drive this process[2-5]. In non-transformed cells, macropinocytosis is induced by growth factors; cancer classes with overexpression or gain of function mutations in epidermal growth factor receptor (EGFR) or the platelet-derived growth factor (PDGF) are likely to perform macropinocytosis as well[6, 7]. Finally, 4T1 murine mammary carcinoma cells perform macropinocytosis although they do not harbor mutations in any of the above signaling pathways demonstrating that additional signals that promote macropinosome formation remain to be identified[8]. In sum, macropinocytosis likely supports the growth of most solid tumors and agents that inhibit macropinocytosis could have broad therapeutic applications across cancer classes.

Although AMPK has historically been classified as a tumor suppressor protein, pro-tumorigenic roles for this stress-activated kinase are being uncovered[9]. While AMPK slows growth in nutrient-replete conditions, when nutrients are limiting, several studies demonstrate that AMPK can promote proliferation by providing access to alternative nutrient sources[10]. We defined an essential role for AMPK in macropinosome formation as an activator of RAC1 consistent with prior studies implicating AMPK in promoting actin polymerization[11-13]. In poorly perfused tumors, AMPK is activated by low oxygen and glucose levels[14]. However, the mutational burden in cancer cells can lead to "oncogenic stress" that activates AMPK even when nutrients are plentiful[15-17]. Although a few breast cancer cell lines were contextually macropinocytic where they required glucose deprivation or AMPK activation to stimulate macropinocytosis, the majority of cancer cells are constitutively macropinocytic (Fig. 3.1A). Even contextually macropinocytic 4T1 mammary cancer cells were robustly macropinocytic in vivo suggesting that the amount of stress in the TME is sufficient to activate AMPK (Fig. 3.1B). PTEN-deficient prostate cancers were wired to constitutively do macropinocytosis in vitro unlike most PTEN-deficient breast cancer cells. Different cancers harboring the same driver mutations can also have different metabolic needs since gene expression patterns would more closely resemble the tissue of origin rather than tissues of other tumor types. K-RAS activating mutations and P53 loss are commonly occurring mutations in both PDAC and non–small cell lung carcinomas (NSCLC). A recent study using a single genetically engineered mouse model with differential expression of Cre to drive $KrasLSL^{G12D/+}$; $Trp53^{flox/flox}$ in both the pancreas and lung tissues[18]. This study identified that NSCLC tumor cells exhibit less macropinocytosis compared to PDAC

tumor cells derived from the same mouse. These differences in macropinocytosis may correlate with differential uptake and utilization of BCAAs. These differences in uptake of BCAAs may also correlate with the perfusion of each of the tumors where NSCLC can derive BCAAs from amino acid transporters directly but poorly perfused PDAC cells might rely on macropinocytosis for replenished scavenged pool of BCAAs. The interesting observation that non-transformed mammary epithelial cells perform macropinocytosis when AMPK is stimulated while normal prostate and pancreas cancer cells do not (Fig. 3.1A and 2.4B) may be related to the fact that the mammary gland undergoes physiologic involution following pregnancy[19, 20]. The mammary gland goes through severe remodeling during this stage, which disperses milk and dying cell corpses in the extracellular space. Ability of these epithelial cells to perform macropinocytosis allows them to scavenge the redistributed milk proteins back into the cell. In addition, tissues that often face nutrient stress like corneal epithelial cells may also rely on macropinocytosis for survival and proliferation[21]. AMPK activation may drive cell-autonomous proliferation in nutrient-stressed cancer cells by stimulating multiple forms of scavenging including entosis and integrin mediated scavenging of ECM proteins, not just macropinocytosis, and can support survival by stimulating autophagy[22-24]. Together, these findings support a paradigm-shift in the field: therapeutic AMPK inhibition, not activation, makes the most sense in established tumors[9, 25-27].

To date, all published studies demonstrating a role for macropinocytosis in tumor anabolism have focused on its ability to supply amino acids from degraded extracellular

proteins. Albumin has been universally supplied as the macropinocytic fuel when nutrient stress is produced by limiting glutamine or non-essential amino acids. However, macropinocytosis is a non-selective, bulk uptake process; many components of the TME are likely to be engulfed in macropinosomes, not just extracellular proteins. Necrosis is present in most solid tumors and negatively correlated with prognosis[10, 28-30]. We have demonstrated that macropinocytosis of necrotic cell corpses provides a wide array of nutrients and supports proliferation under conditions where albumin cannot (Fig. 3.1C) and defined this process as necrocytosis given the extended benefits of scavenging corpses over protein. A novel approach to measuring macropinocytic flux using alkyne-modified nutrients coupled with click chemistry confirmed that necrocytosis can provide macropinocytic cancer cells with lipids, amino acids, sugars, nucleotides and probably most nutrients that are required for biosynthesis. Supplementation with necrotic cells but not albumin maintained lipid droplets in starved prostate cancer cells (Fig. 2.6F) and breast cancer cells (data not shown) suggesting fatty acids are derived via necrocytosis and can be stored in lipid droplets[31]. Unlike albumin, proteins in necrotic cell debris likely contain amino acids at an ideal ratio which can support protein synthesis. Importantly, necrotic cell debris was supplied at only 0.05%-0.2%, a 25- to 40-fold lower concentration than albumin, suggesting that relatively small amounts of necrosis could have a significant impact on tumor growth. Inflammatory signals released by apoptotic cells can drive growth of viable neighboring cells; it is possible that the proliferation of these viable cells could be fueled by necrocytosis[32]. In fact, co-injection of dead cells with viable 4T1 mammary cancer cells accelerates their proliferation in subcutaneous tumor models[33]. This work indicates that in vitro studies where the only

macropinocytic fuel provided is albumin will significantly underestimate the contribution of this process to tumor anabolism and provides a mechanism that could partially explain the association between tumor necrosis and a poor prognosis. It is important to note though macropinocytosis has been established to be support tumor growth in pancreatic and prostate cancers, induction of macropinocytosis in other cancer types can be jeopardizing. Studies have identified that hyperactivation of macropinocytosis or aberrant trafficking of macropinosomes to the lysosomes or recycling of macropinosome to the plasma membrane can result in an accumulation of cytoplasmic vacuoles resulting in cell death[34]. This phenomenon is referred to as methuosis and is selective for tumor cells. Activating mutations in RAS results in methusosis in glialblastomas, gastric cancers and osteocarcinomas[35]. High RAC1 activity is necessary downstream of KRAS signaling and sufficient to induce methuosis in glioblastoma cells. Mutations in either EGFR or K-RAS are relatively common in human lung carcinomas where expression of both mutations together results in synthetic lethality explaining why these genetic events remain mutually exclusive[36]. Increased number of macropinosomes observed upon the combination of both oncogenes leads to cell death. Identifying what accounts for this unique effect in some K-RAS cells but not in others can help identify a novel way of targeting macropinocytosis.

Machinery involved in mediating macropinocytosis are also involved in regulating cell motility and metastasis. Some studies have identified macropinocytosis and cell migration are inversely correlated where highly motile cells are less macropinocytic[37]. This correlation is attributed to redirection of SCAR/WAVE complex, a major nucleator

of actin filaments by elevated PIP3 levels causing a shift towards macropinocytosis rather than cell migration. How these dynamics interplay in tumor cell invasion and metastasis remain to be identified. In other cases macropinocytosis may directly or indirectly aid in promoting cell migration. Degradation of ECM surrounding tumors by macropinocytosis may increase cellular invasion. In addition, internalization of cadherin or other proteins that mediate cell-cell adhesion and cellular mechanics by macropinocytosis may also aid in promoting EMT. Integrins and cadherins also have novel roles in linking macropinocytosis and cell migration. Tumor exosomes have established roles in metastasis initiation and promotion. Therefore, uptake of exosomes by macropinocytosis may also aid this process. It is also tempting to speculate that macropinocytosis may play a role in helping metastatic niches adapt to stresses in a new foreign land. Macropinocytosis may also be the means by which dormant breast cancer cells can acquire nutrients necessary to proliferate and repopulate tumors. Many unanswered questions remain. Can macropinocytosis play a role in selecting and providing an advantage to metastasis initiating cells? Is macropinocytosis regulated differentially in primary vs. metastasized tumors? Can macropinocytosis be differentially regulated depending on the site of secondary metastasis?

Targeting macropinocytosis for cancer therapy

It is widely acknowledged that autophagy contributes to both macroscopic tumor growth and drug resistance, and more than 80 clinical trials are evaluating drugs that limit autophagic flux as single agents or in combination with other cancer therapies[38-40]. This work demonstrates that inhibiting macropinocytosis is likely to have a greater

therapeutic impact than blocking autophagy. Acquiring cell-intrinsic nutrients by autophagy can allow nutrient-deprived cells to survive, but does not support proliferation; autophagy-deficient ATG5 KO MEFs but not macropinocytosis-deficient PAK1 KO MEFs, can proliferate when amino acids are limited (Fig. 2.2G,H). However, the best approach to targeting macropinocytosis in patients is uncertain. To date, no proteins that are involved only in macropinocytosis have been identified, and all inhibitors have pleiotropic effects. The most commonly used macropinocytosis inhibitor, EIPA, targets Na^+/H^+ exchangers (NHE) resulting in pH changes and multifaceted antitumor effects (Table 1)[10]. These pleiotropic effects likely contribute to its anti-cancer activity. As subcutaneous administration every-other-day of EIPA blocks macropinocytosis and caused some tumor regressions in a syngeneic prostate tumor model (Fig. 2.7F-H), the conventional wisdom that EIPA's pharmacologic properties preclude its use in the clinic merits re-evaluation. EIPA inhibits multiple NHE isoforms[41]. Selective NHE1 inhibitors have been tested in clinical trials in a non-oncology context and have been found to be safe[42]. These agents block macropinocytosis more transiently in vitro (data not shown), but given that they may have superior pharmacologic properties, should also be tested in vivo. While RAC1 and p21-activated kinase 1 (PAK1) inhibitors block macropinocytosis and are valuable as tool compounds, their efficacy as clinical agents remain unknown (Table 1). Blocking lysosomal degradation is currently the primary strategy for inhibiting autophagy in tumors[43] and also limits macropinocytic flux. Given that macropinocytosis, but not autophagy, drives growth in nutrient-limiting conditions, the beneficial effects of lysosomal inhibitors like chloroquine (CQ) or its derivative hydroxychloroquine (HCQ) may stem more from the

inhibition of macropinocytosis than from blocking autophagy[44-46]. Alternative inhibitors of lysosomal function with improved pharmacologic properties are under development[47] and may also limit macropinocytosis. It is possible that reported benefits of PI3K inhibitors in pre-clinical and clinical trials partially stem from inhibiting macropinocytosis[7, 48]. In summary, while defining the true anabolic contributions of macropinocytosis to tumorigenesis will require macropinocytosis-specific agents, the most therapeutic value may come from deploying pleiotropic macropinocytosis inhibitors. AMPK activation has been demonstrated to be an effective anti-cancer strategy in some contexts[49]. Some of these anti-tumorgenic effects have been reported with the use of indirect AMPK activators such as metformin which also activate multiple other signalizing cascades. In addition, indirect activation of AMPK via metformin can promote renal tumor growth and thus renal cancers would benefit from AMPK inhibitors rather than activators. Findings that AMPK can promote anabolism through many strategies including macropinocytosis suggest development of AMPK inhibitors is necessary and may be an effective strategy as they would inhibit multiple metabolic adaptions. Macropinocytosis inhibitors could address the critical unmet clinical need for new strategies that prevent or overcome drug resistance. Chemotherapy and irradiation extend survival in patients with solid tumors, but resistance almost invariably develops. Autophagy plays a pivotal role in mediating resistance to these standards of care therapies, but macropinocytosis may make an even greater contribution. Advanced, drug-resistant solid tumors often contain necrotic regions, and tumor necrosis is positively correlated with therapeutic resistance across cancer classes[28-30]. Necrocytosis protected cancer cells from therapies that target de novo nucleotide

synthesis or therapies that mediate genotoxic stress (Fig. 3.6A-D and 3.7C). Triple-negative breast cancer cells that survive chemotherapy accelerate pyrimidine synthesis to alleviate DNA replication stress[50]. Necrocytosis could provide nucleotides without the energetic costs associated with synthesis. It is noteworthy that cisplatin can activate AMPK at the same time it induces DNA damage, potentially stimulating macropinocytosis. Inhibiting AMPK, which would block macropinocytosis, increases cisplatin-induced death[51]. Macropinocytosis may also provide resistance to therapies that disrupt tumor vasculature such as angiogenesis inhibitors; anti-angiogenic therapies are currently being tested in phase III clinical trials in breast cancers[52, 53]. Many other therapeutics that target biosynthesis could be undermined by macropinocytosis as well[54-57]. These findings suggest that inhibiting macropinocytosis could enhance the efficacy of many standard of care therapies.

Future Directions

The oncogenic signals that drive macropinocytosis and the contributions this process makes to tumor initiation, tumor progression, and anti-tumor immunity merit further investigation. The therapeutic potential of inhibiting macropinocytosis should also be more accurately defined. Several critical open questions are defined below:

How do oncogenic signals drive the AMPK activation necessary for macropinosome formation? Further elucidation of the signals that drive macropinocytosis in cancer cells could help identify novel therapeutic targets and identify biomarkers to predict which tumors will respond to macropinocytosis inhibitors.

To what extent does macropinocytosis support different stages of tumorigenesis? Genetic strategies to selectively inhibit macropinocytosis are necessary to identify the contributions macropinocytosis makes to tumor initiation, progression and drug resistance. However, no proteins involved solely in macropinocytosis have been identified. A selective, genetic strategy to inhibit macropinocytosis will be necessary to define whether macropinocytosis fuels the migration and/or survival of metastatic cells.

Does tumor macropinocytosis regulate tumor immunity? Immune cells use macropinocytosis to collect antigens[58]. Before macropinocytosis inhibitors are employed in clinical oncology, it will be vital to determine whether macropinocytosis *limits* or *enhances* tumor immunity. Tumor cell macropinocytosis could *dampen* tumor immunity. Macropinocytic tumor cells may compete with dendritic cells for antigens in the TME suppressing the anti-tumor immune response. In addition, pro-tumorigenic M2 macrophages perform increased rates of macropinocytosis compared to anti-tumor macrophages thus decreasing macropinocytosis could suppress M2 macrophages[59]. To preserve antigen presentation and anti-tumor immunity, it may be necessary to identify signals that specifically regulate macropinocytosis in cancer but not immune cells.

What is the best therapeutic strategy to target macropinocytosis in tumors? AMPK inhibitors should be developed and tested as they will inhibit many metabolic adaptations in parallel. Targeting the lysosome would block all scavenging

mechanisms and recycling via autophagy as they rely on the lysosome for degradation and release of nutrients. However, lysosomal inhibitors may prove unacceptably toxic at effective doses. NHE inhibitors have proven safe in clinical trials and might be employed as pleiotropic macropinocytosis inhibitors in the clinic[60].

Summary statement

Although many open questions remain, our findings provide strong evidence that scavenging via macropinocytosis is a key component of cancer's anabolic supply chain. Necrocytosis likely fuels the growth of many solid tumors and may contribute to drug resistance in many aggressive and lethal cancers including PDAC, castration-resistant prostate cancers, and TNBC. Therapies that target the oncogenes that drive these cancers like KRAS or PI3K may be successful and would also limit macropinocytosis, but if these upstream approaches are too toxic, downstream inhibition may be most effective. Targeting macropinocytosis could improve clinical outcomes in patients and the development of macropinocytosis inhibitors should be prioritized.

Table 1: Scavenging inhibitors with potential value in cancer therapy.

Compound	Target	Pathway Targeted	Step blocked	Tumor class where effective	Ref
EIPA	NHE1/3	MP	Uptake	MIA PaCa-2 xenograft PDAC tumors PTEN- and p53-null prostate tumor isografts	20

Cariporide	NHE1	MP	Uptake	not evaluated in vivo tumor models; clinical trials suggest favorable safety profile	60-62
PI3Ki (pan)*	PI3K	MP	Uptake	BKM120 in clinical trials; progressed to phase III in some cancer classes. Many other PI3K inhibitors (e.g., ZSTK474) in clinical trials with encouraging results	63-65
EHT1864	RAC1	MP	Uptake	BT-474 breast cancer xenografts Fulvestrant-resistant MCF-7 breast cancer xenografts in combination with fulvestrant	66
EHop-016	RAC1/3	MP	Uptake	orthotopic MDA-MB-453 breast cancer tumors MXF8000 myxofibrosarcoma xenografts	67
TBOPP	DOCK1	MP	Uptake	Metastatic ex-3LL Lewis lung carcinoma xenograft DLD-1 colorectal adenocarcinoma xenografts	68
FRAX597	PAK (group I)	MP	Uptake	SC4 NF2-null orthotopic schwannoma tumors	69,70

				Murine Pan02 orthotopic PDAC tumors in combination with gemcitabine	
FRAX1036	PAK (group I)	MP	Uptake	OVCAR3 xenograft tumors in combination with Rotterlin Local and metastatic STS26T and S462TY peripheral neural sheath xenograft tumors in combination with MEK1/2 inhibitor	[71]
Compound c	AMPK**	MP Integrin Entosis	Uptake Trafficking Lysosome biogenesis/function	Single agent in A549 and SMMC-7721 xenograft tumors In combination with cisplatin in HCT116 xenograft tumors	[72, 73]
Apilimod	PIKfyve	All	Lysosomal fusion	B-cell non-Hodgkin lymphoma	[74]
CQ/HCQ	-	All	Lysosomal function	Many tumor models; combinations with chemotherapy successful in clinical trials	[39, 45, 47]
DQ661	PPT1	All	Lysosomal function	Melanoma ($BRAF^{V600E}$-mutant xenograft) Colon cancer (HT29 xenograft) Gemcitabine-resistant PDAC (isograft derived from KPC GEMM model for PDAC)	[75]

Bafilomycin A1	v-ATPase	All	Uptake Lysosomal function	Rat GH3 pituitary xenograft tumors BEL7402 and HepG2 HCC xenograft tumors Capan-1 PDAC xenograft tumors HIF wildtype fibrosarcoma xenograft tumors	51, 73, 76, 77
SH-BC-893	PP2A	All	Lysosomal fusion	Autochthonous and isograft PTEN;p53-null prostate tumors; SW620 colorectal cancer xenografts	72

MP = macropinocytosis; Integrin = integrin-mediated scavenging of ECM; NF2 = neurofibronmin 2; PPT1 = palmitoyl-protein thioesterase 1; PDAC = pancreatic ductal adenocarcinoma; KPC GEMM = genetically engineered mouse model for pancreatic adenocarcinoma KrasLSL.G12D/+; p53R172H/+; PdxCretg/+; HCC = hepatocellular carcinoma; HIF = hypoxia-inducible factor *While isoform-specific inhibitors may be effective in tumors with PI3Kα mutations, dual inhibition of PI3Kα and β was required to block macropinocytosis in PTEN deficient cells **Compound c inhibits AMPK but also has many off-target effect.

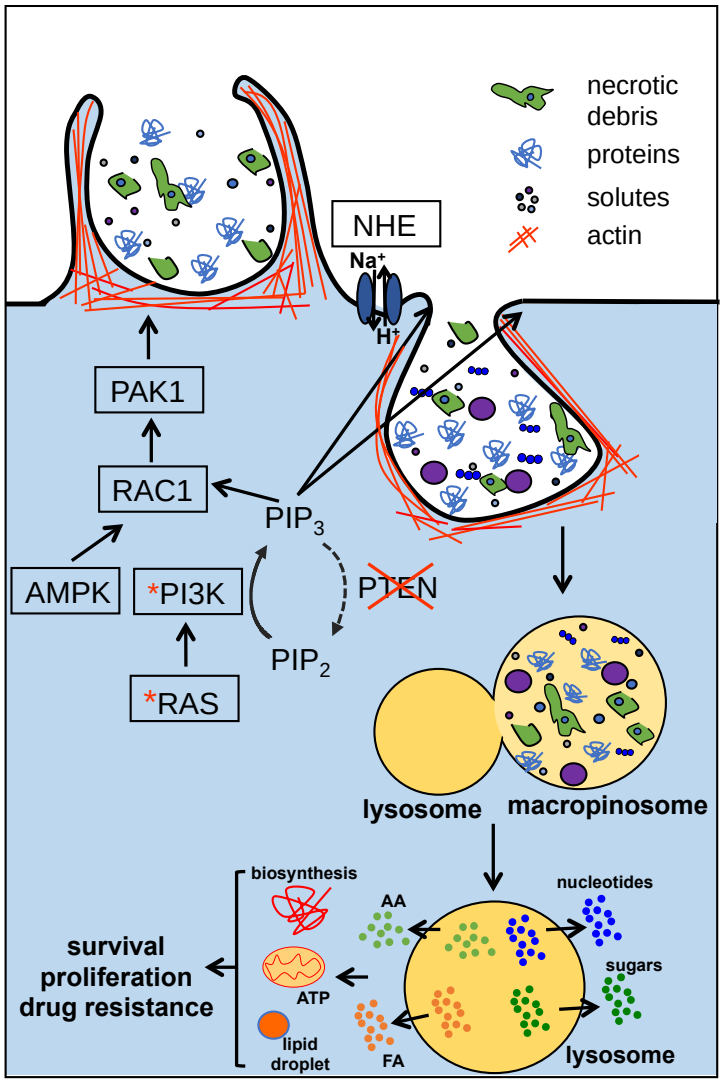

Fig. 4.1: Macropinocytosis stimulated by RAS or PI3K activation promotes cancer cell survival, proliferation and confers drug resistance. Macropinocytosis allows PTEN-deficient prostate cancer cells to proliferate in nutrient-limiting conditions. Phosphatase and tensin homology (PTEN) loss or activation of the PI3 kinase , promote AMP-activated protein kinase (AMPK) dependent macropinosome formation. Macropinocytosis allows non-selective uptake of necrotic cell debris. Lysosomal catabolism of the macromolecules derived via scavenging necrotic cell debris provides anabolic substrates. Boxed proteins are potential targets for pleiotropic macropinocytosis inhibitors. Because macropinocytosis provides access to extracellular macromolecules, it can support both survival and proliferation as well as provide resistance against metabolic therapies. Asterisks (in red) indicate occurrence of oncogenic activating mutations in the respective gene.

References

1. Egami, Y., Taguchi, T., Maekawa, M., Arai, H. & Araki, N. Small GTPases and phosphoinositides in the regulatory mechanisms of macropinosome formation and maturation. *Front Physiol* **5**, 374 (2014).
2. Redelman-Sidi, G. *et al.* The Canonical Wnt Pathway Drives Macropinocytosis in Cancer. *Cancer Res* **78**, 4658-4670 (2018).
3. Tejeda-Munoz, N., Albrecht, L.V., Bui, M.H. & De Robertis, E.M. Wnt canonical pathway activates macropinocytosis and lysosomal degradation of extracellular proteins. *Proc Natl Acad Sci U S A* (2019).
4. Veithen A, Cupers P, Baudhuin P, Courtoy PJ. 1996. v-Src induces constitutive macropinocytosis in rat fibroblasts. *J. Cell Sci*. **109** (Part 8) (2000).
5. Chianale, F. *et al.* Diacylglycerol kinase alpha mediates HGF-induced Rac activation and membrane ruffling by regulating atypical PKC and RhoGDI. *Proc Natl Acad Sci U S A* **107**, 4182-4187 (2010).
6. Yoshida, S. *et al.* Differential signaling during macropinocytosis in response to M-CSF and PMA in macrophages. *Front Physiol* **6**, 8 (2015).
7. Schwartz, S. *et al.* Feedback suppression of PI3Kalpha signaling in PTEN-mutated tumors is relieved by selective inhibition of PI3Kbeta. *Cancer Cell* **27**, 109-122 (2015).
8. Castle, J.C. *et al.* Mutated tumor alleles are expressed according to their DNA frequency. *Sci Rep* **4**, 4743 (2014).
9. Jeon, S.M. & Hay, N. The double-edged sword of AMPK signaling in cancer and its therapeutic implications. *Arch Pharm Res* **38**, 346-357 (2015).
10. Finicle, B.T., Jayashankar, V. & Edinger, A.L. Nutrient scavenging in cancer. *Nat Rev Cancer* **18**, 619-633 (2018).
11. Blume, C. *et al.* AMP-activated protein kinase impairs endothelial actin cytoskeleton assembly by phosphorylating vasodilator-stimulated phosphoprotein. *J Biol Chem* **282**, 4601-4612 (2007).
12. Guest, C.B., Chakour, K.S. & Freund, G.G. Macropinocytosis is decreased in diabetic mouse macrophages and is regulated by AMPK. *BMC Immunol* **9**, 42 (2008).
13. Moser, T.S., Jones, R.G., Thompson, C.B., Coyne, C.B. & Cherry, S. A kinome RNAi screen identified AMPK as promoting poxvirus entry through the control of actin dynamics. *PLoS Pathog* **6**, e1000954 (2010).
14. Laderoute, K.R. *et al.* 5'-AMP-activated protein kinase (AMPK) is induced by low-oxygen and glucose deprivation conditions found in solid-tumor microenvironments. *Mol Cell Biol* **26**, 5336-5347 (2006).
15. Rabinovitch, R.C. *et al.* AMPK Maintains Cellular Metabolic Homeostasis through Regulation of Mitochondrial Reactive Oxygen Species. *Cell Rep* **21**, 1-9 (2017).
16. Liang, J. & Mills, G.B. AMPK: a contextual oncogene or tumor suppressor? *Cancer Res* **73**, 2929-2935 (2013).
17. Park, H.U. *et al.* AMP-activated protein kinase promotes human prostate cancer cell growth and survival. *Mol Cancer Ther* **8**, 733-741 (2009).

18. Mayers, J.R. *et al.* Elevation of circulating branched-chain amino acids is an early event in human pancreatic adenocarcinoma development. *Nat Med* **20**, 1193-1198 (2014).
19. Akhtar, N., Li, W., Mironov, A. & Streuli, C.H. Rac1 Controls Both the Secretory Function of the Mammary Gland and Its Remodeling for Successive Gestations. *Dev Cell* **38**, 522-535 (2016).
20. Commisso, C. *et al.* Macropinocytosis of protein is an amino acid supply route in Ras-transformed cells. *Nature* **497**, 633-637 (2013).
21. Peng, H., Park, J.K. & Lavker, R.M. Autophagy and Macropinocytosis: Keeping an Eye on the Corneal/Limbal Epithelia. *Invest Ophthalmol Vis Sci* **58**, 416-423 (2017).
22. Hamann, J.C. *et al.* Entosis Is Induced by Glucose Starvation. *Cell Rep* **20**, 201-210 (2017).
23. Ross, E. *et al.* AMP-Activated Protein Kinase Regulates the Cell Surface Proteome and Integrin Membrane Traffic. *PLoS One* **10**, e0128013 (2015).
24. Kim, J., Kundu, M., Viollet, B. & Guan, K.L. AMPK and mTOR regulate autophagy through direct phosphorylation of Ulk1. *Nat Cell Biol* **13**, 132-141 (2011).
25. Eichner, L.J. *et al.* Genetic Analysis Reveals AMPK Is Required to Support Tumor Growth in Murine Kras-Dependent Lung Cancer Models. *Cell Metab* **29**, 285-302 e287 (2019).
26. Patra, K.C., Weerasekara, V.K. & Bardeesy, N. AMPK-Mediated Lysosome Biogenesis in Lung Cancer Growth. *Cell Metab* **29**, 238-240 (2019).
27. Endo, H., Owada, S., Inagaki, Y., Shida, Y. & Tatemichi, M. Glucose starvation induces LKB1-AMPK-mediated MMP-9 expression in cancer cells. *Sci Rep* **8**, 10122 (2018).
28. Hiraoka, N. *et al.* Tumour necrosis is a postoperative prognostic marker for pancreatic cancer patients with a high interobserver reproducibility in histological evaluation. *Br J Cancer* **103**, 1057-1065 (2010).
29. Maiorano, E. *et al.* Prognostic and predictive impact of central necrosis and fibrosis in early breast cancer: results from two International Breast Cancer Study Group randomized trials of chemoendocrine adjuvant therapy. *Breast Cancer Res Treat* **121**, 211-218 (2010).
30. Richards, C.H. *et al.* Prognostic value of tumour necrosis and host inflammatory responses in colorectal cancer. *Br J Surg* **99**, 287-294 (2012).
31. Petan, T., Jarc, E. & Jusovic, M. Lipid Droplets in Cancer: Guardians of Fat in a Stressful World. *Molecules* **23** (2018).
32. Labi, V. & Erlacher, M. How cell death shapes cancer. *Cell Death Dis* **6**, e1675 (2015).
33. Huang, Q. *et al.* Caspase 3-mediated stimulation of tumor cell repopulation during cancer radiotherapy. *Nat Med* **17**, 860-866 (2011).
34. Maltese, W.A. & Overmeyer, J.H. Methuosis: nonapoptotic cell death associated with vacuolization of macropinosome and endosome compartments. *Am J Pathol* **184**, 1630-1642 (2014).

35. Bhanot, H., Young, A.M., Overmeyer, J.H. & Maltese, W.A. Induction of nonapoptotic cell death by activated Ras requires inverse regulation of Rac1 and Arf6. *Mol Cancer Res* **8**, 1358-1374 (2010).
36. Unni, A.M., Lockwood, W.W., Zejnullahu, K., Lee-Lin, S.Q. & Varmus, H. Evidence that synthetic lethality underlies the mutual exclusivity of oncogenic KRAS and EGFR mutations in lung adenocarcinoma. *Elife* **4**, e06907 (2015).
37. Veltman, D.M. Drink or drive: competition between macropinocytosis and cell migration. *Biochem Soc Trans* **43**, 129-132 (2015).
38. Wolpin, B.M. *et al.* Phase II and pharmacodynamic study of autophagy inhibition using hydroxychloroquine in patients with metastatic pancreatic adenocarcinoma. *Oncologist* **19**, 637-638 (2014).
39. Levy, J.M.M., Towers, C.G. & Thorburn, A. Targeting autophagy in cancer. *Nat Rev Cancer* **17**, 528-542 (2017).
40. Kocaturk, N.M. *et al.* Autophagy as a molecular target for cancer treatment. *Eur J Pharm Sci* **134**, 116-137 (2019).
41. Masereel, B. An overview of inhibitors of Na+/H+ exchanger. *European Journal of Medicinal Chemistry* **38**, 547-554 (2003).
42. Harguindey, S. *et al.* Cariporide and other new and powerful NHE1 inhibitors as potentially selective anticancer drugs – an integral molecular/biochemical/metabolic/clinical approach after one hundred years of cancer research. *Journal of Translational Medicine* **11**, 282 (2013).
43. Towers, C.G. & Thorburn, A. Therapeutic Targeting of Autophagy. *EBioMedicine* **14**, 15-23 (2016).
44. Mauthe, M. *et al.* Chloroquine inhibits autophagic flux by decreasing autophagosome-lysosome fusion. *Autophagy* **14**, 1435-1455 (2018).
45. Solomon, V.R. & Lee, H. Chloroquine and its analogs: a new promise of an old drug for effective and safe cancer therapies. *Eur J Pharmacol* **625**, 220-233 (2009).
46. Guo, W., Wang, Y., Wang, Z., Wang, Y.P. & Zheng, H. Inhibiting autophagy increases epirubicin's cytotoxicity in breast cancer cells. *Cancer Sci* **107**, 1610-1621 (2016).
47. Chude, C.I. & Amaravadi, R.K. Targeting Autophagy in Cancer: Update on Clinical Trials and Novel Inhibitors. *Int J Mol Sci* **18** (2017).
48. Yang, J. *et al.* Targeting PI3K in cancer: mechanisms and advances in clinical trials. *Mol Cancer* **18**, 26 (2019).
49. Amaravadi, R.K. *et al.* Principles and current strategies for targeting autophagy for cancer treatment. *Clin Cancer Res* **17**, 654-666 (2011).
50. Brown, K.K., Spinelli, J.B., Asara, J.M. & Toker, A. Adaptive Reprogramming of De Novo Pyrimidine Synthesis Is a Metabolic Vulnerability in Triple-Negative Breast Cancer. *Cancer Discov* **7**, 391-399 (2017).
51. Rashtchizadeh, N. *et al.* AMPK: A promising molecular target for combating cisplatin toxicities. *Biochem Pharmacol* **163**, 94-100 (2019).
52. Giuliano, S. & Pages, G. Mechanisms of resistance to anti-angiogenesis therapies. *Biochimie* **95**, 1110-1119 (2013).
53. Gampenrieder, S.P., Westphal, T. & Greil, R. Antiangiogenic therapy in breast cancer. *Memo* **10**, 194-201 (2017).

54. Lin, L., Yee, S.W., Kim, R.B. & Giacomini, K.M. SLC transporters as therapeutic targets: emerging opportunities. *Nat Rev Drug Discov* **14**, 543-560 (2015).
55. Pan, M. et al. Regional glutamine deficiency in tumours promotes dedifferentiation through inhibition of histone demethylation. Nat. Cell Biol. 18, 1090–1101 (2016).
56. Luengo, A., Gui, D.Y. & Vander Heiden, M.G. Targeting Metabolism for Cancer Therapy. *Cell Chem Biol* **24**, 1161-1180 (2017).
57. Mates, J.M., Campos-Sandoval, J.A. & Marquez, J. Glutaminase isoenzymes in the metabolic therapy of cancer. *Biochim Biophys Acta Rev Cancer* **1870**, 158-164 (2018).
58. Platt, C.D. *et al.* Mature dendritic cells use endocytic receptors to capture and present antigens. *Proc Natl Acad Sci U S A* **107**, 4287-4292 (2010).
59. Redka, D.S., Gutschow, M., Grinstein, S. & Canton, J. Differential ability of proinflammatory and anti-inflammatory macrophages to perform macropinocytosis. *Mol Biol Cell* **29**, 53-65 (2018).
60. Murphy, E. & Allen, D.G. Why did the NHE inhibitor clinical trials fail? *J Mol Cell Cardiol* **46**, 137-141 (2009).
61. Karmazyn, M. NHE-1: still a viable therapeutic target. *J. Mol. Cell Cardiol.* **61**, 77–82 (2013)
62. Harguindey, S. et al. Cariporide and other new and powerful NHE1 inhibitors as potentially selective anticancer drugs — an integral molecular/biochemical/metabolic/clinical approach after one hundred years of cancer research. J. Transl Med. 11, 282 (2013).
63. Janku, F., Yap, T.A. & Meric-Bernstam, F. Targeting the PI3K pathway in cancer: are we making headway? *Nat Rev Clin Oncol* **15**, 273-291 (2018).
64. Massacesi, C. *et al.* PI3K inhibitors as new cancer therapeutics: implications for clinical trial design. *Onco Targets Ther* **9**, 203-210 (2016).
65. Zhao, H.F. *et al.* Recent advances in the use of PI3K inhibitors for glioblastoma multiforme: current preclinical and clinical development. *Mol Cancer* **16**, 100 (2017).
66. Dharmawardhane, S. et al. Regulation of macropinocytosis by p21-activated kinase-1. *Mol. Biol. Cell* **11**, 3341–3352 (2000).
67. Hampsch, R. A. et al. Therapeutic sensitivity to Rac GTPase inhibition requires consequential suppression of mTORC1, AKT, and MEK signaling in breast cancer. *Oncotarget* **8**, 21806–21817 (2017).
68. Tajiri, H. *et al.* Targeting Ras-Driven Cancer Cell Survival and Invasion through Selective Inhibition of DOCK1. *Cell Rep* **19**, 969-980 (2017).
69. Licciulli, S. *et al.* Notch1 is required for Kras-induced lung adenocarcinoma and controls tumor cell survival via p53. *Cancer Res* **73**, 5974-5984 (2013).
70. Yeo, D. *et al.* FRAX597, a PAK1 inhibitor, synergistically reduces pancreatic cancer growth when combined with gemcitabine. *BMC Cancer* **16**, 24 (2016).
71. Araiza-Olivera, D. *et al.* Suppression of RAC1-driven malignant melanoma by group A PAK inhibitors. *Oncogene* **37**, 944-952 (2018).
72. Kim, S.M. *et al.* Targeting cancer metabolism by simultaneously disrupting parallel nutrient access pathways. *J Clin Invest* **126**, 4088-4102 (2016).

73. Kim, Y.D. *et al.* Metformin inhibits hepatic gluconeogenesis through AMP-activated protein kinase-dependent regulation of the orphan nuclear receptor SHP. *Diabetes* **57**, 306-314 (2008).
74. Gayle, S. *et al.* Identification of apilimod as a first-in-class PIKfyve kinase inhibitor for treatment of B-cell non-Hodgkin lymphoma. *Blood* **129**, 1768-1778 (2017).
75. Rebecca, V.W. *et al.* A Unified Approach to Targeting the Lysosome's Degradative and Growth Signaling Roles. *Cancer Discov* **7**, 1266-1283 (2017).
76. Lim, J.H. *et al.* Bafilomycin induces the p21-mediated growth inhibition of cancer cells under hypoxic conditions by expressing hypoxia-inducible factor-1alpha. *Mol Pharmacol* **70**, 1856-1865 (2006).
77. Yan, Y. *et al.* Bafilomycin A1 induces caspase-independent cell death in hepatocellular carcinoma cells via targeting of autophagy and MAPK pathways. *Sci Rep* **6**, 37052 (2016).